Pre-print

Malusà M.G., Fitzgerald P.G. (2020) The geologic interpretation of the detrital thermochronology record within a stratigraphic framework, with examples from the European Alps, Taiwan and the Himalayas. *Earth-Science Reviews* 201, 103074

https://doi.org/10.1016/j.earscirev.2019.103074

The geologic interpretation of the detrital thermochronology record within a stratigraphic framework, with examples from the European Alps, Taiwan and the Himalayas

Marco G. Malusà[1*] and Paul G. Fitzgerald[2]

[1] Laboratory for Provenance Studies, Department of Earth and Environmental Sciences, University of Milano-Bicocca, Piazza della Scienza 4 - 20126 Milano – ITALY

[2] Department of Earth Sciences, Syracuse University, Syracuse, NY 13244, USA

*corresponding author: Marco G. Malusà (marco.malusa@unimib.it)

Abstract

Detrital thermochronology studies based on the lag-time approach are increasingly employed to investigate the erosional evolution of mountain belts and perform paleotectonic reconstructions starting from the analysis of sedimentary rocks. However, simple predictions of lag-time conceptual models are often in conflict with observations in sedimentary basins. In this review article, we discuss the major assumptions of the lag-time approach, and present conceptual models to illustrate the main factors that may influence the final complexity of the detrital thermochronologic record in a sedimentary basin. These factors include: (i) the original complexity of the thermochronologic age structure in the source region; (ii) mixing of detritus from multiple source regions characterized by different geologic evolution; (iii) modifications of the original thermochronologic fingerprint from source to sink; (iv) potential post-depositional annealing due to thick sedimentary burial. Based on this synthesis and discussion, we present a list of interpretive guidelines and fundamental criteria for the geologic interpretation of the detrital thermochronologic record derived from the erosion of single and mixed sources. These interpretive guidelines are then applied to published detrital thermochronology datasets from the European Alps, Taiwan and the Himalayas in order to illustrate benefits and pitfalls of the geologic interpretation of thermochronologic age trends through a stratigraphic succession. Results provide evidence for (i) non-steady-state exhumation of the European Alps, (ii) late Miocene onset of arc-continent collision in Taiwan, and (iii) late Miocene morphogenic phase of mountain building in the Himalaya. Concepts presented in this article reinforce existing approaches and provide new perspectives for the application of the detrital thermochronologic approach to tectonic settings where the geologic evolution may be poorly understood. As such, they are expected to guide geologists towards interpretations that are both consistent with evidence provided by different thermochronologic systems, and geologic evidence provided by the rock record.

Keywords: detrital thermochronology; lag time; exhumation; European Alps; Taiwan; Himalaya

1. Introduction

Low-temperature thermochronology has become a routine tool to analyze the erosional evolution of orogenic belts on short-term and long-term timescales, and to perform paleotectonic reconstructions based on the analyses of modern sediment and sedimentary rocks (e.g., Bernet and Spiegel, 2004; Reiners and Ehlers, 2005; Braun et al., 2006; Reiners and Brandon, 2006; Malusà and Fitzgerald, 2019a). Many detrital thermochronology studies are based on the lag-time approach (Zeitler et al., 1986; Cerveny et al., 1988; Brandon and Vance, 1992), i.e., on the comparison between the thermochronologic age recorded by mineral grains found in a sedimentary rock, and the stratigraphic age of that rock that is independently determined by biostratigraphy, magnetostratigraphy or tephrochronology (e.g., Garver et al., 1999; Bernet et al., 2001). According to the simple conceptual model illustrated in Fig. 1a, rocks undergoing exhumation, i.e. moving towards Earth's surface because of overburden removal (England and Molnar, 1990; Stüwe and Barr, 1998), for example during erosion of a mountain range, will cross the closure temperature T_c of a given thermochronologic system at the cooling age t_c (Dodson, 1973) before reaching Earth's surface. There, mineral grains liberated by erosion from the host rock are transported by glaciers, rivers or turbidity currents to be deposited in a sedimentary basin at time t_d (Fig. 1a). Under a range of assumptions, concerning for example the paleogeothermal gradient at the time of exhumation (e.g., Braun et al., 2006) and the transportation time that is assumed to be geologically negligible (Brandon and Vance, 1992), the lag time between t_c and t_d provides an estimate of the average exhumation rate from the depth corresponding to the T_c isotherm to the Earth's surface (Cerveny et al., 1988; Garver et al., 1999; Bernet et al., 2001; Herman et al., 2013; Willett and Brandon, 2013; Bernet, 2019).

Samples for lag-time analyses are generally collected through a stratigraphic succession. Sedimentary successions are expected to reflect, in inverted order, the thermochronologic age structure of the sediment source (e.g., Ruiz et al., 2004; van der Beek et al., 2006). Therefore, the simple "source" scenario illustrated in Fig. 1a would also imply a simple thermochronologic record in the final "sink". Such detrital thermochronologic record should be characterized by a single thermochronologic age peak that becomes progressively younger up section through the sedimentary succession (lower panel of Fig. 1a). Within the conceptual framework of Fig. 1a, different lag-time trends, i.e., decreasing, constant or increasing lag-time values moving up section, can be used to infer whether the mountain belt feeding the sedimentary basin under investigation was under a constructional, steady-state or decay stage of evolution (Bernet et al., 2001; Carrapa et al., 2003; Spotila, 2005; Ruiz and Seward, 2006; Rahl et al., 2007; Zattin et al., 2010; Lang et al., 2016). These trends are also used to provide information on the dynamics of the orogenic wedge during the time interval constrained by thermochronologic data (Carrapa, 2009; Painter et al., 2014).

However, the predictions of the simple conceptual model of Fig. 1a are often in conflict with observations in real sedimentary basins. When thermochronologic ages are determined in detrital mineral grains from a sedimentary rock, resulting grain-age distributions generally include several grain-age populations (Galbraith and Laslett, 1993; Vermeesch, 2019), defining either moving or stationary age peaks (e.g., Brandon and Vance, 1992; Bernet et al., 2006), not a single thermochronologic age peak as predicted by the simple model of Fig. 1a. In order to fit the complexities of real sedimentary basins with the much simpler scenario predicted by the classic lag-time model, geologists often choose to interpret only part of the detrital thermochronology record, for example only the youngest age peak (e.g., Carrapa et al., 2003; Najman et al., 2009), which is often held to be particularly relevant to understanding the dominant tectonic processes of the study region. However, interpretations that only consider part of a dataset are prone to be incorrect. As a result, in spite of the increasing amount of detrital thermochronology data produced in the last decade, scientific debate concerning their geologic interpretation is often vigorous. For example, see Bernet et al. (2001, 2009), Carrapa et al. (2003), Kuhlemann et al. (2006), Carrapa (2009, 2010), Bernet (2010), Stalder et al. (2018) just to consider the long-lasting debate concerning the source-to-sink relationships in the European Alps, or Zeitler et al. (2001, 2014), Bendick and Ehlers (2014), Bracciali et al. (2015, 2016), Najman et al. (2019) for the ongoing debate concerning the timing and mechanisms of exhumation of the Himalayan syntaxial regions.

A careful evaluation of all the factors that may contribute to the complexity of the detrital thermochronology record in a sedimentary basin is the prerequisite for any reliable geologic interpretations based on detrital thermochronology data. Such a complexity may arise from a number of factors that are illustrated in Fig. 1b. They are:

- (I) the original complexity of the thermochronologic age structure in the source region, which may result from a rather complex geologic evolution;
- (II) mixing of detritus from multiple source regions that are characterized by different geologic or upper crustal exhumation histories;
- (III) modifications of the original thermochronologic signal during source-to-sink sediment transport and deposition;
- (IV) potential post-depositional annealing due to thick sedimentary burial.

In this review article, we discuss the major assumptions of the lag-time approach (Section 2) and the main factors (I to IV in Fig. 1b) that determine the potential complexity of the thermochronologic record in a sedimentary basin (Sections 3 to 6). Concepts illustrated in Sections 2 to 6 provide the baseline for a reliable geologic interpretation of detrital thermochronology data from samples collected within a stratigraphic framework.

Selected examples from the European Alps, Taiwan and the Himalayas are presented and discussed in Sections 7 to 9. These examples are not intended to be exhaustive, but they illustrate the potentials and limitations of an approach solely based on detrital thermochronology, the benefits of the integration of detrital thermochronology data with other geologic data sets, and the potentials of the application of the interpretive keys illustrated in Sections 3 and 4. These examples therefore provide new perspectives for the interpretation of detrital thermochronology data in situations where paleotectonic and paleoclimatic reconstructions are still debated.

Figure 1

2. Major assumptions underlying the lag-time approach

The lag-time approach to detrital thermochronology relies on a range of assumptions that may have major implications for data interpretation (Fig. 2). These assumptions should be carefully considered and, whenever possible, independently tested.

2.1 Assumption 1: Ages reflect cooling through closure temperature T_c during exhumation

One major assumption of detrital thermochronology studies based on the lag-time approach is that the thermochronologic fingerprint of eroded bedrock reflects cooling through the closure temperature T_c of the chosen thermochronologic system during exhumation (1 in Fig. 2) (Braun et al., 2006; Reiners and Brandon, 2006; Herman et al., 2013; Willett and Brandon, 2013). As it is well known from thermochronology applied to basement rocks, interpretation of all thermochronologic ages as representing cooling through the T_c isothermal surface during exhumation is often too simplistic (e.g., Gleadow, 1990; Villa, 1998, Williams et al., 2007; Baldwin et al., 2019). During exhumation, rocks transit from a zone characterized by the complete loss of decay products, or total annealing of fission tracks (at higher temperatures), to a zone characterized by near-complete retention of decay products or near-complete retention of fission tracks (at lower temperatures) (Fig. 1c) (Green et al., 1986; Farley, 2000). Between these two zones of complete loss and near-complete retention is the temperature interval characterized by partial stability (Wagner et al., 1977; 1979; Gleadow and Duddy, 1981; Gleadow et al., 1986; Hurford, 2019), which is either referred to as the partial annealing zone (PAZ; Gleadow and Fitzgerald, 1987) or as the partial retention zone (PRZ; Baldwin and Lister, 1998; Wolf et al., 1998) depending on the thermochronologic system under consideration. The concept of a closure temperature and a cooling age only applies in cases of monotonic cooling of a rock across a PAZ/PRZ (cases A and B in Fig. 1c) (Dodson, 1973; Villa, 1998). In those cases, the closure temperature can be defined as the temperature of the rock at its thermochronologic cooling age (Dodson, 1973). A cooling age will depend on the cooling rate (T_c will be higher for more rapid cooling, see e.g., Reiners and Brandon, 2006), will be different for different systems and minerals within those systems, and may also vary according to the mineral composition and/or radiation damage (Green et al., 1986; Barbarand et al., 2003; Rahn et al., 2004; Gautheron et al., 2013; Schneider and Issler, 2019).

The concept of a thermochronologic age being representative of the time a rock cooled through a T_c isotherm cannot be applied for complex cooling paths, such as those indicated by letters C and D in Fig. 1c (e.g., Gleadow et al., 1986), although these ages can still give important insights on the exhumation history of analysed samples. Some thermochronologic methods have kinetic parameters (e.g., confined track lengths for apatite fission-track thermochronology) that can be used to distinguish simple from complex temperature-time paths (e.g., Gleadow et al., 1986; Ketcham, 2005; Gallagher, 2012), and thus determine whether a thermochronologic age can be interpreted as representing the age since the sample cooled through a T_c or not. These kinetic parameters can be applied to bedrock thermochronology studies (see examples in Fitzgerald and Malusà, 2019) and to detrital thermochronology studies using conglomerates and cobbles (e.g., Beamud et al., 2011; Fitzgerald et al., 2019). However, kinetic parameters are seldom applicable to detrital thermochronology studies based on sand and sandstones (Bernet and Garver, 2005) to constrain meaningful temperature-time paths for the source region, although there are examples in the literature (e.g., Carrapa and DeCelles, 2008). For example, kinetic data for AFT must be collected from many apatite grains and, in a detrital sample, all apatite grains cannot be assumed to share the same temperature-time history. Thus, a confined track-length distribution from a sand or sandstone may be meaningless.

In many situations cooling recorded by thermochronometers is not related to the motion of rocks towards Earth's surface (Fig. 3a). For example, cooling may result from the downward motion of a T_c isothermal surface across a rock sample that remains fixed relative to Earth's surface (case 2 in Fig. 3a). This situation can be expected after a transient increase, and subsequent relaxation of the geothermal gradient (Braun, 2016; Malusà et al., 2016a), for example after fast exhumation of deep rocks (e.g., Liao et al., 2018a) or during continental breakup in extensional tectonic settings (e.g., Whitmarsh et al., 2001). Another scenario includes cooling of magmatic rocks (case 3 in Fig. 3a). If magma is emplaced at shallower crustal levels compared to the undisturbed T_c isothermal surface before intrusion (time t_0 in Fig. 3a, case 3), magmatic rocks will cool, after intrusion at temperatures lower than T_c even without moving towards the Earth's surface (time t_1 in Fig. 3a, case 3) (Wagner, 1972; Malusà et al., 2011a; Saylor et al., 2012).

Scenarios illustrated in Fig. 3a imply that thermochronologic ages in detritus cannot be interpreted *a priori* in terms of cooling through the T_c isotherm during exhumation. Notably, the different scenarios of Fig. 3a will determine different and diagnostic thermochronologic fingerprints in bedrock and detritus (see Section 3). Strategies exist to discriminate among different scenarios and minimize the risk of misinterpretations (see discussion in Malusà and Fitzgerald, 2019b). For example, approaches include multiple dating of detrital mineral grains using different thermochronologic systems (see review in Danišík, 2019) in order to identify mineral grains crystallized above the T_c isotherm (Carter and Moss, 1999; Saylor et al., 2012; Bernet et al., 2019). These topics are discussed in more detail in Section 3.

2.2 Assumption 2: T_c isotherms have remained steady during exhumation

The reference frame for the interpretation of thermochronologic data is a thermal reference frame (e.g., Braun et al., 2006). A major assumption of the lag-time approach is that this thermal reference frame has remained steady during exhumation (2 in Fig. 2). However, in active geologic settings, the thermal reference frame is typically dynamic (Mancktelow and Grasemann, 1997; Huntington et al., 2007). The thermal reference frame can evolve as a response to exogenic processes, e.g., due to rapid erosion and exhumation as well as topographic effects. Advection of heat due to rapid erosion will result in an elevated (paleo)geothermal gradient, but lag time can still be estimated using results of thermal models that take into account advection (Braun et al., 2006; Fig 3b). Rugged topography may influence the shape of shallow-depth isotherms and hence affect the interpretation of lower-temperature thermochronologic data, especially in local studies (Stüwe et al., 1994; Mancktelow and Grasemann, 1997; Braun, 2002; see also Fig. 9.5 in Fitzgerald and Malusà, 2019). The impact of these processes can be modelled by numerical methods, e.g., by using Pecube (Braun, 2003; Braun et al., 2012). On a larger scale, the thermal reference frame can also evolve as a result of deep tectonic processes such as subduction (Peacock, 1996; Jamieson and Beaumont, 2013). In this latter case, major deflections of the thermal reference frame are reasonably expected even for those isothermal surfaces that are relevant for the interpretation of higher-temperature thermochronologic data. If relevant isotherms (relevant to the method being applied) have not remained steady during exhumation, an incorrect estimate of the exhumation rate with a resultant impact on lag-time interpretation may result. For example, neglecting the impact of heat advection due to rapid erosion would imply a systematic overestimate of exhumation rates inferred from lag-time analysis (Fig 3b).

Another factor is comparison of lag times and inferred exhumation rates between different thermochronologic methods with different T_c. Isotherms deeper in the crust take longer to respond to rapid removal of material at the surface and to reach steady state as a result of increased surface erosion rates (e.g., Moore and England, 2001; Reiners and Brandon, 2006) (Fig. 3c). Comparison of lag times and resultant exhumation rates determined using different thermochronologic systems should therefore be evaluated carefully. Overall, the applicability of thermochronologic data to constrain exhumation requires that the linkage between the thermal reference frame and Earth's surface is properly assessed. Such strategies to constrain an evolving paleogeothermal gradient based on the geologic record are discussed in Malusà and Fitzgerald (2019c).

2.3 Assumption 3: The lag time pertains to a single eroding source

The conceptual model of Fig. 1a assumes that the lag time pertains to a single eroding source. However, sedimentary successions often record major provenance changes (Clift et al., 2006; Tatzel et al., 2017; Rahl et al., 2018), whereby provenance indicates all characteristics of the source area from which clastic sediments and sedimentary rocks are derived, including relief, weathering and source rocks (Ingersoll, 2014). A reliable provenance assessment may require a multiple-method approach to single-grain analysis (Carter, 2019; Danišík, 2019) and a careful inspection of thermochronologic age trends along the analyzed stratigraphic succession (e.g., Glotzbach et al., 2011). If provenance changes remain undetected, this may lead to an incorrect interpretation of detrital thermochronology data (3 in Fig. 2).

2.4 Assumption 4: Mineral fertility in the eroding source areas is not variable in time and space

Another major assumption underlying the lag-time approach is that the mineral fertility, i.e., the variable propensity of different parent rocks to yield detrital grains of specific minerals when exposed to erosion (Moecher and Samson, 2006; Malusà et al., 2016b), does not vary either regionally within an eroding mountain range, or locally within a single river catchment (4 in Fig. 2).

If mineral fertility varies regionally within a mountain range, lag-time analyses may emphasize the cooling history of small parts of that range, i.e., those parts that are characterized by the highest mineral fertility (Malusà et al., 2017; Gemignani et al., 2018; Glotzbach et al., 2018). On a more local scale, the impact of variable mineral fertility can be also relevant within single river catchments. Thermochronologic ages in detritus are generally older in grains eroded from summits, and younger in grains eroded from valleys (e.g., Stock et al., 2006; Vermeesch, 2007). If bedrock shows variable mineral fertility depending on elevation, drainages that are expected to yield a single age peak, which should reflect the age-elevation relationship in bedrock (e.g., Brewer et al., 2003), may yield instead polymodal grain-age distributions because low-fertility rocks provide no datable mineral grains from specific elevation ranges. This situation may hinder a correct interpretation of lag-time trends in part of the stratigraphic succession. However, this problem is not expected for an entire stratigraphic succession, because different units with different mineral fertility are progressively exposed to erosion through time.

2.5 Assumption 5: Grain-age distributions are not affected by hydraulic sorting

Detrital thermochronology studies are generally based on the assumption that grain-age distributions in detritus provide a faithful mirror of thermochronologic ages in eroded bedrock (Bernet et al., 2004). However, modifications to the original thermochronologic fingerprint of detritus may potentially occur in the source-to-sink transportation environment, for example as an effect of hydraulic sorting (Malusà and Garzanti, 2019) (5 in Fig. 2). In the case of sedimentary basins involving detritus from different eroding sources, a careful evaluation of any factors that may lead to an underestimation, or overestimation, of a specific source of detritus is particularly important (e.g., Sláma and Košler, 2012). These situations will be discussed in detail in Section 4.

2.6 Assumption 6: Sediment transport time is negligible

In order to estimate an average exhumation rate using the difference between the thermochronologic age recorded by a detrital mineral grain (t_c) and its depositional age (t_d) (Fig. 1a), the time elapsed during sediment transport (t_e - t_d in Fig. 1a) should be negligible (Brandon and Vance, 1992; Garver et al., 1999; Bernet et al., 2001). However, temporary storage and reworking of sediment in terraces and floodplains are common processes in drainage systems (e.g., Hippe et al., 2012; Clift and Giosan, 2014; Malatesta et al., 2018). Thus, in some cases, transportation time may become relevant (6 in Fig. 2) and if so, exhumation rates based on lag-time analysis may be underestimated. For example, cosmogenic data from the Amazon reveal that river bedload may require a few millions of years to travel from the Andes to the Atlantic Ocean (Wittmann et al., 2011). For a reliable geologic interpretation of the detrital thermochronologic record, the assumption of zero transport-time should thus be evaluated on a case-by-case basis. Multi-technique studies involving the thermochronologic analysis of different minerals should also consider the different velocities expected for minerals that are chiefly transported as bedload (e.g., apatite and zircon) and minerals that are chiefly transported as suspended load (e.g., micas). These topics are discussed in more detail in Section 5.

2.7 Assumption 7: The detrital thermochronologic signal is preserved after deposition

A further major assumption of lag-time analysis is that the detrital thermochronologic signal is preserved after deposition (7 in Fig. 2). In thick sedimentary successions, this signal is potentially modified by post-depositional annealing due to burial, especially for lower-temperature thermochronologic systems (e.g., Ruiz et al., 2004; Chirouze et al., 2012). Post-depositional annealing may lead to an overestimation of the exhumation rate inferred from lag time. However, post-depositional annealing can be easily recognized thanks to the diagnostic age trends yielded by multiple samples collected through a stratigraphic sequence (van der Beek et al., 2006). This topic is discussed in Section 6.

Figures 2, 3

3. Complexity of thermochronologic data in the source region (I in Fig. 1b)

The complexity of thermochronologic data characterizing a source region (I in Fig. 1b) is one of the main factors contributing to the potential complexity of the detrital thermochronology record in a sedimentary basin. Such complexity may arise from a range of geologic processes depending on the thermochronologic systems under consideration. Relevant processes may include not only annealing and diffusion during erosional exhumation (e.g., Gleadow and Brown, 2000; Reiners and Brandon, 2006; Braun et al., 2006; Ault et al., 2019), but also transient changes of the thermal state of the crust (e.g., Braun, 2016; Malusà et al., 2016a), episodes of magmatic crystallization (e.g., Carter and Moss, 1999; Jourdan et al., 2013), syntectonic growth of metamorphic minerals (e.g., Villa, 2010; Malusà, 2019), late-stage mineral alteration (e.g., Di Vincenzo et al., 2003; Allaz et al., 2011), or the structural juxtaposition of crustal blocks (e.g., Fitzgerald and Gleadow, 1990; Foster and Gleadow, 1996; Niemi et al., 2013). The thermochronologic fingerprint of eroding bedrock may be also complicated by the presence of unreset sedimentary successions reflecting the cooling history of older eroding sources (Bernet and Garver, 2005; Rahl et al., 2007; von Eynatten and Dunkl, 2012).

More localized geologic processes, such as contact metamorphism (Calk and Naeser, 1973; Harrison and McDougall, 1980; Schmidt et al., 2014), frictional heating along major faults (Murakami and Tagami, 2004; Murakami, 2010; Tagami, 2019) and wildfires (Mitchell and Reiners, 2003; Reiners et al., 2007) may be also locally important. However, these processes generally affect small rock volumes, and derived detrital mineral grains are typically volumetrically insignificant in the sedimentary record. Therefore, the impact of these processes on the detrital thermochronologic record will not be considered in this article for the sake of simplicity.

3.1 Origin of thermochronologic complexity in bedrock

Figure 4 presents a range of conceptual models that illustrate the progressive setting of mineral ages in bedrock resulting from the following hypothetical scenarios:

- The progressive erosion of a sedimentary succession and the exhumation of the underlying basement rocks (Fig. 4a)
- The intermittent erosion of bedrock (Fig. 4b)
- The intrusion of magma at depth associated with volcanism at the surface, followed by erosional unroofing of volcanic and plutonic rocks along with their country rocks (Fig. 4c)

- The syntectonic recrystallization of metamorphic minerals at depth during regional metamorphism (Fig. 4b)
- The elevation (upward movement) of isothermal surfaces and subsequent thermal relaxation after continental rifting or fast tectonic exhumation of deep rocks (Fig. 4d).

These conceptual models have been developed from a synthesis of a number of case studies, including some of the earliest applications, from the European Alps (Wagner and Reimer, 1972; Malusà et al., 2011a), Antarctica (Gleadow and Fitzgerald, 1987; Fitzgerald and Gleadow, 1990), the Himalayas (Cerveny et al., 1988; Braun, 2016), Alaska (Fitzgerald et al., 1993; 1995), and the Central Mediterranean (Malusà et al., 2016a). These ideas and concepts have been applied to many other tectonic settings by many workers. The effects of geologic processes considered in the above models are often combined together in the same area, thus determining more complex thermochronologic fingerprints. In the conceptual schemes of Fig. 4, we will consider four thermochronologic systems only: U–Pb on zircon, $^{40}Ar/^{39}Ar$ on mica (mica Ar-Ar hereafter), and fission tracks in zircon (ZFT) and apatite (AFT). However, the same line of reasoning could be extrapolated to other thermochronologic systems with different T_c, such as fission tracks on titanite (TFT) (Kohn et al., 2019) and (U-Th)/He on apatite (AHe) and zircon (ZHe) (e.g., Farley, 2002; Reiners, 2005). The impact of heat advection in these conceptual models is calculated using an equation for transient advection-diffusion in homogeneous media with no heat production, assuming an initial geothermal gradient of 30°C/km (Ehlers et al., 2005). The impact of heat advection is fully considered both in the age-depth diagrams of Fig. 4, and in the hypothetical sedimentary successions illustrated in Sections 3 to 6.

3.1.1 Progressive erosion of sedimentary rocks

Let us consider a hypothetical upper-crustal section including sedimentary rocks lying on top of basement rocks (Figure 4a, upper row). At time t_1, different crustal levels can be distinguished in this crustal section according to the temperature of the rocks. These levels are delimited by the PAZ of the AFT system (lower boundary of level 1), the PAZ of α-damage ZFT (lower boundary of level 2), and the PRZ of mica Ar–Ar (lower boundary of level 3). As shown in the corresponding age-depth diagram (frame t_1 in Fig. 4a lower row), at this stage thermochronologic ages are only set (recorded) at depths shallower than the corresponding isotopic closure, but they are not set at greater depths (i.e., ages are zero below the PAZ/PRZ, dependent on the system). For instance, AFT ages are set in level 1, but they are not set in levels 2 to 4, yet. ZFT ages are set in levels 1 and 2, but they are not set in levels 3 and 4. The polymodal grain-age distributions observed in these sedimentary rocks generally reveal histories of distant sediment sources (e.g., Bernet and Garver, 2005; Carter, 2019).

After the onset of erosion at time t_e , thermochronologic ages are progressively set (recorded) also in rocks originally located beneath the former PAZ/PRZ (frames t_2 and t_3 in Fig. 4a). Once the T_c isotherms have reached the new steady-state depth (see Fig. 3c), these ages will be exclusively controlled by the delayed closure of the thermochronologic system during exhumational cooling. These ages thus represent "exhumation ages" that can be used to constrain the upward motion of rocks towards Earth's surface during erosional exhumation. Exhumation ages are always younger than t_e, they get systematically younger with increasing depth, and define age trends that are progressively shifted towards older ages for higher-temperature systems. The slope defined by exhumation ages in an array of samples from different depths is usually a function of the exhumation rate (see Fitzgerald and Malusà, 2019 for more details). Notably, these ages define a straight line in an age-depth diagram only when the T_c isotherms reach a new steady-state depth, i.e., after the onset of erosion. Higher-temperature isotherms take longer to reach steady state compared to lower-temperature isotherms (Reiners and Brandon, 2006, Fig. 3c), which implies that exhumation ages yielded by higher-T_c systems define non-linear trends for a longer time interval compared to ages yielded by lower-T_c systems (Fig. 4a).

3.1.2 Intermittent bedrock erosion

Let us now assume that the sedimentary succession shown in Fig. 4a has been completely removed by erosion, and that the underlying basement rocks undergo a long period of relative tectonic quiescence before the onset of a new erosional pulse at time t_{e2} (Fig. 4b). At this stage, thermochronologic ages in basement rocks are already set at depths shallower than the corresponding isotopic closure (frame t_4 in Fig. 4b). These ages mainly reflect the previous exhumation pulse corresponding to the removal of the overlying sedimentary rocks.

During tectonic quiescence, tectonic and thermal stability allows the development, within the depth range corresponding to the PAZ/PRZ of each thermochronologic system, of a characteristic shallow-slope age-depth relationship that is typical of any PAZ/PRZ (Fig. 4b, lower row). Notably, the development of this shallow-slope profile requires sufficient time, generally ranging from several tens to hundreds of millions of years (e.g., Fitzgerald and Stump, 1997). For the AFT and ZFT systems, such prolonged residence of rocks within the PAZ maximizes the effects of the variable annealing rate between apatite grains of different chemical compositions (Green et al., 1986; Barbarand et al., 2003), or between zircon grains with different degree of radiation damage (Rahn et al., 2004), leading to a large thermochronologic age dispersion among different grains. A large age dispersion during residence within the PRZ is also expected for the (U-Th)/He systems, because of variations in effective uranium concentration, grain size, grain zonation, and residence time within the PRZ (e.g., Reiners and Farley, 2001; Meesters and Dunai, 2002; Fitzgerald et al., 2006; Flowers et al., 2009; Guenthner et al., 2013). Diagrams quantitatively illustrating these effects for some systems can be found in Fitzgerald and Malusà (2019), their Fig. 9.2.

The shallow-slope profile acquired while in the PAZ/PRZ can be preserved in the geologic record as an exhumed PAZ/PRZ (Naeser, 1976; Gleadow and Fitzgerald, 1987), provided that tectonic quiescence is followed by more rapid cooling due to overburden removal either by erosion (e.g., Fitzgerald et al., 1995) or by low-angle normal faulting (e.g., Fitzgerald et al., 1991, 2009; Stockli, 2005; Foster et al., 2010). In the conceptual model of Fig. 4b, which considers a major erosional pulse at time t_{e2}, thermochronologic ages defining an exhumed PAZ/PRZ are followed by younger thermochronologic ages that define a steeper slope, as typically observed in natural cases (e.g., Fitzgerald and Gleadow, 1988, 1990; Fitzgerald et al., 1993; Miller et al., 2010). These younger ages are set during erosional exhumation and can be used to constrain the exhumation rate after time t_{e2}. Notably, many age-depth profiles documenting an exhumed PAZ/PRZ in the thermochronologic record are unlikely to have formed within a period of "complete and absolute" tectonic and thermal stability. What is particularly important, however is the contrast in thermal and tectonic regimes between the formation of a PAZ and subsequent more rapid cooling/exhumation that preserves the classic PAZ form (see discussion in Fitzgerald and Malusà, 2019). The time corresponding to the break in slope, marked by a green star in Fig. 4b, does represent the transition from a relatively stable tectono-thermal regime to a period of more rapid cooling. However, the age of the break in slope generally underestimates the time of such transition, because rocks take time to transit the PAZ/PRZ. Ages within an exhumed PAZ/PRZ do not represent closure ages (cf. Fig. 1c), and thus should not be used to constrain the exhumation rate using the lag-time approach.

3.1.3 Magmatic crystallization

Let now assume that the period of tectonic quiescence (frame t_4 in Fig. 4c) is followed by intrusion of magma at depth and emplacement of volcanoes at the surface at time t_m. Zircon U-Pb ages yielded by these magmatic rocks will be equal to t_m and identical within error at any intrusion depth (frame t_5 in Fig. 4c). These U-Pb ages represent "magmatic ages" (e.g., Malusà et al., 2011a) that mark the time of magma crystallization (Dahl, 1997; Mezger and Krogstad, 1997). These U-Pb magmatic ages will be systematically younger than the zircon U–Pb ages in adjacent country rocks (frame t_5 in Fig. 4c). Whenever magma is intruded into the upper crust, where country rocks are resident at temperatures cooler than the PAZ, for example in the case of shallow intrusions and volcanoes, the time elapsed between crystallization and the first retention of fission tracks is shorter than the resolution of the fission-track dating method. In those cases, ZFT and AFT ages will be indistinguishable within error from the zircon U-Pb age in the same magmatic rock, and thus will also be considered as magmatic ages. In the absence of mineral retrogression (e.g., Villa, 2010), mica Ar-Ar ages are also potentially indistinguishable in levels 1 to 3 from zircon U-Pb ages in the same magmatic rock. As these magmatic ages at shallow levels are set before the onset of erosional exhumation at time t_{e2}, they cannot be used to constrain the exhumation rate since time t_{e2} using the lag-time approach. Notably, "magmatic ages" for lower temperature systems are not recorded in those magmatic rocks that were intruded at depths below (and temperatures higher than) a PAZ/PRZ of the thermochronologic system as identified at time t_4, because in those levels temperatures will remain higher than T_c until subsequent erosion.

After the onset of progressive erosional unroofing of volcanic and plutonic rocks along with their country rocks at time t_{e2} (frame t_6 in Fig. 4c), thermochronologic ages are progressively set also in magmatic and country rocks originally located beneath the PAZ/PRZ of the thermochronologic system under consideration. These ages are controlled by the delayed closure of the thermochronologic system during undisturbed exhumational cooling, and thus can be used to constrain exhumation. These ages get systematically younger with increasing depth, and are generally the same in magmatic rocks and adjacent country rocks. However, ages defined by ZFT in magmatic rocks (zero-damage trend in Fig. 4c) are expected to be slightly older compared to the ages defined by ZFT in country rocks (α-damage trend in Fig. 4c), because magmatic zircon crystallized at time t_m has less α-damage and thus higher T_c (Rahn et al., 2004) than older zircons of the country rocks.

After the onset of erosion, the upper-crustal section of Fig. 4c is thus characterized by diagnostic combinations of magmatic and exhumation ages in country rocks and magmatic rocks depending on the crustal level. For example, level 1 is characterized, for all the thermochronologic systems under consideration, by magmatic ages in the intruded rocks and older pre-intrusion ages in country rocks (unless country rocks are partially reset or fully reset because of proximity to the intrusion, e.g., Calk and Naeser, 1973). Level 2 additionally shows AFT exhumation ages younger than the magmatic age t_m, and level 3 also includes ZFT exhumation ages older than the AFT ages but younger than the magmatic ages recorded by zircon U-Pb and possibly mica Ar-Ar. Similar relationships are also expected for magmatic rocks intruded within a sedimentary rock sequence. In that case, country rocks will have the same thermochronologic age structure as in Fig. 4a.

3.1.4 Syntectonic mica (re)crystallization during regional metamorphism

Modifications to the thermochronologic age-depth relationships previously described for mica Ar-Ar can be introduced by syntectonic (re)crystallization of micas that have grown at temperatures lower than the isotopic closure of the Ar-Ar system, for example during low-grade metamorphism (e.g., Baldwin et al., 2019; Malusà, 2019). In metamorphic rocks, micas generally show microtextural evidence of petrological disequilibrium (Challandes et al., 2008; Glodny et al., 2008). Different generations of micas define foliations formed at different times and at different pressure-temperature conditions during exhumation of a metamorphic rock towards Earth's surface (Spear, 1993). However, all of the micas within a rock sample, if they grow at temperatures that exceed the diffusion-only isotopic closure, will cross the T_c of the Ar-Ar system during subsequent exhumation. Ar-Ar ages from progressively deeper rock samples should thus get progressively younger with increasing depth, providing constraints on the exhumation rate (frame t_5 in Fig. 4b). However, micas of the youngest generations may have grown at temperatures lower than diffusion-only isotopic closure (orange arrows in frame t_5, Fig. 4b). These micas should not be used to constrain exhumation using the lag-time approach, because they have not crossed the T_c isotherm during exhumation (e.g., Malusà, 2019).

3.1.5 Elevation (upward movement) of isothermal surfaces followed by thermal relaxation

Let us consider a hypothetical scenario where isothermal surfaces rise (are elevated or uplifted) through the same upper-crustal section of Fig. 4b (frame t_4 in Fig. 4d). This thermal perturbation is expected to produce a systematic rejuvenation of thermochronologic ages in selected crustal levels, thus modifying the thermochronologic age structure produced during the previous stages of erosional exhumation and residence within the PAZ/PRZ. Subsequent thermal relaxation since time t_r (frame t_5 in Fig. 4d) will determine the downward motion of relevant T_c isotherms across rock samples that have remained fixed relative to Earth's surface. Such thermal relaxation will produce near-invariant thermochronologic ages with depth. Notably, these ages cannot be used to constrain exhumation, because they are not set during motion of rocks towards Earth's surface (Braun, 2016; Malusà et al., 2016a). At a later stage, after the onset of erosion since time t_{e2}, thermochronologic ages are progressively set also in rocks originally located beneath the former PAZ/PRZ (frame t_6 in Fig. 4d). These ages are controlled by the delayed closure of the thermochronologic system during undisturbed exhumational cooling, and can be used to constrain exhumation.

According to this scenario, diagnostic combinations of thermochronologic ages from different systems should be expected according to the crustal level. For example, near-invariant mica Ar-Ar ages will be expected in crustal level 3 and perhaps part of level 2. Near invariant ZFT ages will be expected in level 2 and perhaps part of level 1. Near invariant AFT ages will be expected in the lowermost part of level 1. Invariant ages are not found in the uppermost part of this hypothetical crustal section (unlike the case of magmatic crystallization illustrated in Section 3.1.3), because the elevated isotherms (unlike magma in Fig. 4c) do not reach the Earth's surface. Within a single crustal level, near-invariant ages will be generally associated with exhumation ages that are provided by lower-temperature thermochronologic systems. These exhumation ages get progressively younger with depth, and are systematically younger than the thermochronologic ages set during thermal relaxation.

Figure 4

3.2. Detrital thermochronologic age patterns from single sources

Detritus derived from erosion of the hypothetical crustal sections described in Section 3.1 is expected to be accumulated in reverse order in sedimentary basins. For the sake of simplicity, we will assume that the sedimentary successions in those basins consist of four stratigraphic units (A to D in Fig. 5), each one exclusively derived from progressive erosion, at a rate of 1 km/Ma, of one of the four crustal levels identified in the source.

3.2.1 Thermochronologic age pattern in detritus derived from erosion of a sedimentary succession

Let us consider the progressive erosion of the hypothetical sedimentary succession discussed in Section 3.1.1 (Fig. 5a). The oldest stratigraphic unit A, entirely eroded from level 1, includes sandstones that generally yield polymodal grain-age distributions (e.g., Galbraith, 2005; Vermeesch, 2019). These thermochronologic ages form individual peaks that are always older than time t_e, i.e., older than the onset of erosion in the source region (Fig. 5a). These "recycled" ages reflect the geologic history of older sediment sources that have fed, in the past, the sedimentary succession now undergoing erosion.

Starting from stratigraphic unit B, which is entirely derived from erosion of crustal level 2, apatite grains will start showing unimodal AFT age distributions with a single age peak that is younger than t_e (Fig. 5a). This peak becomes increasingly younger up section, and is thus referred to as a "moving age peak". Thermochronologic ages belonging to this moving age peak are set during exhumation. When plotted in a classic lag-time diagram that reports stratigraphic age vs. thermochronologic age and lines of equal lag time (in green in Fig. 5), this moving age peak can provide direct constraints on exhumation, taking into account the caveats described in Section 2 such as the effect of heat advection during erosion (Fig. 3b). Within stratigraphic unit B zircon grains and mica flakes still yield ZFT and Ar-Ar ages older than t_e, which reflect the history of the older eroding sources thus these provide no direct constraint on exhumation since time t_e. The moving age peak defined by detrital ZFT ages first appears in unit C (entirely eroded from level 3), whereas the moving age peak defined by detrital mica Ar-Ar ages only appears in unit D (entirely derived from level 4). These peaks get systematically younger up section, and the trends they define are progressively shifted towards older ages for progressively higher-T_c systems. The lag time gets progressively longer for higher-T_c systems because it reflects exhumation from greater depths.

This example shows that only a single moving age peak is expected from a single eroding source. Moreover, the appearance of any moving age peak (of a particular thermochronologic method/mineral) only takes place when the whole rock pile with a thermochronologic fingerprint (relative to each thermochronologic method/mineral) acquired before the onset of erosion is completely removed. The delay in such response depends on the T_c of the thermochronologic system under consideration, and on the erosion rate (e.g., Rahl et al., 2007). The delay is greater for higher temperature systems and may exceed 10 Ma, even if erosion is relatively fast (on the order of 1 km/Ma) (e.g., Malusà et al., 2011a). This delay means that the detrital signal of rapid cooling/exhumation may not be part of the stratigraphic sequence derived from erosion associated with this rapid cooling/exhumation episode, but may be instead part of the stratigraphic sequence derived from a subsequent episode of erosion (see example below).

3.2.2 Thermochronologic age pattern in detritus derived from intermittent bedrock erosion

We can now consider the progressive erosion of the hypothetical sedimentary succession discussed in Section 3.1.2 (see Fig. 5b). After complete removal of its sedimentary cover, the underlying basement rocks undergo a period of tectonic quiescence before the reprise of erosion at a rate of 1 km/Ma. This younger erosional pulse has produced the detritus now deposited in inverted order in the hypothetical sedimentary succession of Fig. 5b.

According to the above scenario, exhumation ages defining single moving age peaks are already found in stratigraphic unit A, which is eroded from level 1. Notably, these exhumation ages reflect a previous exhumation pulse (also occurred at a rate of 1 km/Ma) corresponding to the removal of the overlying sedimentary rocks before tectonic quiescence, and are not due to the erosion providing detritus to the analyzed sedimentary basin. Thermochronologic ages set during prolonged residence within the PAZ/PRZ are found in different stratigraphic units depending on the thermochronologic system (unit A for the AFT system, unit B for the ZFT system, and unit C for the mica Ar-Ar system), and ideally in the uppermost part of these units. Ages set during prolonged residence within the PAZ/PRZ cannot be interpreted as closure ages, and thus provide no direct constraint on exhumation.

Moving age peaks reflecting exhumation at rate of 1 km/Ma after tectonic quiescence appear at later stages in the sedimentary record. The timing of their first appearance depends on the thermochronologic system under consideration, as already discussed in Section 3.2.1 (Fig. 5b). Within the same stratigraphic unit, a moving age peak may be either related to an older erosion event, if detrital thermochronologic ages are provided by a system with relatively high T_c, or to a young erosion event, if ages are provided by a system with lower T_c. For example, in stratigraphic units B and C (Fig. 5b) the moving age peak defined by mica Ar-Ar data reflects erosion before tectonic quiescence, whereas the moving age peak defined by AFT data reflects erosion after tectonic quiescence. The onset of erosion after tectonic quiescence can be constrained by the age of the oldest peaks defining the moving age trends.

The diagrams in Fig. 5b provide different lag-time values (either for ZFT or mica Ar-Ar) for moving age peaks that refer to the ancient and to the recent erosion events, despite both events taking place at the same rate of 1 km/Ma. This is due to the fact that the longer time lag recorded in the oldest stratigraphic units also includes the period of tectonic quiescence before the onset of the younger erosional pulse. Notably, the sharp shift from a longer to a shorter lag time, which is observed at different stratigraphic levels depending on the thermochronologic system, does not mark a sudden change from a period of slower exhumation to a period of faster exhumation. Instead, it marks the end of a period of relative tectonic quiescence, between periods characterized by similar rapid erosion rates.

3.2.3 Thermochronologic age pattern in detritus derived from erosion of a magmatic complex

The hypothetical section of a volcanic-plutonic complex discussed in Section 3.1.3 (Fig. 4c) includes: (i) pre-intrusion ages that are set before magmatic activity and are exclusively found in country rocks; (ii) syn-intrusion magmatic ages that are set during crystallization of a magmatic intrusion and volcanism at the surface at time t_m, and are exclusively found in magmatic rocks; and (iii) exhumation ages that are set during progressive erosion of the volcanic-plutonic complex and are found both in magmatic and country rocks. Erosion of the volcanic–plutonic complex produces sand-sized grains of apatite, zircon, micas or other minerals, either derived from magmatic rocks or from country rocks, that are deposited in inverted order in a sedimentary basin.

In the oldest stratigraphic unit of the basin (unit A), entirely derived from level 1, sandstones will contain not only grains eroded from the country rock, which are expected to yield thermochronologic ages older than t_m, but also grains eroded from volcanic and shallow intrusive rocks yielding an age peak around the magmatic age t_m. This latter peak is constant up section, and is referred to as a "stationary age peak". This stationary age peak coexists with older ages that are either set during the pre-intrusion history of the country rock (Fig. 5c), or inherited from its protolith. All of these ages are set before the onset of the erosional unroofing of the volcanic-plutonic complex. Therefore, they provide no direct constraint on its exhumation.

In stratigraphic unit B, grains of zircon and micas in sandstones are expected to define composite grain-age distributions in the ZFT, Ar-Ar and U–Pb systems, with a stationary age peak still corresponding to the magmatic crystallization age t_m. Apatite grains, however, will show unimodal AFT age distributions with a single peak that is younger than t_m, and that becomes increasingly younger up section. This moving age peak is defined by thermochronologic ages set during exhumation. Therefore, it can be used to directly constrain the erosional unroofing of the volcanic-plutonic complex using the lag-time approach.

Stratigraphic unit C is entirely eroded from level 3. It yields exhumation fission-track ages not only on apatite grains, but also on α-damaged zircon grains that have been eroded from the country rock. As a result, AFT and ZFT ages in sandstones define moving age peaks younger than t_m. If a sandstone sample includes zircon grains with both low and high levels of α-damage, and thus different T_c, the resulting ZFT age distribution is potentially bimodal. Mica Ar–Ar and zircon U–Pb ages are expected to yield composite distributions, also including a stationary peak corresponding to the magmatic crystallization age t_m. In stratigraphic unit D, exhumation ages are the rule, with the only exception being zircon U–Pb ages.

In summary, the detrital thermochronology record shown in Fig. 5c includes stationary age peaks and moving age peaks. Moving age peaks are set during progressive cooling of rocks as a result of exhumation, and can be used to investigate the long-term erosional evolution of the source area using the lag-time approach. Stationary age peaks are invariant up section. They are formed by thermochronologic ages that are set during magmatic crystallization, and before the onset of erosional exhumation. Therefore, they provide no direct constraint on exhumation. Stationary peaks formed by magmatic ages are potentially found starting from the lowermost units of a sedimentary basin, and for different thermochronologic systems in the same stratigraphic level. Stationary age peaks can be associated with a moving age peak. However, a stationary age peak is always younger than a moving age peak from the same source, for the same thermochronologic method and mineral.

The identification of mineral grains yielding magmatic crystallization ages in detritus is of primary importance for a correct interpretation of detrital grain-age distributions in terms of exhumation (Bernet, 2019). If magmatic activity is characterized by multiple magmatic pulses, magmatic ages provided by lower-temperature systems are expected not only in the oldest stratigraphic units of the final sink, but also in much younger stratigraphic levels (see Fig. 16.2c in Malusà, 2019). A suitable approach for the identification of magmatic crystallization ages is provided by double dating, for example U-Pb and fission-track dating of the same zircon or apatite grain (e.g., Carter and Moss 1999; Carter, 2019; Danišík 2019). As shown in Fig. 6a, magmatic zircons crystallized at shallow depth (i.e., from volcanic or shallow-level plutonic rocks) should display identical U-Pb and ZFT ages within error, because of rapid magma crystallization in the upper crust, where country rocks are at temperatures cooler than the PAZ of the ZFT system. Conversely, zircon grains crystallized at greater depth, and recording cooling across the T_c isotherm during exhumation, should display a ZFT age younger than the corresponding U-Pb age. These latter ZFT ages can be used to constrain the long-term exhumation history of the source rocks according to the lag-time approach. Notably, the recognition of magmatic crystallization ages by double-dating is relatively straightforward for zircon grains showing no internal U-Pb age zonation. However, if zircon grains show an internal U-Pb age zonation, and ablation for U-Pb analysis is routinely performed in the centre of the grain (e.g., Jourdan et al., 2018), U-Pb ages older than ZFT ages may just reflect the presence of an older xenocrystic core (Bernet et al., 2016; 2019). In that case, shallow-depth crystallization of the zircon rim, implying a ZFT age not related to exhumation, cannot be safely ruled out (Fig. 6a). Examples of application of the double-dating approach for the identification of magmatic crystallization ages are reported, among the others, from the Himalayas (Carter et al., 2010), Taiwan (Kirstein et al., 2010), the Andes (Saylor et al., 2012), the European Alps (Jourdan et al., 2013), the Apennines (Stalder et al., 2018) and Alaska (Enkelmann et al., 2019).

3.2.4 Thermochronologic age pattern in detrital micas recording synmetamorphic crystallization

Micas are common minerals in many metamorphic rocks. These rocks generally include different generations of micas, possibly characterized by different Ar-Ar ages. Some of these micas grow at temperatures higher than diffusion-only isotopic closure (e.g., micas D1 and D2 in Fig. 6b). During exhumation, these micas will then cross the T_c isothermal surface of the Ar-Ar system and, despite having potentially different crystallization ages, will yield the same Ar-Ar age. Resulting Ar-Ar ages in detritus will define a moving age peak that becomes increasingly younger up section, because these ages reflect the delayed closure of the Ar-Ar thermochronologic system during undisturbed exhumational cooling. The evolution of this age peak can be used to constrain the long-term exhumation history of the source rocks using the lag-time approach.

However, metamorphic rocks often include syntectonic micas (D3 in Fig. 6b) that have grown at lower temperatures than the diffusion-only Ar-Ar isotopic closure (e.g., Villa, 2010). These micas will not cross the T_c isothermal surface during exhumation (Fig. 6b). When eroded, they may define a stationary age peak. The age of that peak is controlled by the age of the tectono-metamorphic event associated with syntectonic mica recrystallization during low-grade to very-low-grade metamorphism. Such a stationary age peak provides no direct constraint on exhumation, and is always younger than the moving age peak defined by micas from older foliation planes.

Because syntectonic growth of metamorphic mica is only expected for relatively deep levels of an active orogen, stationary age peaks due to metamorphic (re)crystallization are generally not expected in the lowermost units of a sedimentary basin, unless Ar-Ar ages of those micas reflect much older metamorphic events (see Fig. 5b).

3.2.5 Thermochronologic age pattern in detritus recording thermal relaxation in bedrock

Stationary age peaks are found not only in detritus recording the progressive erosion of a magmatic complex or syntectonic growth of mica during regional metamorphism. Stationary age peaks are also expected in the case of erosion of an upper-crustal section where thermal perturbations, associated with an increase in paleogeothermal gradient, are followed by thermal relaxation over a time interval that is shorter than the uncertainty of typical thermochronometers, as in the case illustrated in Section 3.1.5. Stationary age peaks that reflect past thermal-relaxation events in bedrock should occur in progressively younger stratigraphic units for progressively higher-T_c systems. This is illustrated in the hypothetical sedimentary succession of Figure 5d, where a stationary peak is defined by ZFT ages in stratigraphic unit B, and another one is defined by mica Ar-Ar ages in the uppermost part of unit B and in the whole unit C. These stationary age peaks are never associated, in the same stratigraphic level, with moving age peaks from the same source. They are best exemplified by higher-temperature thermochronologic systems, because higher-temperature isothermal surfaces are expected to show larger shifts during orogeny than lower-temperature isotherms.

Figures 5, 6

3.3. Sensitivity of the detrital thermochronology record to erosion rate variations

Stationary age peaks in the detrital thermochronology record are not sensitive to variations in erosion rate. In fact, they are defined by mineral grains originally showing, in the source region, thermochronologic ages that are invariant with depth. If a source providing a stationary age peak is eroded slowly, the resulting stationary age peak is expected to be found in a long chronostratigraphic interval within the sedimentary succession of the final sink.

Moving age peaks are defined by thermochronologic ages that get increasingly younger with depth in the source region. These peaks are instead affected by variations in erosion rates (e.g., Rahl et al., 2007). The left panel of Figure 7a shows the thermochronologic record in a hypothetical upper-crustal section where rocks are eroded at rates of 0.5 km/Ma until time t_b (also corresponding to the onset of sedimentation in the hypothetical sedimentary basin to the right). The erosion rate suddenly increases to 1 km/Ma after time t_b. Lag-time diagrams on the right illustrate the expected thermochronologic age pattern in the basin. In the basal part of the basin, marked with "A", lag time reflects the erosion rate before time t_b. In the overlying strata, lag-time values progressively decrease up section until they reflect, starting from the point marked with "B", the new bedrock erosion rate of 1 km/Ma. In the interval between A and B, the lag time is not a reliable mirror of the exhumation rate, as it underestimates the true exhumation rate. The time elapsed between A and B is shorter for lower-T_c systems such as AFT, and much longer for higher-T_c systems such as ZFT and mica Ar-Ar. In the specific case of Fig. 7a, the time elapsed between A and B is longer than 10 Ma for the Ar-Ar system on mica that will mirror the new erosion rate in the sedimentary succession only after time t_3, i.e., in stratigraphic unit D. The low sensitivity of detrital thermochronology data in recording changes in erosion rate implies that a sharp change in erosion rate is barely distinguishable from a more progressive change in erosion rate on a detrital thermochronologic basis, especially in the case of higher-temperature thermochronologic systems.

In the same fashion of Figure 7a, Fig. 7b shows the impact of a sharp decrease in erosion rate at time t_b, from 1.0 to 0.5 km/Ma. Because of the slower bedrock exhumation compared to Fig. 7a, lag-time values reflecting the new slower erosion rate values will be observed in much younger strata of the sedimentary succession. AFT data will record the new erosional regime in detritus only after time t_2, ZFT data only after time t_3, and the highest-T_c systems may even fail to fully reveal the new erosion regime, as illustrated in the case of mica Ar-Ar in Fig. 7b. In case of a sharp decrease in erosion rate, the lag-time approach will lead to an overestimation of the exhumation rate in the whole stratigraphic interval between A and B. Notably, such overestimation reflects the fact that the thermochronologic fingerprint of bedrock was acquired during a previous stage of faster erosion, and is independent from overestimations due to heat advection discussed in Section 2.2.

Figure 7

3.4. Summary of fundamental criteria for the interpretation of the detrital thermochronologic record from a single source

The conceptual models described in this section show that different geologic processes produce diagnostic combinations of stationary and moving age peaks in the detrital thermochronologic record derived from a single eroding source. Fundamental criteria (C1 to C15) for a correct interpretation of these thermochronologic age patterns, and for a correct application of the lag-time approach in detritus derived from erosion of a single source, are listed below:

C1) Moving age peaks are defined by thermochronologic ages set during bedrock erosion. They get progressively younger up section, and can be used to infer past exhumation rates.

C2) Stationary age peaks remain fixed up section. They are defined by thermochronologic ages set either during episodes of magmatic/metamorphic crystallization, or during episodes of thermal relaxation in eroded bedrock. They should not be used to infer past exhumation rates.

C3) For a given thermochronologic system, only one moving age peak is expected from a single eroding source.

C4) The first appearance of a moving age peak occurs in detritus well after the onset of erosion, and with a time delay that is greater for higher-T_c thermochronologic systems.

C5) The onset of an erosion event is broadly constrained by the age of the oldest peak that defines a moving-age trend.

C6) Systems with progressively higher T_c tend to provide information on progressively older exhumation events. Within a given stratigraphic interval, moving age peaks defined by different thermochronologic systems potentially relate to exhumation events of different age.

C7) Detrital thermochronology ages reflecting former residence of mineral grains within a PAZ/PRZ, and thus showing remarkable age dispersion, are expected at different stratigraphic levels in a basin depending on the thermochronologic systems under consideration.

C8) Stationary age peaks defined by magmatic crystallization ages are potentially detected starting from the lowermost units of a sedimentary succession derived from unroofing of a magmatic complex, and will characterize different thermochronologic systems within the same stratigraphic level.

C9) Magmatic crystallization ages in detritus can be detected by double dating (e.g., zircon U-Pb and ZFT dating of the same grain), but this approach could be misleading for zircon grains that have or have had (since abraded) U-Pb age zonation.

C10) Stationary age peaks due to metamorphic crystallization are generally not expected in the lowermost units of a sedimentary basin, unless they relate to much older metamorphic events.

C11) Stationary age peaks due to magmatic or metamorphic crystallization can be associated with a moving age peak derived from the same source. However, that moving age peak will be always older than the stationary age peak.

C12) Stationary age peaks due to thermal relaxation are never associated, in the same stratigraphic level, with moving age peaks from the same source. These stationary age peaks are found in progressively younger stratigraphic units for progressively higher-T_c systems.

C13) A sharp change in erosion rate is barely distinguishable from a more progressive change in erosion rate with respect to the detrital thermochronologic record.

C14) A sharp change from slower to faster erosion (or from faster to slower erosion) will produce a more progressive variation in lag-time values recorded by moving age peaks in detritus. These variations are even smoother for higher-temperature thermochronologic systems.

C15) The onset of erosion after a period of relative tectonic quiescence where there is no erosion can be revealed by a sharp decrease in lag time, which is recorded at different levels of the stratigraphic succession depending on the thermochronologic system (i.e., deeper stratigraphic levels for lower-T_c systems, shallower stratigraphic levels for higher-T_c systems).

4. Impact of mixed provenance in lag-time interpretations (II in Fig. 1b)

Large sedimentary basins preserved in the geologic record and accreted in mountain belts are generally fed by multiple sources of detritus, which are often characterized by different geologic or upper crustal exhumation histories (II in Fig. 1b). The detrital thermochronologic record in these basins is thus expected to be more complex than the detrital thermochronologic record in small sedimentary basins that were possibly fed by erosion of a single bedrock source. Complexities in case of a mixed provenance arise not only from the combination of the different thermochronologic age patterns described in Section 3, but also from the possible modifications determined, for example, by variations in erosion rate either in space or time, or by incorporation of detritus from different paleo-depths in regions of high topographic relief.

4.1. Recognition of lag-time trends in stratigraphic successions derived by multiple bedrock sources

The conceptual model of Fig. 8 illustrates the potential impact of a mixed provenance in the thermochronologic record of a sedimentary basin, and the potential implications for lag-time analysis. The hypothetical sedimentary basin in Fig. 8 is fed from detritus derived from two different bedrock sources (source 1 and source 2), which are assumed to have the same size and zircon fertility. The ZFT age-depth relationship of source 1 is the same previously described in Fig. 7b. It results from progressive erosion of bedrock at a rate of 1 km/Ma until time t_b, and at rate of 0.5 km/Ma after time t_b. The ZFT age-depth relationship of source 2 is the same previously described in Fig. 5c. It results from progressive removal of the overburden at a rate of 1 km/Ma, followed by relative tectonic quiescence with negligible erosion at rate of 0.01 km/Ma, and subsequent erosion after time t_b at rate of 1 km/Ma.

In single-source detritus, both source 1 and source 2 will define a moving age peak that gets progressively younger up section. When detritus from these two sources is combined and accumulated in the hypothetical sedimentary basin starting from time t_b (right panel in Fig. 8), the resulting grain-age distribution will show two sets of peaks. The relative size of these peaks will be a function of the size of the eroding source, of the mineral fertility in the parent bedrock, and of the short-term erosion rate (Bernet et al., 2004; Resentini and Malusà, 2012). Because source 1 is eroded at a slower rate compared to source 2, the peak defined by zircon grains from source 1 will be smaller than the peak defined by zircon grains from source 2.

If provenance from these different sources remains undetected, the composite grain-age distribution in the final sink, showing a moving age peak with constant lag time from the bottom to the top of the sedimentary succession (red arrow in Fig. 8), may erroneously suggest a steady-state evolution of the eroding mountain belt (cf. Fig. 1a). However, this interpretation is incorrect, because the trend underlined by the red arrow actually includes peaks from two different source areas, both eroded during part of their geologic evolution at a rate of 1 km/Ma. Source 1 controls the youngest age peak in the lowermost part of the stratigraphic succession, source 2 controls the youngest age peak in the uppermost part of the stratigraphic succession. If the mixed provenance is correctly detected, for example by using Hf isotopic compositions of the same zircon grains, these detrital thermochronologic data would support migration of erosion across a mountain belt where steady state is not attained, in line with the initial hypothesis of Fig. 8. This example illustrates the importance of an independent provenance discrimination of dated mineral grains in order to provide reliable geologic interpretations of thermochronologic age trends in detritus.

Potential detection of multiple age peaks by thermochronologic analysis of sedimentary rocks is a function of the uncertainty of single grain-age measurements, and how many grains have been measured (Vermeesch, 2004). In detrital thermochronology studies, different age peaks from the same sample are often indicated in lag-time diagrams by different colors according to their relative age (e.g., Bernet et al., 2006; Shen et al., 2016), and are generally labeled *a priori* as peak P1, P2 etc. As a result, situations like those illustrated in Fig. 8 are easily overlooked. Such *a priori* attribution of grain-age populations to predetermined age peaks is thus discouraged. We alternatively suggest using different colors or symbols to either visualize parameters that may constrain the provenance of dated mineral grains, or to visualize other information (such as the size of the age population forming each peak) that may help revealing major potential provenance changes through the analyzed stratigraphic sequence. The advantages of this approach are demonstrated by case studies illustrated in Sections 7 to 9.

4.2. Detection of a mixed provenance in the detrital thermochronology record

Some of the fundamental criteria for the interpretation of the detrital thermochronologic record from a single source, as illustrated in Section 3.4, can be also used to detect a mixed provenance. For a given thermochronologic system, only one moving age peak is expected from a single eroding source (criterion C3 in Section 3.4). Therefore, the presence of two or more moving age peaks in detritus provide strong indication of a mixed provenance, which should be carefully considered during data interpretation.

Useful indications are also provided by the relationships between stationary age peaks and moving age peaks. Stationary age peaks due to thermal relaxation are never associated with a moving age peak from the same source (criterion C12 in Section 3.4). The presence of a moving age peak associated with a stationary age peak mirroring thermal relaxation in bedrock thus implies a mixed provenance. Notably, stationary age peaks due to magmatic or metamorphic crystallization can be associated with a moving age peak derived from the same eroding source. However, that moving age peak must be older than the stationary age peak derived from the same source (criterion C11 in

Section 3.4). The presence of a moving age peak that is younger than the stationary age peak in the same sedimentary layer thus provides strong indication for a mixed provenance.

4.3. Detection of major provenance changes through a stratigraphic succession

Sedimentary successions often record major provenance changes that can be detected, under favourable conditions, by inspecting the trends of detrital thermochronologic ages observed through the stratigraphic succession under consideration. In fact, if provenance does not change, the detrital thermochronologic record should follow trends either including stationary age peaks, or moving age peaks that get progressively younger up section. The sudden appearance of older grain-age populations moving up section along a stratigraphic succession provides strong evidence for a major provenance change and involvement of new sources of detritus, e.g. due to tectonic and/or drainage reorganization in the source regions (e.g., Ruiz et al., 2004; Glotzbach et al., 2011).

An example of this simple principle is provided in Fig. 9a, which shows the detrital AFT age populations in sedimentary rocks from the Gediz Graben succession, western Turkey (Asti et al., 2018). In each formation, age peaks become increasingly younger up section, which is consistent with the progressive erosion of deeper rocks in the source. However, jumps to older age peaks (marked by solid black dots) are observed at the base of the Caltilik and Kaletepe formations, which provides evidence for two major provenance changes (marked by white arrows) in the late Miocene and the Quaternary.

Changes in the pattern of bedrock erosion might also be revealed by sharp changes, through a stratigraphic succession, of the size of grain-age populations defining a stationary age peak. If mineral fertility variations with depth can be excluded, a sharp increase in the size of a stationary age peak may imply a coeval sharp increase in erosion rate in the corresponding eroding source. Under favourable conditions, stationary age peaks may thus reveal variations in erosion rate even more readily than moving age peaks (see Section 3.3). However, this requires that the size of the age population forming each peak is properly visualized in a lag-time diagram (see Section 7).

Provenance changes are more reliably detected when thermochronologic age trends are compared for different thermochronologic system along the same stratigraphic succession. As illustrated in Section 3, the same geologic event is generally recorded in detritus at different levels of the stratigraphic succession, depending on the thermochronologic system under consideration. And variations in bedrock erosion rate, even if sharp, are recorded gradually in the detrital thermochronologic record, and at different stratigraphic levels in different thermochronologic systems. Within this framework, a sharp change in the thermochronologic fingerprint of detritus that is simultaneously recorded by different thermochronologic systems and at the same stratigraphic level of the sedimentary succession, provides compelling evidence for a major provenance change.

Potential provenance changes may be further supported by the analysis of framework minerals and heavy mineral suites in the stratigraphic units already analyzed by detrital thermochronology techniques (e.g., Baldwin et al., 1986; Garver and Brandon, 1994; Lonergan and Johnson, 1998; Ruiz et al., 2004; Tatzel et al., 2017; Rahl et al., 2018).

4.4. Independent provenance discrimination of dated mineral grains

Provenance of grain-age populations can be preliminarily constrained by thermochronologic data from bedrock and detritus following a simple principle: thermochronologic ages in detritus within a stratigraphic succession, unless reset by burial, must be equal to or older than the thermochronologic ages now observed in bedrock within the potential source areas. Bedrock units showing older thermochronologic ages can be safely excluded as a potential source. Applications of this simple principle can be found, for example, in Kirstein et al. (2010) and Li et al. (2019). However, provenance constraints exclusively based on cooling ages are often poor for older stratigraphic units, because of the wide range of thermochronologic ages consistent with potential sources, which makes it necessary for an integration by complementary provenance analyses (see reviews by von Eynatten and Dunkl, 2012; Carter, 2019).

Provenance information for apatite grains dated by the AFT method may also be constrained by apatite U-Pb ages (Thomson et al., 2012), which can reveal cooling in the temperature range of ~375-570 °C (see Chew et al., 2011 and Danišík, 2019 for further information on apatite double and triple dating). Apatites from different rock types have distinctive absolute and relative abundances of halogens and many trace elements including rare-earth elements, Sr, Y, Mn, and Th that can be exploited as a provenance tool (e.g., Belousova et al., 2002; O'Sullivan et al., 2018; Ansberque et al., 2019). Foster and Carter (2007) combined detrital AFT data and in situ Sm–Nd isotopic measurement to link detrital AFT age populations in modern river sands to specific bedrock sources eroded at different rates in the Himalayas (Carter and Foster, 2009). In a similar fashion, Malusà et al. (2017) linked the trace-element composition of detrital apatite grains in modern river sands shed from the European Alps with the composition of apatite crystals in the potential eroding sources. They also provided an example of provenance discrimination based on Nd isotopic analysis on apatite, which is illustrated in Fig. 9b.

Potential complementary tools for provenance discrimination of detrital zircon grains include zircon color linked to α-damage (Fielding, 1970; Garver and Kamp, 2002), zircon crystal morphology (Pupin, 1980; Dunkl et al., 2001) and Ti content controlled by zircon crystallization conditions (Watson et al., 2006; Fu et al., 2008). Robust constraints on zircon provenance are also provided by Hf isotopes, which can be measured on zircon grains together with U-Pb ages (Carter, 2007).

Figure 9c provides an example of provenance discrimination based on zircon U-Pb ages and Hf isotopic compositions, as applied to magmatic zircon grains in sedimentary rocks of the Alpine foreland basin and the Adriatic foredeep (Jacobs et al., 2018; Lu et al., 2018; 2019). The reference fields for the potential Periadriatic sources are from Ji et al. (2019). South of the Alps, sedimentary rock samples include zircon grains consistent with a provenance from the Adamello magmatic unit (AD) and the Bergell pluton (BG), but no grains from the Biella (BI) and Traversella (nTR, sTR) plutons (Fig. 9c). The same provenances are documented farther south in samples from the Elba Island. North of the Alps, zircon grains are initially consistent with an Adamello source but they show a trend of increasing $\varepsilon_{Hf}(t)$ values that is different from the boomerang-shaped trend with decreasing $\varepsilon_{Hf}(t)$ values recognized for the Periadriatic plutons (Ji et al., 2019). This may suggest a different source area for the uppermost part of the North Alpine sedimentary succession. Previous work, based on preliminary reference datasets of zircon U-Pb ages and Hf isotopic compositions for the potential bedrock sources (Jacobs et al., 2018; Lu et al., 2019), have ascribed the Oligocene magmatic zircon grains from different sites of the Adriatic foredeep either to a dominant Bergell source (Elba Island) or to a mixed Biella-Bergell source (Como Conglomerate), in spite of the similar Hf isotopic compositions measured in zircon grains from these different sites (see Fig. 9c). However, based on a more comprehensive reference dataset reported in Fig. 9c, which was not available at that time to Jacobs et al. (2018) and Lu et al. (2019), major supply from a Biella source appears unlikely. This example underlines the importance of a robust reference dataset as a starting point to perform reliable provenance interpretations.

4.5. Impact of mineral fertility in case of multiple bedrock sources

In the mixed-provenance conceptual model of Fig. 8, different sources are assumed to have the same mineral fertility, i.e., the same propensity to yield specific mineral grains when exposed to erosion. Most detrital thermochronology studies do assume negligible changes in mineral fertility (e.g., Malusà et al., 2009; Zhang et al., 2012; Glotzbach et al., 2013; Saylor et al., 2013; He et al., 2014; Braun et al., 2018). However, constant mineral fertility is rarely observed in real geologic settings, and the constant-fertility assumption of many studies, while understandable is generally untenable.

The conceptual model of Fig. 10 illustrates the impact of variable mineral fertilities on lag-time interpretations in case of a mixed provenance. The hypothetical sedimentary basin of Fig. 10 is fed from detritus supplied from two different bedrock sources (source 1 and source 2). The ZFT age-depth relationship of source 1 (in red) is the same as previously described in Fig. 7a. This relationship results from progressive erosion of bedrock at a rate of 0.5 km/Ma until time t_b, and at rate of 1.0 km/Ma after time t_b. The ZFT age-depth relationship of source 2 (in blue) is the same as previously described in Fig. 7b. It results from progressive erosion of bedrock at a rate of 1.0 km/Ma until time t_b, and at rate of 0.5 km/Ma after time t_b. Detritus from these two sources is combined and accumulated in the hypothetical sedimentary basin starting from time t_b (right panel in Fig. 10). Notably, the volume of eroded material from source 2 is much smaller than from source 1. However, its mineral fertility is much larger (100 mg/kg vs 1 mg/kg). As a result, in spite of the larger area and higher erosion rate (black arrows) characterizing source 1 since time t_b, zircon grains from source 2 are overwhelming in the final sink (yellow bells). Only one moving age peak will be recognized in the detrital thermochronology record: it derives from source 2, and will define a trend of increasing lag time up section.

According to this hypothetical scenario, the detrital thermochronology record in the final sink is prone to be incorrectly interpreted in terms of decreasing exhumation rates that would have characterized the entire mountain belt. Instead, most of the orogen underwent an increase in exhumation rate since time t_b, not a decrease in exhumation rate. This underlines the importance of reliable mineral fertility determinations for lithologies in the eroding orogen to support the geologic interpretation of detrital thermochronology data.

Variations in mineral fertility in real geologic settings may be even greater than those assumed in the conceptual model of Fig. 10 (Malusà et al., 2016b; Resentini et al., in review). For example, zircon fertility values measured in the European Alps varies from <0.5 mg/kg to ~100 mg/kg (Fig. 11a). High zircon fertility values characterize the Lepontine dome gneisses (10–70 mg/kg), migmatites and granitoid rocks of the Mont Blanc and Argentera Massifs (80–100 mg/kg), and Carboniferous-to-Permian metasediments of the Paleogene wedge (50–90 mg/kg), whereas the lowest zircon fertility values are found in sedimentary successions of the Southern Alps (0.5–6 mg/kg) and the Northern Apennines (0.5–7 mg/kg). In Taiwan, zircon fertility values range from ~1 mg/km to >100 mg/kg. The highest fertility values characterize the Tananao Complex but, in places, also the Western Foothills (Fig. 11b).

While there is often a well-defined relationship between bedrock geology and mineral fertility, major mineral fertility variations are sometimes observed even in tectonic units ascribed to the same palaeogeographic domain, and potentially considered to be similar *a priori*. For example, the Dora-Maira and Gran Paradiso Massifs of the European Alps (DM and GP in Fig. 11a) both formed by subduction and eclogitization of European continental crust during the Paleogene, yet have zircon fertilities that differ over an order of magnitude or more (DM = 0.4–1.2 mg/kg; GP = 5–8 mg/kg). We conclude that the relationships between bedrock geology and mineral fertility are complex and difficult to predict. They depend not only on lithology, but in general more on the whole magmatic, sedimentary or metamorphic evolution of the source rocks. A major role in determining the fertility of a rock is also played by its texture, since datable minerals in detritus are often found as inclusions in larger framework mineral grains.

Careful approaches to mineral fertility determinations are thus encouraged. However, these approaches invariably require that the source area has not been completely eroded away. Point counting under a microscope (e.g. Silver et al., 1981; Tranel et al., 2011; Gemignani et al., 2018) is inherently imprecise and time-consuming. Geochemical approaches to fertility determinations (e.g., Cawood et al., 2003; Dickinson, 2008) are prone to introduce further unquantifiable bias (Malusà et al., 2016b). A more effective approach to mineral fertility determination that requires only minor modifications to the standard concentration procedures adopted in most thermochronology laboratories, is based on the analysis of modern sands. Details on this procedure are described in Malusà and Garzanti (2019).

4.6. Other potential sources of bias in case of mixed provenance

Beside variations in mineral fertility, in cases of mixed provenances other factors that may potentially produce an underestimation (or overestimation) of the contribution of datable mineral grains from a specific source area should be carefully accounted for, and their impact on geologic interpretations should be carefully evaluated. Some of these potential sources of bias, namely the U-concentration bias and the etching bias (Malusà et al., 2013), are specific to detrital ZFT datasets, but may also propagate to other datasets whenever zircon grains are subject to double or triple dating. The U-concentration bias is due to the fact that zircon grains with [U] >1000 ppm generally show uncountable (very high density) overlapping fission tracks, and are thus undatable by the ZFT method using the classic approach and an optical microscope (Montario and Garver 2009; Ohishi and Hasebe, 2012; Gombosi et al., 2014). In the European Alps, these undatable U-rich grains exceed 40% of the total zircon load in the final sink (Malusà et al., 2013). This implies that, in case of sediment mixing from two or more sources yielding zircon grains with different [U] (for example because of the different metamorphic evolution of the eroding tectonic units), sources supplying the larger amounts of U-rich grains will be systematically under-represented in the detrital ZFT record. The impact of U-concentration bias can be predicted in certain situations, by measuring the distribution of [U] in zircon grains from each potential source by LA-ICP-MS (see Malusà et al., 2013, their Fig. 15), although this example deals with modern river sediments and not with sedimentary rocks preserved in a stratigraphic succession.

The etching bias is due to the differential etching response characterizing zircon grains with different amounts of α-damage (e.g., Gleadow et al., 1976; Kasuya and Naeser, 1988; Tagami et al. 1990, 1996). Accumulated α-damage is a function of [U] and effective accumulation time (Tagami et al., 1996; Garver and Kamp, 2002). Revelation of spontaneous fission tracks for zircon dating requires chemical etching (Garver, 2003; Kohn et al., 2019). Zircons that are old and have more accumulated α-damage require a shorter etching time to reveal fission tracks for counting, whereas young zircons with less α-damage require a much longer etching time (Bernet and Garver, 2005). Within this framework, older zircon grains with higher levels of α-damage are often selectively overetched and eventually lost during routine etching, even in case of multiple etching times to reveal the full spectra of ZFT ages. Whenever different source areas shed zircon grains with different levels of α-damage, for example because of the different age of their protoliths, sources yielding zircon grains with old U–Pb ages and high levels of α-damage will be systematically under-represented in the final sink.

Detrital apatite grains have much lower [U] compared to zircon, and the above sources of bias are not an issue. However, in some situations the abundance of young U-poor apatite grains without spontaneous tracks, if not properly accounted for, may lead to an under-representation of specific source areas in the detrital AFT record. Bias may also occur during the preparation of grain mounts for AFT and ZFT dating if a relationship exists between grain age and grain shape or size. When mounted in epoxy or Teflon for polishing and etching, elongated grains tend to align themselves parallel to the c-axis, and most of them are thus suitably oriented for fission-track counting (e.g., Kohn et al., 2019). Equidimensional grains tend instead to be randomly oriented, leading to a lower proportion of grains suitably oriented for counting. This implies that source areas supplying a higher proportion of elongated detrital grains are generally over-represented in the detrital AFT and ZFT record.

4.7. Summary of fundamental criteria for the interpretation of the detrital thermochronologic record derived from two or more sources

Useful criteria for the identification and interpretation of the detrital thermochronology record derived from the mixing of detritus from two or more sources are summarized below:

M1) The presence of two (or more) moving age peaks in detritus is compelling evidence of a mixed provenance.

M2) The presence of a moving age peak that is younger than a stationary age peak in the same sedimentary layer provides strong support for a mixed provenance.

M3) The presence of a moving age peak beside a stationary age peak mirroring thermal relaxation in bedrock also suggests a mixed provenance.

M4) The sharp change of thermochronologic fingerprint in detritus simultaneously recorded in the same stratigraphic level by different thermochronologic systems provides compelling evidence for a major provenance change and addition of detritus from new sources.

M5) The sudden appearance of older grain-age populations moving up section through a stratigraphic succession is also evidence for a major provenance change and addition of detritus from new sources.

M6) Sharp changes in the size of stationary and moving age peaks moving through a stratigraphic succession may also provide support to a change in provenance, if variations in mineral fertility with depth in the source can be excluded.

M7) Detrital thermochronologic ages observed in a stratigraphic succession, if not rejuvenated by post-depositional annealing, should be equal to or older than thermochronologic ages observed today in the potential sources.

M8) In case of sediment mixing from two or more sources, detrital mineral grains shed from a high-fertility source are generally overwhelming in the final sink, irrespective of the rate of erosion of that source.

M9) In case of sediment mixing from two or more sources, those sources supplying larger amounts of U-rich zircon grains will be under-represented in the detrital ZFT record (U-concentration bias).

M10) In case of sediment mixing from two or more sources, those sources supplying zircon grains with older U-Pb ages and higher levels of α-damage will be under-represented in the detrital ZFT record (etching bias).

M11) In case of sediment mixing from two or more sources, those sources supplying a higher proportion of rounded, equidimensional detrital grains will be under-represented in the detrital AFT and ZFT record

Figures 8, 9, 10, 11

5. Potential modifications of the original thermochronologic signal during sediment transport (III in Fig. 1b)

Grain-age distributions in detritus are ideally regarded as being a faithful mirror of thermochronologic ages in eroded bedrock. However, during transportation and before final deposition detritus may undergo significant modification. Clastic detritus may experience 10’s, 100’s or even 1000’s of km of transportation, either as bedload or as suspended load, before reaching a deep-sea sink (Graham et al., 1975, Ingersoll et al., 2003; Garzanti, 2019). During this stage, the detrital thermochronologic signature acquired in the source area may undergo modifications by physical and chemical processes (III in Fig. 1b). Mineral grains are sorted in clastic detritus according to their size, density and shape, and they may also suffer abrasion and mechanical breakdown (Schuiling et al. 1985). Drastic modifications in detritus are also induced by the different chemical stability of detrital minerals during weathering and burial diagenesis (Johnsson, 1993; Worden and

Burley 2003). However, like other single-mineral methods, detrital thermochronology minimizes both the impact of differential mineral density during transport and deposition, and the impact of differential mineral dissolution during weathering and diagenesis (Morton and Hallsworth, 1999; von Eynatten and Dunkl, 2012). An appropriate approach to detrital thermochronology may thus provide information on the source area that is largely independent from physical and chemical modifications taking place during transport, deposition and diagenesis (Fig. 12a).

5.1. Impact of selective entrainment of mineral grains

In sorted sediments, dense minerals that are commonly employed in detrital thermochronology (e.g., apatite and zircon) are usually associated with coarser lower-density framework minerals such as quartz and feldspars, according to the principle of hydraulic equivalence (Rubey, 1933, Garzanti et al., 2008). The settling velocity of a grain in a fluid reflects the balance between drag resistance and gravitational force, and depends on the density and size of the settling grains (Schuiling et al., 1985; Komar, 2007). Mineral grains with the same settling velocity are deposited together: the greater the difference in density between settling-equivalent grains, the greater their difference in size, which is also referred to as the size shift (Rittenhouse, 1943). Metamict zircon grains, due to their lower density (Ewing et al., 2003), have smaller size shifts (relative to quartz) than hydraulically equivalent non-metamict zircon grains. Settling velocity in micas, beside density and size, is also controlled by grain shape. Micas settle slower than quartz in spite of their higher densities, just because of their platy shape (Doyle et al., 1983; Komar and Wang, 1984; Le Roux, 2005). The hydraulic behavior of bedload sediment can be easily modelled mathematically (Resentini et al., 2013), but the behavior of micas, largely transported as suspended load, is more difficult to predict.

Particle size and density play a major role not only during grain settling, but also in controlling the process of selective entrainment during transport (Komar and Li, 1988; Komar, 2007). In bedload sand, smaller and higher-density mineral grains are less easily entrained by tractive currents than settling-equivalent coarser and lower-density mineral grains. In fact, coarser and lower-density mineral grains project higher above the bed and experience greater flow velocities and drag forces (Slingerland and Smith, 1986; Garzanti et al., 2009). As a result, the original neutral bedload is separated into a fraction of entrained sediment depleted in denser minerals (antiplacer deposit), and a smaller lag fraction strongly enriched in denser minerals (placer deposit). Placer deposits can be easily detected either by their bulk grain density, or by geochemical methods (Malusà et al., 2016b). Whenever relationships exist in the source areas between grain age and grain size, selective entrainment may have a large impact on the grain-age distributions observed in the final sink (e.g., Najman et al., 2019) (Fig. 12b). Dated mineral grains should be always tested for potential age-size relationships (e.g., by plotting grain age versus equivalent spherical diameter) and, if any relationship exists, particular care should be used to test the analyzed samples against selective entrainment effects (Malusà and Garzanti, 2019). In case of a correlation between grain age and grain size, selective entrainment may have led to grain-age distributions that are not fully representative of the thermochronologic fingerprint of eroded bedrock.

5.2. Mechanical grain breakdown during transport

During sediment transport, detrital mineral grains may undergo mechanical breakage and thus mineral inclusions are possibly liberated from their host grains, forming new individual detrital grains that start to be sorted during tractive transport according to their size, density and shape. The downstream grain-size reduction in natural sedimentary systems primarily occurs in the uppermost and higher relief parts of the catchment (e.g., Fedele and Paola, 2007; Allen and Allen, 2013; Lavarini et al., 2018), whereas mechanical breakdown of sand-sized grains during river transport across the floodplain is generally minor (Russel and Taylor, 1937; Kuenen, 1959). This has been recently confirmed by Malusà and Garzanti (2019) by comparing the concentration of individual zircon grains in bedload (measured according to the approach described in their Fig. 7.8) with the zirconium concentration in the same bulk sediment samples as indicated by chemical analysis. If the production of additional individual zircon grains by mechanical breakdown of the host minerals in the floodplain was relevant, then the ratio between individual-zircon-grain concentration and zirconium concentration should increase downstream along the floodplain. However, in the Po river catchment such an increase is not observed, confirming the negligible impact of mechanical grain breakage in detrital thermochronology studies (Fig. 12b).

5.3. Abrasion and rounding of detrital mineral grains during transport

During sediment transport, detrital mineral grains may undergo progressive abrasion and rounding depending on their physical and mechanical properties, with consequent potential removal of their external rims (Fig. 12b). Metamict zircon grains may also be selectively destroyed by abrasion during river transport (Fedo et al., 2003; Hay and Dempster, 2009), but this possibility is poorly supported by observational evidence (Malusà et al., 2013). The analysis of modern river systems suggests that lower-density metamict zircon may survive long distance river transport, because mechanical wear in these settings is much less effective than in the eolian environment (Russell and Taylor, 1937; Kuenen 1959, 1960; Garzanti et al., 2015). In many cases, rounding of mineral phases such as zircon may reflect chemical abrasion by metamorphic fluids in the source rocks, rather than mechanical abrasion during transport (Malusà et al., 2013).

The removal of the external rims by grain abrasion has major implications in (U-Th)/He dating, because it affects the α-ejection correction factor applied to raw He ages (e.g., Reiners and Farley, 2001; Hourigan et al., 2005). Implications are also relevant for zircon double dating (Carter and Moss, 1999), because the removal of an outer zircon rim may also remove the evidence of its original U-Pb age zonation. As a result, some ZFT ages that are apparently associated with much older zircon U-Pb ages may be incorrectly interpreted in terms of exhumation, despite that they just reflect the age of a coeval magmatic event (Fig. 6a). This may have an impact on the identification of lag-time trends.

5.4. Temporary storage and reworking of sediment

As mentioned previously, mineral grains may travel either as bedload (e.g., apatite and zircon) or as suspended load (e.g., micas) (Fig. 12a). The minimum time required by suspended load to reach the final sink is equal to the time needed by a flood wave to reach the closure section of a basin during a major flood event. However, the actual transit time is generally much longer. In fact, sediment can be temporarily deposited on levees, crevasse splays or even far from the active river channel, to be re-eroded and transported downstream during subsequent flood events (Clift and Giosan, 2014; Malatesta et al., 2018). The transfer time of bedload is generally longer than the transfer time of suspended load, and a substantial time delay can be expected in the detrital thermochronology signals provided by apatite and zircon (transported as bedload) compared to the thermochronologic signal provided by micas (entrained as suspended load). Based on the analysis of ^{238}U–^{234}U–^{230}Th radioactive disequilibria in river sediments derived from the Himalaya, Granet et al. (2010) suggested a transit time of > several 10^5 a for bedload, and a much shorter transit time for associated suspended load (<20–25 10^3 a). A bedload transit time of 1–3 Ma has been suggested by Wittmann et al. (2011) for the Amazon basin, based on the ratio of *in situ*-produced cosmogenic ^{26}Al and ^{10}Be in sediment, which implies a similar delay in the exhumation signal potentially preserved in the detrital thermochronology record. Even greater delay (>10 Ma) is expected in case of reworking of sediment that has been temporarily stored in a wedge-top basin to be transferred into the final sink at a later stage (Fig. 12a). This situation has been documented, for example, in the Northern Apennines, where Oligocene-Miocene detritus derived from Alpine erosion (Garzanti et al., 2012) and initially stored on top of the Apenninic wedge (Cibin et al., 2001) has been re-eroded and transferred into the Po Plain after major Pliocene uplift of the Northern Apennines (Malusà and Balestrieri, 2012).

The analysis of thermochronologic age trends through a stratigraphic succession can provide evidence to detect (or exclude) major recycling of sediment into the final sink after long-term sediment storage and reworking. This is illustrated in the conceptual model of Fig. 13, where the hypothetical crustal section undergoing erosion is the same as described in Section 3.1.1. In this conceptual model, part of the detritus eroded from levels 1 to 3 since time t_e, and forming units A-to-C in Fig. 13, is temporarily stored in a wedge-top basin where it is not affected by post-depositional annealing. Starting from time t_3, thrust fault activity determines the uplift and erosion of sediment previously stored in the wedge-top basin. Sediment reworked from units A-to-C is thus admixed in the final sink with sediment derived from erosion of level 4, forming the new sedimentary unit D. As a result, unit D is expected to include not only the young moving age peaks defined by AFT, ZFT and mica Ar-Ar ages measured in mineral grains eroded from level 4 (cf. Fig. 5a). Unit D will also include all of the major grain-age populations inherited from units A-to-C (dashed lines in Fig. 13). Only the smallest grain-age populations of units A-to-C are prone to remain undetected in unit D, because they may fall below the detection limit (see Vermeesch et al., 2004) after sediment mixing. In unit D, the age peaks inherited from recycled units will be invariably older than the age peaks derived from erosion of level 4. The inherited peaks might represent the youngest peaks in unit D, but only if unit D is entirely derived from recycled material, which is unlikely. Recognition of specific intervals of a stratigraphic succession recycled within a basin after long-term storage and reworking is favoured by the presence of moving age peaks. Whenever a sedimentary rock does not include all of the major age peaks found in the underlying rocks, major sediment recycling can be excluded. An example of thermochronologic evidence of major recycling of sediment after long-term storage and reworking is provided in Fig. 9a by the Quaternary Kaletepe Fm (Gediz Graben, western Turkey). The Kaletepe Fm includes all of the major AFT age populations detected in the underlying Miocene-Pliocene formations of the Gediz Graben succession (Asti et al., 2018), consistent with predictions of the conceptual model of Fig. 13.

5.5 Chemical weathering

The original compositional fingerprint of sediment is generally modified by selective dissolution of unstable minerals during transient sediment storage and exposure on the floodplain. At low latitudes, severe dissolution in soils affects not only the more unstable minerals such as olivine or garnet, but also tourmaline, zircon and quartz (Cleary and Conolly, 1972; Nickel, 1973; Velbel, 1999; Van Loon and Mange, 2007). In bedload sand carried by equatorial rivers, zirconium concentrations are often markedly lower than the upper continental crust standard (e.g., Dupré et al., 1996; Garzanti et al., 2013), which suggests that metamict zircon may undergo dissolution in lateritic soils (Carroll, 1953; Colin et al., 1993). Apatite is very soluble in acidic soils (Lång, 2000; Morton and Hallsworth, 2007). A few decades in a peat bog might be sufficient for a complete apatite dissolution (Le Roux et al., 2006), but apatite grains are anyway preserved in many peat-bog sediments (e.g., Szopa et al., 2019). AFT and ZFT ages determined from fresh and partially weathered rock samples show no major effect of weathering on thermochronologic ages (Gleadow and Lovering, 1974). This suggests that the potential impact of chemical weathering on thermochronologic data interpretation is probably negligible (Fig. 12b).

5.6 Burial diagenesis

The time and temperatures available for chemical reactions during burial diagenesis are much longer and higher than the time and temperatures during transient storage and exposure of sediment on the floodplain. Consequently, diagenetic effects are generally more drastic than those of weathering (e.g., Andò et al., 2012; Morton, 2012). Diagenetic effects are responsible for the decreasing mineral diversity generally observed in sedimentary successions with increasing burial depths (Morton, 1979; Cavazza and Gandolfi, 1992; Milliken, 2007). During burial diagenesis, pyroxene, amphibole, epidote, titanite, staurolite and garnet are typically dissolved, partially or even completely with increasing depth, but minerals such as zircon, apatite, monazite and rutile have a high probability of survival (Morton and Hallsworth, 2007), and their relative proportions in ancient sandstones generally increases.

Figures 12, 13

6. Impact of post-depositional annealing on lag-time trends (IV in Fig. 1b)

Despite burial diagenesis not being very likely to dissolve detrital mineral grains that are the target of most detrital thermochronology studies, post-depositional annealing (or diffusion) towards the base of a thick sedimentary succession has an impact on lag-time trends that must be carefully detected and accounted for during geologic interpretation (IV in Fig. 1b). This impact is illustrated in the conceptual model of Fig. 14, where the initial age structure is the same as Fig. 5a, but it is modified by heating due to additional sedimentary burial (in brown). The original trend of decreasing AFT ages that define, in units B-to-D of Fig. 5a, a moving age peak, is replaced in the lowermost units of Fig. 14 by AFT ages that become increasingly younger down section (Ruiz et al., 2004; van der Beek et al., 2006; Fitzgerald et al., 2019). These ages define a trend that is opposite to trends observed in the uppermost stratigraphic levels of the sedimentary succession under consideration. Such a reversal is not observed in higher T_c systems within the same stratigraphic level (e.g., Malusà et al., 2011a). Post-depositional annealing may eventually lead to negative lag-time values (e.g., Chirouze et al., 2012). If undetected, reduction in lag-time values due to post-depositional annealing may determine a systematic overestimation of inferred exhumation rates.

Figure 14

7. Application to sedimentary successions: European Alps

The European Alps are the result of Cretaceous-to-Present convergence between Africa and Eurasia (Dewey et al., 1989; Jolivet and Faccenna, 2000; Schmid et al., 2004). Tectonic plate convergence led to the progressive subduction of the Alpine Tethys and adjoining European plate margin under the Adriatic microplate (Piromallo and Faccenna, 2004; Zhao et al., 2015; 2016; Sun et al., 2019), followed by hard collision since the Oligocene (Lickorish et al., 2002; Rosenberg et al., 2015; Liao et al., 2018b). (Fig. 15a). Analysis of detrital thermochronology studies in the European

Alps (e.g., Bernet et al., 2001, 2009; Carrapa et al., 2003; 2004; Fellin et al., 2005; Kuhlemann et al., 2006; Carrapa, 2009; 2010; Bernet, 2010; Glotzbach et al., 2011; Jourdan et al., 2013) is particularly informative, as it demonstrates how interpretations and ideas evolve when new data are available from a given study area. In the Alpine case, this task is facilitated by the huge amount of data collected by geologists in the past two centuries (see reviews in Handy et al., 2010; Malusà et al., 2015), and by recent provenance studies based on different independent constraints (see below).

7.1. Published detrital thermochronology studies in the Alpine region

The first detrital thermochronology study using the lag-time approach in the European Alps is provided by Bernet et al. (2001). They analyzed the ZFT fingerprint of the Neogene succession (15 Ma or younger deposits) exposed in the Northern Apennines, which led to the recognition of two different age components with rather constant lag times of ~8 Ma and ~17 Ma. Based on these data, Bernet et al. (2001) proposed that the Western and Central Alps were exhumed in steady state due to a combination of erosion and tectonic processes.

Two years later, Carrapa et al. (2003) applied the Ar-Ar method to detrital micas of the Oligocene-Miocene clastic sediments of the Tertiary Piedmont Basin. These sediments are exposed south of the Alps on top of the Alpine metamorphic wedge, and are considered to be derived from erosion of the Western Alps. This study found a young, persistent age peak around 37-38 Ma through the entire sedimentary succession, that was interpreted as the evidence of fast cooling and exhumation of the Western Alps prior to ~38 Ma, followed by a period of slower cooling and exhumation of crustal rocks with uniform Ar-Ar signature. These processes would have produced the observed trend of regularly increasing lag times up section. Note that this interpretation of rapid exhumation followed by slow exhumation of the Western Alps proposed by Carrapa et al. (2003) is not consistent with the steady-state exhumation model proposed by Bernet et al. (2001). One year later, Spiegel et al. (2004) provided additional detrital ZFT ages from the opposite sides of the Alps and underlined the issue of zircon recycling for data interpretation. In the Molasse of the North Alpine foreland basin, Spiegel et al. (2004) reported Cenozoic cooling ages that define a relatively constant lag time of ~10 Ma between 21 Ma and 19 Ma, decreasing to ~6 Ma between 19 and 14 Ma. Based on these data, they excluded exhumational steady-state conditions in the Central Alps before 14 Ma. They also presented detrital ZFT data from the Miocene deposits of the South Alpine foredeep, describing a stationary age peak at ~30 Ma associated with an older moving age peak also found in the same sedimentary layers. In the same Miocene deposits, Fellin et al. (2005) detected a stationary age peak at ~30 Ma defined by detrital AFT ages. Evidence against exhumational steady state was later presented by Kuhlemann et al. (2006), based on AFT data from detrital apatites shed from the Eastern Alps.

Three years later, Bernet et al. (2009) presented a more comprehensive dataset of detrital ZFT data from the Oligocene-to-Present sedimentary successions exposed on the opposite sides of the European Alps. They confirmed the presence of fairly constant lag-time values defined by youngest age peaks, supporting their proposal of a steady-state evolution of the Alpine belt since the Oligocene. According to Bernet et al. (2009), available detrital ZFT data would not provide any indications of major long-term changes of tectonic or climatic forcing during Alpine evolution. However, a different conclusion was reached in the same year by Carrapa (2009), who compiled the existing detrital thermochronologic datasets for the European Alps, and concluded that exhumation trends in the pro-foreland and retro-foreland basins correlate with orogenic wedge states inferred from propagation rates of the Alpine thrust fronts. In the pro-foreland of the Central and Eastern Alps, a trend of decreasing lag-time values suggested increasing exhumation rates from 30 to 10 Ma and subcritical taper conditions. The pro-foreland of the Western Alps recorded increasing exhumation rates between 38 and 36 Ma (suggesting a subcritical wedge state) and decreasing exhumation rates between 16 and 8 Ma (suggesting a supercritical state). In the retro-foreland of the Western Alps, the youngest age peak remained constant for >30 my, and therefore suggested to Carrapa (2009) rapid cooling and episodic exhumation of the Internal Crystalline Massifs (e.g., Gran Paradiso and Dora-Maira, GP and DM in Fig. 11a) and of the Periadriatic plutons (subcritical wedge state) followed by slower cooling (supercritical state). Changes in lag-time trends defining the transition between different wedge states are recorded synchronously by different thermochronologic systems within a single stratigraphic level (Carrapa, 2009), although such an occurrence should not be possible. This is because, as underlined by Bernet (2010), each thermochronologic system has a different sensitivity to upper crustal processes, and a different response time to changes in exhumation rates.

A few years later, Glotzbach et al. (2011) presented detrital AFT data from the North Alpine foreland successions to better resolve Miocene to Present exhumation in the Western Alps. They documented young AFT age peaks with lag times of less than 3 Ma before 13 Ma, and AFT age peaks with constant lag times around ~6 Ma during the last 10 Ma. According to Glotzbach et al. (2011), these data provided evidence of a steady state Miocene–Pliocene exhumation of the Western Alps, with the lag-time shift around 10-6 Ma reflecting a coeval drainage reorganization. Following a few years after the Glotzbach et al. study, Jourdan et al. (2013) published detrital AFT and ZFT data from Oligocene-Miocene sediments on the opposite sides of the Alps, integrated with zircon double dating. Their results were interpreted as evidence for short-lived fast erosional exhumation of the Paleogene wedge of the Western Alps between 30 and 28 Ma, followed by a slow down of erosion to rates similar to the rates observed today in the Western Alps.

7.2. Integration with information provided by other geologic data sets

Contrasting interpretations derived from different thermochronologic datasets from the same region (as described above in Section 7.1), can help in understanding potentials and limitations of a detrital thermochronologic approach solely based on the interpretation of selected age peaks. During the past decade or so, our understanding of the erosional evolution of the Alpine belt has been progressively improved by a number of independent provenance studies. For example, Garzanti and Malusà (2008) based on the analysis of bulk compositions, heavy minerals and ZFT from sedimentary rocks of the Adriatic foredeep, demonstrated that the Oligocene - middle Miocene successions of the Northern Apennines were chiefly fed by erosion of the Lepontine dome (in green in Fig. 15a), with only minor inputs (around 10% each) from the Western Alps and the Southern Alps. This implies that the dataset of Bernet et al. (2009) for the Adriatic foredeep largely records the exhumation history of the Lepontine dome, not of the entire Western and Central Alps. A few years later, Malusà et al. (2013) catalogued zircon U-Pb fingerprints of all the major sources of detritus of the Western and Central Alps. Those fingerprints were subsequently used to detect a switching of erosional foci from the eastern part of the Lepontine dome to its western part at 24-23 Ma, synchronous with a major tectonic phase of strike-slip activity along the Insubric Fault (Malusà et al., 2016c). LASS-ICP-MS depth-profiling of detrital zircons in the Aveto Formation (Anfinson et al., 2016) indicates that early Oligocene erosion was likely focused to the east of the Lepontine dome (Bergell area). This would imply a progressive shift of the site of erosion in the Central Alps, from the east to the west during the Oligocene-Miocene, rather than tectonic steady state. Zircon fertility maps for the European Alps, first produced in the same year (Malusà et al., 2016b), revealed that zircon fertility is particularly high in the Lepontine dome, especially in its eastern part. Therefore, the detrital ZFT record in the Apenninic foredeep is probably dominated by a Lepontine signal not only because of the sediment dispersal paths towards the Apenninic foredeep, but also because of the uneven distribution of mineral fertility in the Alpine source rocks. However, zircon grains, likely derived from the Adamello batholith in the Southern Alps have been detected in the upper Miocene deposits of the Adriatic foredeep based on their diagnostic U-Pb age fingerprint (Stalder et al., 2018), and a thermochronologic signal from the Western Alps can be still recognized in the sedimentary successions of the Adriatic foredeep by a careful analysis of thermochronologic age trends (see Section 7.3). A major impact of mineral fertility on the thermochronologic fingerprint of detritus is documented also in modern Alpine sediments (Fig. 9b), thanks to the integration of apatite trace-element and Nd-isotope analyses, fertility measurements, and cosmogenic-derived erosion rates

(Wittmann et al., 2016; Malusà et al., 2017). Within this framework, erosion of the Western Alps should be best recorded in the North Alpine foreland basin and in Tertiary Piedmont Basin, rather than in the Apenninic foredeep, where the detrital thermochronology record is likely dominated by inputs from the Central Alps (Fig. 15a). Different detrital thermochronology datasets previously published in the Alpine region may thus shed light on the long-term erosion history of different segments of the Alpine belt.

7.3. New interpretive keys applied to previous detrital thermochronology data sets

As presented above there is a wealth of detrital thermochronologic data for the European Alps. We present a synthesis of representative data sets from sedimentary basins surrounding the Alps (Fig. 15) that include ZFT from the Adriatic foredeep (Fig. 15b) , mica Ar-Ar from the Tertiary Piedmont Basin (Fig. 15c), ZFT (Fig. 15d) and AFT (Fig. 15e) from the North Alpine foreland basin (after Bernet et al., 2001, 2009; Dunkl et al., 2001; Carrapa et al., 2003, 2004; Glotzbach et al., 2011; Jourdan et al., 2013; Stalder et al., 2018). Different color intensities indicate the different size of each grain-age population, according to the keys reported on the top-right of Fig. 15. In the diagrams (in colors) on the left side of each frame (b-to-e), grain age populations are not ascribed *a priori* to any specific peaks, in order to avoid any preconceived interpretations. In the greyscale diagrams on the right side of each frame interpretive age trends are presented. All available grain-age populations younger than 50 Ma are reported with associated error (see original publications for details).

All of the diagrams of Fig. 15 invariably show several grain-age populations. This rules out the simplest lag-time scenario of Fig. 1a, which should imply only one single thermochronologic age peak that becomes progressively younger up section. The interpretation of these age patterns may thus benefit from the application of the guidelines and fundamental criteria summarized in Section 3.4 (criteria C1 to C15) and Section 4.7 (criteria M1 to M11). When these interpretation keys are applied, different thermochronologic systems provide a consistent picture of the Cenozoic evolution of the Alpine region, which is comparable to the complex tectonic evolution derived from independent geologic constraints, and indicates that exhumational steady state in the European Alps was not attained.

7.3.1. Detrital ZFT age trends, Adriatic foredeep

Detrital ZFT age distributions in sedimentary rocks from the Adriatic foredeep (Bernet et al., 2001; 2009; Dunkl et al., 2001; Stalder et al., 2018) (Fig. 15b) include several moving or stationary thermochronologic age peaks, marked by dots, which provide compelling evidence of a mixed provenance (criteria M1 and M2). The age of the youngest peaks progressively decreases up section, as expected in case of erosional exhumation (criterion C1). These youngest age peaks are more prominent (i.e., they have a darker color) in strata older than 20-15 Ma, and less prominent (i.e., they have a paler color) in strata younger than 20-15 Ma. This change in size of moving age peaks through a stratigraphic succession may support a major change in provenance during the Miocene (for example from an area characterized by higher zircon fertility to an area characterized by lower zircon fertility) (criterion M6). Other provenance changes are possibly suggested in the Adriatic foredeep data in Fig. 15b by the appearance of older grain-age populations moving up section (criterion M5), for example at ~23 Ma (A' in Fig. 15b). This scenario is consistent with information provided by other provenance studies, which suggest a shift in erosional foci in the Oligocene-Miocene from the eastern side of the Lepontine dome, where zircon fertility is higher, to the western side of the Lepontine dome, where zircon fertility is lower (see Section 7.2). Notably, lag-time values in Fig. 15b vary through time. They initially decrease from ~12 Ma to ~5 Ma in Oligocene strata (from A to B in Fig. 15b) and then progressively increase to >20 Ma (trend 1 in Fig. 15b). A trend of decreasing lag-time values up section is also observed in Miocene strata (from A' to B' in Fig. 15b), with lag-time values reaching ~7-10 Ma in Pliocene and modern strata (trend 2 in Fig. 15b). In this situation, changing lag-time values could either reflect a progressive change in erosion rate or a progressive readjustment of the thermochronologic age signal after a sharp tectonic event (see criterion C13 and Fig. 7a), for example the reactivation of the Insubric Fault between 30 Ma and 20 Ma (i.e., the ZFT ages corresponding to the changes in slope, B and B' in trends 1 and 2). The data set of Fig. 15b which previously may have been interpreted as being representative of apparent steady-state exhumation is therefore more suggestive of the situation illustrated in the conceptual model of Fig. 8, where age peaks from two different sources attest to migration of erosion across a mountain belt where steady state is not attained. In those cases, if mixed provenance is not detected, detrital thermochronology data may be erroneously interpreted as the evidence of steady state exhumation.

Classic reconstructions of the Adriatic foredeep evolution (e.g., Ricci Lucchi, 1986, 2003) have suggested major recycling of Burdigalian-Serravallian turbidites into the Adriatic foredeep during the late Miocene. Based on the concepts illustrated in Section 5.4 and Fig. 13, this hypothesis is not supported by detrital ZFT data. In fact, the prominent ZFT age peaks at 30-28 Ma detected in middle Miocene strata (J in Fig. 15b) are not found in upper Miocene strata, which indicates that sediment recycling, if any, was not overwhelming. The diagram of Fig. 15b also shows a stationary age peak at 34-33 Ma (trend 3 in Fig. 15b), progressively decreasing in population size from upper Oligocene to upper Miocene strata. Coexistence of this peak with a younger moving age peak ascribed to the Lepontine dome is supportive of an additional source of detritus (criterion M2) likely located outside of the Lepontine area. The ZFT ages that define this 34-33 Ma stationary age peak are consistent (criterion M7) with bedrock ZFT ages of ca. 34-30 Ma that are observed in the Paleogene wedge of the Western Alps (Malusà et al., 2005). The lack of a stationary age peak at 34-33 Ma defined by mica Ar-Ar ages (Fig. 15c) and of older moving age peaks defined by ZFT ages in Miocene strata (cf. criteria C8 and C11), are strong indications of thermochronologic ages set during thermal relaxation of eroded bedrock (criterion C12), as reasonably expected after fast exhumation of (ultra)high pressure rocks in the late Eocene (e.g., Liao et al., 2018a). Persistence of this stationary ZFT age peak from upper Oligocene to upper Miocene strata is supportive of slow erosion in the source area, in line with bedrock thermochronologic ages in the Western Alps attesting to exhumation rates of 0.1-0.3 km/Ma during the Neogene (Malusà and Vezzoli, 2006; Vernon et al., 2008). The impact of differential zircon fertility between rocks exposed in the Western Alps and more fertile rocks exposed in the Lepontine dome (Fig. 11a) is partly counterbalanced, in the detrital record of the Adriatic foredeep, by the larger area of the Western Alpine sources, which allows detection of the stationary ZFT age peak ascribed to the Western Alps even after sediment mixing. The Southern Alps represent an additional source of detritus delivered to the Adriatic foredeep (see Section 7.2). They have experienced fast erosion in the late Miocene, as shown by bedrock AFT data (Reverman et al., 2012; Zanchetta et al., 2015). However, no moving ZFT-age peak mirroring such erosion is found in the stratigraphic record of the Adriatic foredeep. This is because the rock pile with a ZFT fingerprint acquired before the onset of late Miocene erosion has not been completely removed in the Southern Alps, yet (criterion C4), as attested by bedrock ZFT ages invariably older than the Miocene (Bertotti et al., 1999; Viola et al., 2001).

7.3.2. Detrital mica Ar-Ar age trends, Tertiary Piedmont Basin

Application of the interpretive keys of Sections 3.4 and 4.7 to mica Ar-Ar data from the Tertiary Piedmont Basin (Fig. 15c) is even more informative. The dataset presented by Carrapa et al. (2003, 2004) includes two stationary age peaks at ~37-38 Ma (trend 4 in Fig. 15c) and ~43-45 Ma (trend 5 in Fig. 15c) that provide no direct constraint on exhumation (criterion C2). In fact, these peaks are likely the result of distinct episodes of syntectonic mica crystallization during metamorphism of the lower-grade units now exposed in the Paleogene wedge (Fig. 11a). They are not related to exhumation of the Dora-Maira, which was suggested by Carrapa (2009), because the Dora-Maira was still undergoing subduction at that stage (Rubatto and Hermann, 2001). Ar-Ar on micas from the Tertiary Piedmont Basin are fully consistent with P-T-t paths of metamorphic units exposed in the frontal part of the Alpine metamorphic wedge, to the west of the Dora-Maira. These units were already exhumed and at the surface while the Dora-Maira was undergoing subduction (Malusà et al., 2011b). The stationary age peaks documented by Carrapa et al. (2003, 2004) are also clearly unrelated to thermal relaxation after fast exhumation, with exhumation occurring at a later stage (i.e., after 35 Ma). Moreover, thermal relaxation would be expected to produce a single stationary age peak (criterion

C12), unlike what is observed. The overwhelming abundance of old Ar-Ar ages >50 Ma in micas of the Tertiary Piedmont Basin suggests mixing of detritus derived, in some cases, from tectonic units largely unaffected by Alpine metamorphism. Persistence of the young thermochronologic age signal at ~37-38 Ma, which is never prominent through the stratigraphic sequence, suggests slow erosion of the corresponding source. This is in accordance with the absence of moving age peaks, which indicates that the removal of the rock pile with a thermochronologic fingerprint acquired before the onset of erosion is still largely incomplete (criterion C4).

7.3.3. Detrital ZFT and AFT age trends, North Alpine foreland

In the North Alpine foreland basin, detrital ZFT age distributions (Fig. 15d) include several age peaks attesting to mixed provenance (criterion M1). ZFT ages of ~30 Ma in lower Oligocene strata (K in Fig. 15d) may either indicate short lag-times attesting to fast erosion, or magmatic crystallization linked to the Alpine magmatic climax (vertical dashed line in the lag-time diagram). Notably, despite zircon double-dating being performed on samples from the North Alpine foreland basin, shallow-depth zircon crystallization cannot be safely excluded, because U-Pb ages were collected from zircon cores (Jourdan et al., 2018) which may be inherited. In that case, the old (50-45 Ma) moving age peaks documented by Bernet et al. (2009) and Jourdan et al. (2013) in Oligocene strata to the west of the Alps (trend 6 in Fig. 15d) may provide information on the geologic evolution of the country rock (criterion C11). The lag-time decrease recorded in lower Miocene strata (from A to B, trend 7 in Fig. 15d) likely reflects an increase in erosion rate at 24-23 Ma that is also documented in the detrital thermochronology record of the Adriatic foredeep (cf. Fig. 15b).

Detrital AFT data, in the upper Miocene succession of the North Alpine foreland basin, define a sharp decrease in lag times for the youngest grain-age population (trend 9 in Fig. 15e) (Glotzbach et al., 2011; Jourdan et al., 2013). The youngest AFT age peaks are statistically overwhelming and progressively larger in sedimentary rocks as young as 12-10 Ma, but much less prominent in sedimentary rocks younger than 6 Ma. Such variations in peak size, also corresponding to a jump towards older ages (L in Fig. 15e) moving up section, provide further support to the hypothesis of Glotzbach et al. (2011) of a major provenance change in the late Miocene (criterion M6), which is possibly linked to the exhumation of the External Massifs. Detrital thermochronology data from the North Alpine foreland basin thus indicate contributions from different eroding sources. These sources are different from those (e.g., the Lepontine dome) identified in the sedimentary successions of the Adriatic foredeep (cf. Section 7.3.1), which confirms that previously-published data sets provide constraints on the long-term erosion history of different segments of the Alpine belt.

Figure 15

8. Application to sedimentary successions: Taiwan

The late Cenozoic Taiwan orogen is a crucial region for the development of critical wedge models of mountain building (Suppe, 1981; Davis et al., 1983; Dahlen et al., 1984; Willett et al., 2003). This region currently experiences some of the highest exhumation rates in the world (3-5 km/Ma) (e.g., Liu et al., 2000; Dadson et al., 2003; Fuller et al., 2006; Lee et al., 2015; Hsu et al., 2016; Resentini et al., 2017). Detrital thermochronology studies from Taiwan are thus particularly relevant to demonstrate how the interpretive criteria illustrated in Sections 3.4 and 4.7 can be applied to a young active orogen, where the time elapsed between cooling and deposition can be particularly short, and the erosion pattern may vary through time as a response to active tectonic processes.

8.1. Tectonic setting of Taiwan

Taiwan is located at the boundary between the Philippine Sea plate and the Eurasian plate (Fig. 16a). This area has evolved from being part of an east-dipping intra-oceanic subduction zone with a volcanic arc and a submarine accretionary wedge to become a ~4 km-high subaerial orogen following Neogene collision of the Luzon arc with the Chinese continental margin (Suppe, 1984; Lundberg et al., 1997; Lin et al., 2003; Fisher et al., 2007; Mesalles et al., 2014). Plate-motion constraints (Seno et al., 1993; Yu et al., 1987) and the marked obliquity of the Luzon arc relative to the Chinese margin (CMMA in Fig. 16a) suggest that arc-continent collision may have propagated southward at a rate of ~60 km/Ma (Byrne and Liu, 2002).

According to most authors, the onset of arc-continent collision in northern and central Taiwan lies between 6.5 and 4 Ma (see review in Byrne et al., 2011). An age of ~4 Ma was first proposed for the onset of collision in northern Taiwan by Suppe (1981) on the basis of plate-tectonic reconstructions, whereas an age of ~6.5 Ma is supported by a regional unconformity recognized in the foredeep succession west of Taiwan, possibly marking the onset of flexurally controlled foreland-basin deposition (Lin et al., 2003). The stratigraphic record in the Coastal Range, on the eastern side of the island, suggests that a proto-Taiwan orogenic belt was likely first exposed to subaerial erosion since at least the early Pliocene (Dorsey and Lundberg, 1988; Kirstein et al., 2010). A steady southward propagation of arc-continent collision has been proposed by several authors (e.g., Willett et al., 2003; Simoes et al., 2007; Stolar et al., 2007), whereas other authors have argued for a more complicated collision history, with punctuated events possibly controlled by the irregular shape of the subducted continental margin (Lee et al., 2006; Mouthereau and Lacombe, 2006; Hsu et al., 2016). Unlike the European Alps and the Himalaya, where hard collision and subaerial topographic growth occurred well-after the onset of submarine continental accretion

(Gansser, 1982; Malusà and Garzanti, 2012), Taiwan is characterized by a much shorter time interval between these two different tectonic stages, which makes the interpretation of thermochronologic data challenging (Mesalles et al., 2014; Chen et al., 2019). A careful inspection of detrital thermochronologic age trends in sedimentary successions is thus particularly important. On the retro-side (eastern) of the Taiwan orogen, where erosion is faster, bedrock ZFT ages are generally younger than 3 Ma (Willett et al., 2003; Lee et al., 2015; Chen et al., 2019), and zircon grains presently exposed at Earth's surface have been completely reset during the Neogene (Fig. 16a).

8.2. Detrital thermochronology record in the Coastal Range

Owing to the high erosion rates documented in Taiwan, bedrock thermochronologic data mainly record the latest stages of orogen development. However, the early stages of mountain growth are recorded in Plio-Pleistocene stratigraphic successions exposed, for example, in the Coastal Range on the upper-plate side of the island (Kirstein et al., 2010; 2014). The Coastal Range includes kilometres of Taiwan-derived Plio-Pleistocene sediments lying on top of Miocene volcanic and volcaniclastic rocks of the Luzon arc (Dorsey, 1992). Sedimentological observations document dominant sediment transport directions towards the east and the south-southeast, and no major provenance change during the last 5-4 Ma (Chen and Wang, 1988; Dorsey, 1988; Dorsey and Lundberg, 1988).

8.2.1 Detrital ZFT age trends and application of interpretive keys

Published detrital ZFT data from the sedimentary successions of the northern Coastal Range (Kirstein et al., 2010) are summarized in Fig. 16b. As in Fig. 15, populations younger than 50 Ma are reported with associated errors (see the original publication for details) and are not ascribed *a priori* to any specific peaks. Different color intensities indicate the different size of each grain-age population. As underlined by Kirstein et al. (2010), ZFT ages in sediments older than ~2 Ma were not reset by the Neogene Taiwan orogeny (Fig. 16b). Grain-age distributions in these sediments are in fact markedly polymodal, with the presence of several moving age peaks generally older than 50 Ma, suggesting sediment mixing from different sources (criterion M1). These peaks therefore do not provide a direct measure of exhumation rates during arc-continent collision, as they reflect the geologic history of older sediment sources located outside of the orogenic wedge. By contrast, much younger ZFT age peaks are found in sediments younger than 2 Ma (trend 1 in Fig. 16b). Short lag times associated with these peaks suggest that exhumation, transport and deposition occurred within 0.4-1.5 Ma, which would point to exhumation rates around 1.6-2.5 km/Ma (Kirstein et al., 2010). These young peaks become progressively larger moving up section. Young age peaks are dominant in samples with depositional age around ~1 Ma (Fig. 16b), and overwhelming in modern sediments (Fellin et al., 2017) as shown by the progressively darker colors in the lag-time diagram of Fig. 16b. However, small older-age peaks are still found in sediments younger than 2 Ma (e.g., J in Fig. 16b), which suggests that mixing between reset and (likely minor) unreset sources also occurred, prior to deposition, in higher (younger) stratigraphic levels. A similar detrital ZFT record is also reported from the orogen pro-side on the western side of Taiwan (Mesalles et al., 2014), where Pleistocene sediments include young age peaks at 6.7 and 4.3 Ma, and Pliocene sediments only include age peaks not younger than 22 Ma (small red dots in Fig. 16b).

In summary, the lower part of the Plio-Pleistocene succession of the northern Coastal Range likely reflects the early stage removal of the sedimentary cover during the onset of arc-continent collision, before the first appearance of a young moving age peak that can be used to constrain the syn-collisional exhumation rate (criterion C4). The onset of fast erosion in the accretionary wedge west of the northern Coastal Range can be constrained to be not younger than ~4±1 Ma, as indicated by the ZFT ages that define the youngest moving-age peaks (K in Fig. 16b, criterion C5). However, this is a conservative estimate. Because of the sudden increase in erosion rates after the onset of arc-continent collision, isotherms have initially moved (were advected) with the same velocity of the rocks relative to Earth's surface, until they have reached a new steady state depth (cf. Fig. 3a). This implies that arc-continent collision may have started a few millions of years earlier than the age recorded by ZFT, i.e. in the late Miocene, which is consistent with the age of the regional unconformity recognized in the foredeep succession on the orogen pro-side (~ 6.5 Ma; Lin et al., 2003).

Detrital ZFT data from the northern Coastal Range demonstrate that most of the rock pile with a thermochronologic fingerprint acquired before the onset of arc-continent collision was removed by 2 Ma, as indicated by the progressive appearance of young ZFT ages in sediments younger than 2 Ma. Notably, a young ZFT age peak is also found in sediments as old as 3 Ma (L in Fig. 16b), but it is volumetrically minor and likely derived from a source of reset zircon grains possibly located farther north, and initially exhumed at an earlier stage of arc-continent collision as discussed in Section 8.3.

In the southern Coastal Range, sediments from the 2-1 Ma stratigraphic interval are dominated by old ZFT age peaks (Fig. 16c). These old age peaks indicate that the rock pile with a thermochronologic fingerprint acquired before the onset of arc-continent collision was not completely removed one million years ago (Kirstein et al., 2014). However, it is now completely eroded away, as attested by ZFT data in bedrock (Lee at al., 2015) and modern sediments (Fig. 16c). The onset of erosion along this orogenic section cannot be determined precisely, because of the sparse sampling density in the 0-1 Ma stratigraphic interval (Fig. 16c). However, it can be bracketed, as a conservative estimate, between 0.6 Ma (the age of the youngest peak in modern sediment, M in Fig. 16c) and ~ 4 Ma (the age of the youngest peak in Pleistocene samples, N in Fig. 16c).

The inferred north-south delay in the removal of the unreset sedimentary cover, as inferred by detrital thermochronology data in the northern and southern Coastal Range, is consistent with the tectonic framework presented in Section 8.1 (Byrne et al., 2011), and with a progressive southward propagation of arc-continent collision. Fast erosion rates may have initially affected, in the late Miocene, the accretionary wedge in front of the northern Coastal Range, followed one million year later by rapid erosion of the accretionary wedge in front of the southern Coastal Range. However, at that time fast erosion rates had not yet affected the Hengchun Peninsula in southern Taiwan (HoP in Fig. 16a). The Hengchun Peninsula forms the recently emerged portion of the accretionary wedge, and presently shows subdued topography and exposure of rocks with partially reset AFT ages (Chen et al., 2019).

8.2.2. Impact of variable zircon fertility on the detrital ZFT record of eastern Taiwan

The variable mineral fertility of eroded bedrock can have an impact on the potential detection of a thermochronologic signal marking the onset of arc-continent collision in the stratigraphic record. Based on the zircon fertility map of Taiwan (Fig. 11b), and the evolution depicted in Section 8.2.1, the impact of differential mineral fertility on the detrital thermochronologic record of Fig. 16 is expected to be potentially relevant. On the orogen retro-side, zircon fertility values are particularly high in rocks of the Tananao Complex exposed between latitude 23°N and latitude 24°N, but they are 4-to-8 times lower in rocks exposed north of latitude 24°N and south of latitude 23°N. Therefore, the ZFT reset zone, delimited by the dashed purple line in Fig. 16a, can be divided into three parts based on the zircon fertility: a northern low-fertility part, a central high-fertility part, and a southern low-fertility part. A similar uneven distribution of zircon fertility could be reasonably expected also in the late Miocene.

Because of the progressive southward propagation of arc-continent collision, fast erosion rates may have first affected the northern low-fertility part of the ZFT reset zone, and only at a later stage the central high-fertility and southern low-fertility parts. Zircon grains determining the first appearance of a young ZFT-age peak in the sedimentary record should thus derive from low-fertility rocks of the northern part of the ZFT reset zone. Notably, these zircon grains are likely mixed in the final sink with zircon grains derived from higher-fertility rocks of the central part, yielding at this stage zircon grains with older ZFT ages. Older ZFT ages will be thus overwhelming in the final sink, just because of the higher zircon fertility of the corresponding source (criterion M8). Instead, the onset of fast exhumation in the northern part of the ZFT reset zone, which should be revealed by the first appearance of a young ZFT age peak in the sedimentary record, may even remain undetected (see Fig. 10). Within this framework, the small relatively young ZFT age peak (L in Fig. 16b) detected by Kirstein et al. (2010) in sediments deposited ~3 Ma ago (peak age = 7.6 ±1 Ma; peak size = 1%; see) may reflect the onset of arc-continent collision in the northern part of the ZFT reset zone, providing further support to a southward progression of arc-continent collision as proposed by previous work (Byrne et al., 2011).

Figure 16

9. Application to sedimentary successions: Himalaya

The Himalayas mark the Cenozoic collision zone between India and Eurasia (Fig. 17a) and form the highest mountains on Earth (Gansser, 1964; LeFort, 1975; Najman et al., 2010a; Hu et al., 2016). A reliable reconstruction of Himalayan topographic and denudational evolution is the starting point for studies aimed at understanding collision processes and the potential feedbacks between tectonics and climate (e.g., Molnar et al., 1993; Raymo, 1994; Thiede et al., 2004; Grujic et al., 2006; Clift et al., 2008; Godard et al., 2014; Clift and Webb, 2018). However, available reconstructions of the spatial and temporal evolution of the Himalayas still remain controversial (e.g., Burbank et al., 1993; Métivier et al., 1999; Clift and Gaedicke, 2002, Vance et al. 2003, Vannay et al., 2004; Thiede and Ehlers, 2013; Tremblay et al., 2015; Stübner et al., 2018). Because of the fast exhumation characterizing parts of the Himalaya, thermochronologic systems such as mica Ar-Ar, ZFT and AFT, when applied to bedrock typically yield very young ages on the order of few millions of years (e.g., Zeitler et al., 2001; Herman et al., 2010; Gemignani et al., 2018), and do not address earlier geologic events. Many scientists have thus applied a detrital thermochronologic approach to reveal the exhumation history of the Himalaya on longer timescales, based on the thermochronologic analysis of the sedimentary successions either accreted on the southern side of the orogen, or accumulated in the Himalayan foreland basin and in the Indus and Bengal fans, largely fed by Himalayan erosion (e.g., Cerveny et al., 1988; Copeland et al., 1990; Corrigan and Crowley, 1990; White et al., 2002; Szulc et al., 2006; van der Beek et al., 2006; Zhuang et al., 2015; Clift, 2017; Najman et al., 2019; Stickroth et al., 2019). The Himalayan region is therefore an ideal site not only to illustrate the detrital thermochronologic age trends defined by different thermochronologic systems in a large source-to-sink system, but also to compare the detrital thermochronologic record in distal and more proximal sediment sinks.

9.1. Tectonic framework of the Himalayas

The Himalayan mountain belt is classically subdivided into four tectonic domains parallel to the orogen trend. From the North to the South, they are: the Tethys Himalaya, the Greater Himalaya, the Lesser Himalaya, and the Sub-Himalaya (e.g., Hodges, 2000; DeCelles et al., 2016; Garzanti, 2019). These tectonic domains are separated by north-dipping crustal-scale faults developed above the subducting Indian plate (Zhao et al., 1993; Yin and Harrison, 2000; Avouac, 2003) (Fig. 17a).

The Tethys Himalaya includes Cambrian-to-Eocene sedimentary and low-grade metamorphic rocks, exposed along the southern border of the Tibetan Plateau and separated from the underlying Greater Himalaya by the extensional Southern Tibetan Detachment fault (Burg et al., 1984). The Greater Himalaya forms the topographic backbone of the Himalayan range. It consists of high-grade metamorphic rocks intruded by upper Oligocene - Miocene (25-15 Ma) leucogranites (Guillot et al., 1994, Hodges et al., 1996; Weinberg, 2016), and overthrust onto the Lesser Himalaya along the Main Central Thrust (Searle et al., 2008). Based on classic tectonic models, simultaneous activity of the Southern Tibetan Detachment and the Main Central Thrust at 25-15 Ma would have allowed extrusion of rocks now forming the Greater Himalaya from beneath the Tibetan Plateau (Hodges, 2000; Beaumont et al., 2001; Godin et al., 2006). The Lesser Himalaya mainly includes Proterozoic-to-Paleozoic (meta)sedimentary rocks that overthrust the Neogene Siwalik successions of the Sub-Himalaya along the Main Boundary Thrust (Meigs et al.,1995; DeCelles et al., 2001; Huyghe et al., 2005). The Siwalik successions are in turn accreted along the Main Frontal Thrust onto the Himalayan foreland (DeCelles et al., 1998; Burgess et al., 2012) (Fig. 17a).

Two major syntaxes, namely the Nanga Parbat and Namche Barwa syntaxes, are found at either ends of the orogen, where the Indus and Yarlung Tsangpo rivers cut impressive gorges across crustal-scale antiforms (Burg et al., 1998; Rolland et al., 2001; Finnegan et al., 2008). Along the Himalayan syntaxes, exposure of granulite-facies rocks and anatectic granites as young as the Plio-Pleistocene indicates extremely fast erosion, as confirmed by the very young (even < 1 Ma) thermochronologic ages in bedrock and modern sediments (Zeitler et al. 2001; Enkelmann et al., 2011; Bracciali et al., 2016; Lang et al., 2016; Gemignani et al., 2018).

9.2. Detrital thermochronology data from the Sub-Himalaya

Starting from the pioneering work of Cerveny et al. (1988), the Neogene successions of the Sub-Himalaya have been characterized by detrital AFT, ZFT and mica Ar-Ar thermochronologic data with progressively more detail (e.g., White et al., 2002; Bernet et al., 2006; Szulc et al., 2006; van der Beek et al., 2006; Najman et al., 2009; Chirouze et al., 2012; Stickroth et al., 2019). Cerveny et al. (1988) applied a detrital ZFT approach to the Indus River modern sands and to the Neogene successions deposited by the ancestral Indus River over the past 18 Ma. They systematically detected distinctive populations of young zircon grains yielding ZFT ages that are 1 to 5 Ma older than the depositional age of the sandstones. Based on their results, Cerveny et al. (1988) concluded that a series of uplifted blocks, analogous to the contemporary Nanga Parbat massif, have been continually present in the Himalaya since 18 Ma, and that over that time the elevation and relief of the Himalaya have been essentially constant.

More recently, White et al. (2002) provided mica Ar-Ar data from the lower–middle Miocene (21-12.5 Ma) molasse of Northern India (Dharamsala and Lower Siwalik Formations). They found that Ar-Ar ages of detrital micas in the 21-17 Ma Lower Dharamsala Formation contrast strongly with the detrital mica ages in the 17-12.5 Ma Upper Dharamsala and Lower Siwaliks Formations. This would suggest a major reorganization of the Himalayan orogenic wedge at 17 Ma, after cessation of rapid exhumation of the Greater Himalaya and subsequent thrust propagation towards the foreland. A few years later, Szulc et al. (2006) extended the analysis of White at al. (2002) to the Siwaliks of southwestern Nepal (stratigraphic age range 16-1 Ma). They documented detrital mica Ar-Ar ages defining peaks at 20-15 Ma, interpreted as the period of most extensive exhumation of the Greater Himalaya. According to Szulc et al. (2006), lag times <5 Ma persisting until 10 Ma suggested Greater Himalaya exhumation at rates up to 2.6 km/Ma, whereas a lag-time increase since 10 Ma would suggest a switch since then in the dynamics of the orogen, such that strain began to be accommodated by structures within the Lesser Himalaya. These studies were further developed by Najman et al. (2009, 2010b), who provided detrital mica Ar-Ar data from a more complete stratigraphic succession spanning through the entire Miocene. Najman et al. (2009, 2010b) detected short lag times until 16 Ma and a major provenance change at 6–7 Ma. These data, according to Najman et al. (2009, 2010b), would suggest a slow down in Greater Himalaya exhumation at 16–17 Ma, subsequent thrust propagation south of the Main Central Thrust, and progressive erosion of the Lesser Himalaya with final exposure of the metamorphosed Inner Lesser Himalaya by 6 Ma.

Van der Beek et al. (2006) analyzed sediments from Siwalik successions of the western and central Nepal using a detrital AFT approach. They showed that samples from the upper part of the analyzed successions are unreset and thus retain a signal of source-area exhumation, at rates ranging from 1.8 km/Ma (in central Nepal) to 1-1.5 km/Ma (in western Nepal) over the last 7 Ma. In the uppermost part of the analyzed sections, they described potential evidence for major apatite recycling within the Siwalik belt, whereas the partially reset deeper samples record the activation of the Main Frontal Thrust at ~2 Ma. Bernet et al. (2006) applied a double-dating approach (ZFT and zircon U-Pb analyses) to the same stratigraphic successions analyzed by van der Beek et al. (2006), and were able to discriminate different zircon sources based on the diagnostic U-Pb age signatures of the Lesser, Greater and Tethys Himalayas (Parrish and Hodges, 1996; DeCelles et al., 2000, 2004). In the detrital ZFT record of the Siwaliks, Bernet et al. (2006) recognized two age peaks at 80-150 Ma and ~16 Ma, interpreted as stationary age peaks, and a younger moving age peak that suggests continuous exhumation of rocks of the Greater and the Lesser Himalayas at a rate of ~1.4 km/Ma since the middle Miocene. According to Bernet et al. (2006), the older "stationary" age peak at 80-150 Ma reflects the evolution of source rocks eroded from the Tethys Himalaya, whereas the stationary age peak at ~16 Ma, defined by zircons likely derived from the Greater and the Lesser Himalayas, would attest cooling related to a combination of tectonics and erosion during simultaneous activity of the Main Central Thrust and the Southern Tibetan Detachment. More recently, Braun (2016) analyzed the dataset provided by Bernet et al. (2006) using a numerical modeling approach. According to Braun (2016), the young stationary age peak (at ~16 Ma) described by Bernet et al. (2006) could be explained by a sudden cessation of rock extrusion due to channel flow (see Beaumont et al., 2001) at 13-15 Ma, and subsequent relaxation of isotherms that "may have created a thick iso-age crustal plug south of the Southern Tibetan Detachment that has been progressively exhumed at a much slower rate by isostatically-driven erosional rebound or motion along a more frontal structure such as the Main Frontal Thrust or Main Boundary Thrust" (Braun, 2016).

Studies by van der Beek et al. (2006) and Bernet et al. (2006) were subsequently integrated by Chirouze et al. (2012), who performed additional detrital AFT and ZFT analyses in the Siwaliks of eastern Nepal, and by Stickroth et al. (2019), who extended the existing detrital ZFT and mica Ar-Ar datasets to the lower Miocene successions of southern Nepal, also providing detrital monazite Th-Pb and zircon U-Pb ages. The polymodal grain-age distributions reported by Stickroth et al. (2019) include prominent ZFT age peaks at ~28-24 Ma, and small mica Ar-Ar age peaks at ~40-30 Ma, representing the youngest grain-age populations of each method in lower Miocene strata. According to Stickroth et al. (2019), the analyzed lower Miocene succession was dominated by detrital inputs from the Tethys Himalaya. Lag times of ~10 Ma for the youngest ZFT age peaks, and ~20 Ma for the youngest mica Ar-Ar age peaks, when compared with results from previous work in the middle-upper Miocene successions, would be consistent with an overall acceleration of Himalayan exhumation from ~40 Ma to the Present.

9.3. Detrital thermochronology data from the Bengal Fan

Starting with Ocean Drilling Program (ODP) Leg 116 core samples (Cochran et al., 1990), low-temperature thermochronologic techniques have been also applied to sediments of the Bengal Fan (Copeland and Harrison, 1990; Corrigan and Crowley, 1992; Najman et al., 2019). These sediments, beside minor contributions from the Indo-Burma Range and Peninsular India, mainly derive from erosion of the central-eastern Himalaya (France-Lanord et al., 2016; Blum et al., 2018), also including the Namche Barwa syntaxis. Corrigan et al. (1990) and Copeland and Harrison (1990) first applied the Ar-Ar technique to detrital micas and K-feldspars of the ODP Leg 116 cores, in strata from the distal Bengal Fan with depositional ages between 0 Ma and 17 Ma. In each sample, they found micas with thermochronologic ages essentially identical to the depositional ages. Based on these results, they concluded that a significant portion of the material in the Bengal Fan was first-cycle detritus derived from the Himalaya, and that the southern slope of the orogen, near the Main Central Thrust, experienced fast erosion during the entire Neogene. In the same years, Corrigan and Crowley (1990, 1992) analyzed samples from ODP Leg 116 cores by the AFT method. They reported pooled AFT ages that are 0 to 10 Ma older than the depositional ages (i.e., lag-times of 0 to 10 Ma) suggesting a rapidly cooled source, which was also supported by AFT length distributions measured in these distal sediments. According to Corrigan and Crowley (1992), the detrital AFT record in the distal Bengal Fan provides evidence for a nearly continuous unroofing of a large source area, similar to the dimensions of the present Himalayan and southern Tibetan Plateau deformation front, and of an efficient transport system supplying sediment to the Bengal Fan since the early Miocene. Shorter lag times in the detrital AFT record since 6-7 Ma led them to suggest accelerated denudation in the source area, possibly due to the gravitational collapse of the Tibetan Plateau (Corrigan and Crowley, 1992).

More recently, a multi-method detrital thermochronology study of mid-Bengal Fan sediments, on samples collected during the International Ocean Discovery Program (IODP) Expedition 354 (France-Lanord et al., 2016) involved apatite and rutile U-Pb, mica Ar-Ar and ZFT (Najman et al. (2019). Based on the ZFT and rutile U-Pb data, Najman et al. (2019) detected a shift towards very short lag times (<1 Ma) at ~4 Ma, interpreted to mark the onset of extremely rapid exhumation of the Namche Barwa syntaxis, which would rule out a previous hypothesis of rapid syntaxial exhumation stretching back to 10 Ma (Zeitler et al., 2014). The Najman et al. data also negates previous indications of a continuous record of fast exhumation during the entire Neogene which was suggested by detrital mica Ar-Ar data (Copeland and Harrison, 1990). Lag times <1 Ma, detected by Najman et al. (2019) in the 17 to ~14 Ma stratigraphic interval, were interpreted to reflect the rapid exhumation of the Greater Himalaya, whereas longer lag times in the 12 to 5 Ma stratigraphic interval would mirror subsequent passive erosion of Greater Himalayan rocks. Najman et al. (2019) found that the detrital mica Ar-Ar dataset from the mid-Bengal fan was not sensitive to syntaxial exhumation, possibly due to a low mica fertility in lithologies of the Namche Barwa syntaxis. This latter observation underlines the importance of reliable mineral fertility determinations for a fruitful approach to detrital thermochronology studies. Mineral fertility maps are not available for the Himalaya, yet, but should be a primary target for future studies.

9.4. Application of interpretive keys to datasets from Sub-Himalaya and Bengal Fan

Figure 17 shows a synthesis of detrital thermochronology data sets from sedimentary successions of the Sub-Himalaya (b-to-d; White et al., 2002; Bernet et al., 2006; Szulc et al., 2006; van der Beek et al., 2006; Najman et al., 2009; Chirouze et al., 2012; Stickroth et al., 2019) and the Bengal Fan (e-to-g; Corrigan and Crowley, 1990; Najman et al., 2019) deposited during the past 17 Ma. In the diagrams (in colors) on the left side of each frame, grain-age populations younger than 25 Ma are reported with associated error, and are not ascribed *a priori* to any specific peaks. Different color intensities (blue = AFT; purple = ZFT; orange = mica Ar-Ar) indicate different population size according to the keys reported on the top-right of Fig. 17. In the greyscale diagrams on the right side of each frame (b-to-g in Fig. 17) are shown the interpretive age trends discussed in the text. Grain-age populations in these lag-time diagrams are progressively shifted towards older ages for progressively higher-T_c systems, as normally expected during erosional unroofing of an orogenic belt (see Section 3).

9.4.1. Detrital AFT age trends, Sub-Himalaya

Detrital AFT data from the Siwaliks (van der Beek et al., 2006; Chirouze et al., 2012) are summarized in the lag-time diagram of Fig. 17b. In the uppermost part of the stratigraphic succession, including sediments deposited during the past 7-8 Ma, detrital AFT ages define two major moving age peaks and a stationary peak, attesting to a mixed provenance (criterion M1). The youngest moving age peak (trend 1 in Fig. 17b) is more prominent, as indicated by darker colors. Associated lag-time values are rather constant being generally <5 Ma and thus indicative of rapid exhumation, but lag-times may vary according to the location of analyzed successions along the Himalayan orogenic front (see van der Beek et al., 2006 for details). The second moving age peak (trend 2, from A to B in Fig. 17b) is less prominent, as indicated by paler colors, and is associated to lag-time values progressively decreasing up section (indicative of increasing rates of exhumation), from ~15 Ma (for depositional ages around 8-7 Ma) to <5 Ma (for depositional ages around 6-5 Ma). The stationary age peak (trend 3 in Fig. 17b) is defined by AFT ages around 15 Ma and can be recognized in sediments deposited from ~7 Ma to ~3 Ma. The geologic processes behind this stationary age peak are discussed in more detail below.

A different AFT age pattern is observed in Siwalik sediments older than 7-8 Ma. In this stratigraphic interval, the youngest and most prominent age peak gets progressively younger down section (Fig. 17b), defining a trend (4a in Fig. 17b) that is opposite to the trend observed in the uppermost stratigraphic levels (van der Beek et al., 2006). Lag-time values associated with this peak consequently decrease down section, and become negative in sediments older than 8-9 Ma. Such a reversal is not observed in higher-temperature-method detrital datasets (ZFT and mica Ar-Ar) from the same stratigraphic levels (see Fig 17c, d). The diagnostic trend exhibited by detrital AFT data in this interval documents the major role exerted by post-depositional AFT annealing towards the base of the thick Siwalik succession (van der Beek et al., 2006) (see Section 6). A smaller population of apatite grains, yielding AFT ages around 12-15 Ma in sediments older than 7-8 Ma, also exhibits a reverse age trend that is less pronounced (trend 4b in Fig. 17b). This smaller population likely includes more retentive apatites that are less affected by post-depositional annealing during sedimentary burial.

In the uppermost part of the Siwalik successions, older AFT age peaks >20 Ma suddenly appear in sediment deposited at ~5 Ma (K in Fig. 17b), whereas the youngest AFT age peak shows a marked shift towards older ages in sediments deposited between 4-3 Ma and ~1 Ma (L in Fig. 17b). These observations are supportive of major provenance changes during the last 5 Ma (criterion M5), which may also reflect the activation of the Main Frontal Thrust. Thermochronologic evidence of activation of the Main Frontal Thrust at ~2 Ma is provided by modelling of AFT length distributions in the most deeply buried and strongly annealed samples of the Siwalik successions, which constrains the exhumation of the frontal Siwaliks at ~2 Ma (van der Beek et al., 2006). The stationary AFT age peak at ~15 Ma, detected in the stratigraphic interval between ~7 Ma and ~3 Ma (trend 3 in Fig. 17b), is also marked by detrital ZFT ages (but in the stratigraphic interval between ~5 Ma and 0 Ma, see Section 9.4.2). The observation that these stationary age peaks are found in progressively younger stratigraphic units for progressively higher-T_c systems, supports the hypothesis of a thermochronologic fingerprint acquired during thermal relaxation of eroded bedrock after fast exhumation (criterion C12). In Pliocene or younger sediments, the lack of major AFT age peaks inherited from older strata rules out the hypothesis of major post-Miocene sediment recycling in the Siwalik basin (see Section 5.4).

9.4.2. Detrital ZFT age trends, Sub-Himalaya

Detrital ZFT data from the Siwaliks (Bernet et al., 2006; Chirouze et al., 2012; Stickroth et al., 2019) are summarized in the lag-time diagram of Fig. 17c. According to Bernet et al. (2006), who plotted the first detrital ZFT data from this region using a logarithmic scale for the ZFT age axis, a young moving age peak exists in the Siwalik data set, as well as two older "stationary" age peaks at ~16 Ma and 80-150 Ma. Based on the fundamental criteria listed in Section 4.7, the presence of a moving age peak that is younger than a stationary age peak in the same stratigraphic level provides evidence for a mixed provenance (criterion M2). However, a word of caution about lag-time diagrams that use a logarithmic scale to report detrital thermochronologic ages is that they may lead to an overestimation of old "stationary" age peaks, at the expense of moving age peaks which may remain undetected. When detrital ZFT data from the Siwaliks are plotted using a linear scale for ZFT age (Fig. 17c), the resulting thermochronologic age trends are much more informative. Besides a young moving age peak recognized in the entire stratigraphic succession (trend 5a-5b in Fig. 17c), and the previously mentioned stationary age peak at ~15-14 Ma best detected in sediments younger than 5 Ma (trend 6 in Fig. 17c), a second moving age peak (trend 7 in Fig. 17c) generated by an additional eroding source becomes evident between A and B starting from sediments at least as old as 8 Ma.

The youngest ZFT age peak of Fig. 17c is most prominent in samples older than 10 Ma (trend 5a). In sediments belonging to the 17-10 Ma stratigraphic interval, lag-time values progressively decrease up section from ~7 Ma to ~3 Ma. In sediments deposited at 10-9 Ma, the youngest ZFT age peak shows a sharp shift towards older ages (J in Fig. 17c), with consequent lag-time increase to >5 Ma. This sharp shift is also supportive of a major provenance change and input of detritus from an additional eroding source since ~10 Ma (criterion M5). In sediments younger than 9 Ma (trend 5b in Fig. 17c), lag-time values progressively decrease up section from >5 Ma (for depositional ages around 9 Ma) to ~4 Ma (for depositional ages around 7 Ma) and remain steady since then.

The second moving age peak (trend 7 in Fig. 17c), previously undetected, is quite prominent in strata of 8 to 5-4 Ma and associated with lag-time values decreasing up section from ~17 Ma (for depositional ages around 8 Ma) to ~5 Ma (for depositional ages around 5-4 Ma). Double-dated grains (Bernet et al., 2006) that define this peak have a diagnostic Lesser Himalayan signature, given by U-Pb ages of ~1.8 and ~2.5 Ga. This signature, indicated by black squares in Fig. 17c, contrasts with the Greater Himalayan signature (i.e., dominant U-Pb ages of 1.1 Ga, in addition to ages of 1.5, 1.7 and 2.5 Ga) shown by double-dated zircon grains of the youngest moving-age peak, at least in sediments older than 5-4 Ma (white lozenges in Fig. 17c). A Greater Himalayan U-Pb signature is also detected in zircon grains defining the stationary age peak at 15-14 Ma (trend 6 in Fig. 17c).

Starting from 5-4 Ma (B in Fig. 17c), the second moving age peak merges with the youngest moving age peak, and double-dated zircon grains from the youngest ZFT age peak start including a Lesser Himalayan U-Pb age signature. The progressive decrease in lag-time values recorded by the second moving age peak, from A to B, does not necessarily imply a progressive increase in exhumation rate from ~25 to ~10 Ma (criterion C14, see Fig. 7). Instead, it likely reflects a sharp increase in exhumation rate at ~10 Ma (i.e., the ZFT age corresponding to point B) in the new eroding source, represented by the Lesser Himalaya. In the AFT diagram of Fig. 17b, similar information is provided by the second and less prominent moving age peak (trend 2) also associated with decreasing lag-time values up section. As for ZFT data, such a decrease in lag-time values is consistent with a sharp increase in exhumation rate at ~10 Ma. Notably, the signal of increased exhumation rate, if provided by a lower-T_c system should be observed in older stratigraphic levels, and if provided by a higher-T_c system should be observed in younger stratigraphic levels for the same geologic event (see Fig. 7). In the lag-time diagrams of Fig. 17b,c, the onset of Lesser Himalayan exhumation is recorded in 6-5 Ma old sediments by AFT data, and in 5-4 Ma old sediments by ZFT data, in line with predictions of Fig. 7.

Two independent lines of thermochronologic evidence thus concurrently constrain the onset of fast exhumation of the Lesser Himalaya to ~10 Ma. Firstly, the sharp shift of the youngest ZFT age peak towards older ages, observed in ~10 Ma old sediments (J in Fig. 17c). This signal, supportive of inputs from a new eroding source since ~10 Ma, is not observed in the corresponding detrital AFT record because it is completely reset by post-depositional annealing. Secondly, the progressive decrease in lag-time values recorded at different stratigraphic levels by ZFT and AFT data in upper Miocene – lower Pliocene sediments. This signal is consistent with a sharp increase in exhumation rate in the Lesser Himalaya at ~10 Ma (B in Fig. 17b, c). Because of the expected variations in zircon and apatite fertilities in Greater Himalayan and Lesser Himalayan rocks, this second signal is provided by a ZFT age peak (trend 7 in Fig. 17c) that is more prominent than the corresponding AFT age peak (trend 2 in Fig. 17b), despite the source of these two peaks likely being the same. The onset of Lesser Himalaya exhumation at ~10 Ma is fully consistent with independent Sm-Nd constraints reported by Najman et al. (2009; 2010).

9.4.3. Detrital mica Ar-Ar age trends, Sub-Himalaya

Detrital mica Ar-Ar data from the Siwaliks (White et al., 2002; Szulc et al., 2006; Najman et al., 2009; Stickroth et al., 2019), summarized in the lag-time diagram of Fig. 17d, confirm all of the major provenance changes previously detected by AFT and ZFT data (J, K and L in Fig. 17d). In sediments older than 17 Ma (not shown in Fig. 17d), detrital mica Ar-Ar data point to decreasing lag-time values up section. In sediments deposited between 17 and 10 Ma, detrital mica Ar-Ar data define prominent young peaks (trend 8 in Fig. 17d) associated to rather constant lag-time values around ~5 Ma (White et al., 2002, Najman et al., 2009). A sharp change in detrital mica Ar-Ar fingerprint is observed in Siwalik sediments since 10-9 Ma (J in Fig. 17d), when the youngest peak becomes stationary with mica Ar-Ar ages invariably around 14-15 Ma (trend 9 in Fig. 17d), and much less prominent. The sharp change in size of the youngest age peak, and its sharp shift towards older ages at 10-9 Ma, concurrently indicate a major provenance change at that time (criteria M5 and M6). A change in Ar-Ar fingerprint can be recognized in detrital micas from sediments deposited since 6-5 Ma (K in Fig. 17d), and an age shift towards older ages can be detected in sediments deposited at ~2 Ma (L in Fig. 17d), suggesting the involvement of new sediment sources.

Lessons learnt from the European Alps, and concepts illustrated in Section 3, suggest that most of the peaks in the polymodal grain-age distributions of Fig. 17d likely reflect distinct episodes of syntectonic mica (re)crystallization, rather than undisturbed exhumational cooling through the T_c

isotherm. Crystallization or recrystallization of mica is also suggested by recent Ar-Ar studies in bedrock (e.g., Montemagni et al., 2019). If there was simple cooling through the T_c isotherm, a single moving-age peak should be produced from each eroding source (Fig. 6b). If cooling was related to thermal relaxation after Greater Himalaya exhumation (e.g., Braun, 2016), the associated mica Ar-Ar signal should be exclusively found in stratigraphic levels younger than 5 Ma (criterion C12). In fact, the ZFT signal mirroring such event is not recorded in sediments older than ~5 Ma, and the corresponding AFT signal is found in sediments deposited between 7 Ma and 3 Ma (see Section 9.4.1), which reinforces the idea that the mica Ar-Ar signal in most of the Siwalik succession is controlled by (re)crystallization processes rather than diffusion processes.

However, detrital mica Ar-Ar data summarized in Fig. 17d still provide major pin-points to constrain Himalayan exhumation. The prominent young peaks, in the range between 25 and 15 Ma, observed in sediments older than ~10 Ma (trend 8 in Fig. 17d), can be reasonably associated to micas derived from Greater Himalayan migmatites and leucogranites emplaced in the late Oligocene – early Miocene. Lag-time values around 5 Ma associated with these micas would thus reflect the time required for exhumation from the depth of emplacement (or formation) of these rocks to Earth's surface. If this scenario is correct, and such lag time is used to infer an exhumation rate, the inferred value may be an overestimate, because micas may have grown at temperature lower than diffusion-only isotopic closure (see Section 3).

The lack of significant age peaks younger than 14-15 Ma in Siwalik sediments deposited during the past 10 Ma (trend 9 in Fig. 17d) indicates that syntectonic mica (re)crystallization was negligible in most of the Himalaya during the last 15 Ma. More specifically, the lack of a young moving age peak in upper Miocene or younger sediments indicate that the rock pile with an Ar-Ar thermochronologic fingerprint acquired during the 25-15 Ma time interval has not been completely removed by erosion, yet (criterion C4), in spite of the strong rock uplift associated to the formation of the highest mountains on Earth.

9.4.4. Comparison with thermochronologic age trends in the Bengal Fan

Detrital AFT data from the distal Bengal Fan (Corrigan and Crowley, 1990) are illustrated in Fig. 17e. They largely reproduce the age trend observed in the unreset uppermost part of the Siwalik succession (trend 1 in Fig. 17b), but in a smoother fashion due to the lower sampling density, and possibly also as a result of modifications of the thermochronologic signal due to sedimentary processes in the flood plain (see Section 5.4). Evidence of post-depositional annealing due to thick sedimentary burial is only found in the lowermost stratigraphic levels, i.e., in samples with depositional ages >14 Ma (trend 10 in Fig. 17e). This means that the detrital AFT data set from the distal Bengal-Fan sediments can reveal the exhumation history of the Himalaya on a longer time scale (see trend 11 in Fig. 17e) compared to the AFT data set from the Siwaliks where samples with depositional ages >7-8 Ma are instead affected by post-depositional annealing due to burial (trends 4a and 4b in Fig. 17b). As shown in Fig. 17e, lag-time values in the detrital AFT record of the Bengal Fan progressively decrease up section (trend 11), from ~8 Ma (for depositional ages around 11-10 Ma) to ~2 Ma (for depositional ages around 6 Ma).

Detrital ZFT and mica Ar-Ar data from the mid-Bengal Fan published by Najman et al. (2019) are shown in Fig. 17f and g. We also plotted the youngest grain age populations from these data sets in the corresponding lag-time diagrams for the more proximal sediment sinks (red dots in Fig. 17c, d), in order to highlight the detrital thermochronology fingerprint of the Namche Barwa syntaxis. Notably, thermochronologic age trends observed in the mid-Bengal Fan share many similarities with the corresponding age trends in the Sub-Himalaya (Fig. 17c, d). Major thermochronologic-age peaks detected in the proximal Sub-Himalayan sediment sink are also found in the more distal sink of the mid-Bengal Fan. However, these datasets (proximal Siwaliks vs distal Bengal Fan) also show major differences. For example, the youngest ZFT age peaks associated to very short lag times, detected by Najman et al. (2019) in upper Pliocene – Pleistocene sediments of the mid-Bengal Fan (trend 12 in Fig. 17f), are not observed in the corresponding data set of the Siwaliks (Fig. 17c). These young ZFT age peaks reflect the extremely fast erosion of the Namche Barwa syntaxis, which is not recorded in sediments of the Siwaliks. The first appearance of these young ZFT age peaks constrains the onset of very rapid exhumation of the Namche Barwa to ~4 Ma (Najman et al., 2019). A young ZFT age peak associated with a longer lag time is found in ~7 Ma Bengal Fan sediments (M in Fig. 17f). This young peak, not detected in the Siwaliks, may reflect the early stages of exhumation of the syntaxial area. Following the same line of reasoning, the small young peaks at 10-12 Ma, defined by mica Ar-Ar ages in upper Miocene to Pleistocene sediments of the mid-Bengal Fan (trend 13 in Fig. 17g), may also reflect the progressive unroofing of the Namche Barwa syntaxis (cf. Fig. 17d). This suggests that crustal sections with an Ar-Ar fingerprint acquired before the onset of very fast erosion at ~4 Ma were not completely removed in the Namche Barwa area until the Pleistocene, when rocks with very young mica Ar-Ar ages started to be exposed at Earth's surface as they are observed today (e.g., Gemignani et al., 2018). The signal of fast syntaxial exhumation is not detected in the detrital AFT dataset of Corrigan and Crowley (1990) (Fig. 17e), possibly due to a fertility bias or underestimation of zero-track grains in analyzed samples.

9.4.5. Tectonic implications and Himalaya topographic growth

Different thermochronologic system applied to proximal and distal sedimentary successions derived from Himalayan erosion provide a relatively consistent yet complex picture for the post-Oligocene evolution of India-Eurasia collision. Detrital thermochronology data are supportive of a progressive thrust propagation towards the Himalayan foreland in the south, and consequent progressive involvement of new eroding sources through time. The onset of fast exhumation in the Lesser Himalaya is invariably constrained to ~10 Ma by different thermochronologic methods and independent lines of evidence. Coeval fast exhumation is also recorded in detritus derived from the Greater Himalaya, which is supportive of a major morphogenic phase of mountain building in the late Miocene (~10 Ma). The late Miocene morphogenic phase in the Himalaya, also suggested by data from Tibet (Tremblay et al., 2015), precedes the onset of fast exhumation in the Namche Barwa syntaxis, which is constrained as ~4 Ma (Najman et al., 2019).

Figure 17

10. Conclusions

The lag-time approach to detrital thermochronology is increasingly employed to analyze the evolution of orogenic belts starting from the analysis of samples collected through a stratigraphic succession. However, simple predictions that follow from the classic lag-time conceptual model are often in conflict with the detrital thermochronology record observed in sedimentary basins. The observed thermochronologic complexity results from: (i) the original complexity of the thermochronologic age structure in the source region; (ii) mixing of detritus from multiple source regions that are characterized by different geologic or upper crustal exhumation histories; (iii) modifications of the original thermochronologic signal during sediment transport and deposition; and (iv) post-depositional annealing after sedimentary burial. A careful analysis of these processes provides interpretive keys that can be used for an improved interpretation of detrital thermochronology data from samples collected within a stratigraphic framework, shedding new light on the complex and often debated evolution of orogenic belts and associated sedimentary basins.

Application of these concepts to published detrital thermochronologic data sets reveals that: (i) exhumational steady state in the European Alps was not attained, but erosion shifted progressively westward during the Oligocene-Miocene, and towards more external areas of the orogen in the late Miocene; (ii) arc-continent collision in Taiwan migrated progressively from north to south starting from the late Miocene, consistent with stratigraphic evidence; (iii) India-Eurasia collision determined a progressive propagation of thrusting towards the Himalayan foreland, and a major morphogenic phase of mountain building in the Himalaya in the late Miocene (~10 Ma), prior to the onset of fast exhumation in the Namche Barwa syntaxis.

Acknowledgments

This article is an outcome of Project MIUR – Dipartimenti di Eccellenza 2018–2022. It benefited from discussions and inputs from chapter authors and reviewers who contributed to the book entitled "Fission-Track Thermochronology and its Application to Geology", and colleagues at University of Milano-Bicocca. Fitzgerald also acknowledges support from National Science Foundation grant EAR-1550034. Comments by associate editor David Chew and three anonymous reviewers helped to improve the clarity of the manuscript.

References

Allaz, J., Engi, M., Berger, A., & Villa, I. M. (2011). The effects of retrograde reactions and of diffusion on $^{40}Ar/^{39}Ar$ ages of micas. Journal of Petrology, 52(4), 691-716.

Allen, P. A., & Allen, J. R. (2013). Basin analysis: Principles and application to petroleum play assessment. John Wiley & Sons.

Andò, S., Garzanti, E., Padoan, M., & Limonta, M. (2012). Corrosion of heavy minerals during weathering and diagenesis: A catalog for optical analysis. Sedimentary Geology, 280, 165-178.

Anfinson, O. A., Malusà, M. G., Ottria, G., Dafov, L. N., & Stockli, D. F. (2016). Tracking coarse-grained gravity flows by LASS-ICP-MS depth-profiling of detrital zircon (Aveto Formation, Adriatic foredeep, Italy). Marine and Petroleum Geology, 77, 1163-1176.

Ansberque, C., Mark, C., Caulfield, J. T., & Chew, D. M. (2019). Combined in-situ determination of halogen (F, Cl) content in igneous and detrital apatite by SEM-EDS and LA-Q-ICPMS: A potential new provenance tool. Chemical Geology, 524, 406-420.

Asti, R., Malusà, M. G., & Faccenna, C. (2018). Supradetachment basin evolution unravelled by detrital apatite fission track analysis: the Gediz Graben (Menderes Massif, Western Turkey). Basin Research, 30(3), 502-521.

Ault, A. K., Gautheron, C., & King, G. E. (2019). Innovations in (U-Th)/He, fission-track, and trapped-charge thermochronometry with applications to earthquakes, weathering, surface-mantle connections, and the growth and decay of mountains. Tectonics.

Avouac, J. P. (2003). Mountain building, erosion, and the seismic cycle in the Nepal Himalaya. Advances in geophysics, 46, 1-80.

Baldwin, S. L., Harrison, T. M., & Burke, K. (1986). Fission track evidence for the source of accreted sandstones, Barbados. Tectonics, 5(3), 457-468.

Baldwin, S. L., & Lister, G. S. (1998). Thermochronology of the South Cyclades Shear Zone, Ios, Greece: Effects of ductile shear in the argon partial retention zone. Journal of Geophysical Research: Solid Earth, 103(B4), 7315-7336.

Baldwin, S. L., Fitzgerald, P. G., & Malusà, M. G. (2019). Crustal Exhumation of Plutonic and Metamorphic Rocks: Constraints from Fission-Track Thermochronology. In Fission-Track Thermochronology and its Application to Geology (pp. 235-257). Springer, Cham.

Barbarand, J., Carter, A., Wood, I., & Hurford, T. (2003). Compositional and structural control of fission-track annealing in apatite. Chemical Geology, 198(1-2), 107-137.

Beamud, E., Muñoz, J. A., Fitzgerald, P. G., Baldwin, S. L., Garcés, M., Cabrera, L., & Metcalf, J. R. (2011). Magnetostratigraphy and detrital apatite fission track thermochronology in syntectonic conglomerates: constraints on the exhumation of the South-Central Pyrenees. Basin Research, 23(3), 309-331.

Beaumont, C., Jamieson, R. A., Nguyen, M. H., & Lee, B. (2001). Himalayan tectonics explained by extrusion of a low-viscosity crustal channel coupled to focused surface denudation. Nature, 414(6865), 738.

Belousova, E. A., Griffin, W. L., O'Reilly, S. Y., & Fisher, N. I. (2002). Apatite as an indicator mineral for mineral exploration: trace-element compositions and their relationship to host rock type. Journal of Geochemical Exploration, 76(1), 45-69.

Bernet, M. (2010). Tracing exhumation and orogenic wedge dynamics in the European Alps with detrital thermochronology: COMMENT. Geology, 38(11), e226-e226.

Bernet, M. (2019). Exhumation studies of mountain belts based on detrital fission-track analysis on sand and sandstones. In Fission-Track Thermochronology and its Application to Geology (pp. 269-277). Springer, Cham.

Bernet, M., & Garver, J. I. (2005). Fission-track analysis of detrital zircon. Reviews in Mineralogy and Geochemistry, 58(1), 205-237.

Bernet, M., & Spiegel, C. (Eds.). (2004). Detrital thermochronology: Provenance analysis, exhumation, and landscape evolution of mountain belts (Vol. 378). Geological Society of America.

Bernet, M., Zattin, M., Garver, J. I., Brandon, M. T., & Vance, J. A. (2001). Steady-state exhumation of the European Alps. Geology, 29(1), 35-38.

Bernet, M., Brandon, M. T., Garver, J. I., & Molitor, B. R. (2004). Fundamentals of detrital zircon fission-track analysis for provenance and exhumation studies with examples from the European Alps. Special Papers – Geological Society of America, 25-36.

Bernet, M., Van Der Beek, P., Pik, R., Huyghe, P., Mugnier, J. L., Labrin, E., & Szulc, A. (2006). Miocene to Recent exhumation of the central Himalaya determined from combined detrital zircon fission-track and U/Pb analysis of Siwalik sediments, western Nepal. Basin Research, 18(4), 393-412.

Bernet, M., Brandon, M., Garver, J., Balestieri, M. L., Ventura, B., & Zattin, M. (2009). Exhuming the Alps through time: clues fromdetrital zircon fission-track thermochronology. Basin Research, 21(6), 781-798.

Bernet, M., Urueña, C., Amaya, S., & Peña, M. L. (2016). New thermo and geochronological constraints on the Pliocene-Pleistocene eruption history of the Paipa-Iza volcanic complex, Eastern Cordillera, Colombia. Journal of Volcanology and Geothermal Research, 327, 299-309.

Bernet, M., Piraquive, A., Urueña, C., López-Isaza, J. A., Bermúdez, M. A., Zuluaga, C., ... & Villamizar, N. (2019). Multidisciplinary petro-geo-thermochronological approach to ore deposit exploration. Ore Geology Reviews, 103017.

Bertotti, G., Seward, D., Wijbrans, J., Ter Voorde, M., & Hurford, A. J. (1999). Crustal thermal regime prior to, during, and after rifting: a geochronological and modeling study of the Mesozoic South Alpine rifted margin. Tectonics, 18(2), 185-200.

Blum, M., Rogers, K., Gleason, J., Najman, Y., Cruz, J., & Fox, L. (2018). Allogenic and autogenic signals in the stratigraphic record of the deep-sea Bengal Fan. Scientific reports, 8(1), 7973.

Bracciali, L., Najman, Y., Parrish, R. R., Akhter, S. H., & Millar, I. (2015). The Brahmaputra tale of tectonics and erosion: Early Miocene river capture in the Eastern Himalaya. Earth and Planetary Science Letters, 415, 25-37.

Bracciali, L., Parrish, R. R., Najman, Y., Smye, A., Carter, A., & Wijbrans, J. R. (2016). Plio-Pleistocene exhumation of the eastern Himalayan syntaxis and its domal 'pop-up'. Earth-Science Reviews, 160, 350-385.

Brandon, M. T., & Vance, J. A. (1992). Tectonic evolution of the Cenozoic Olympic subduction complex, Washington State, as deduced from fission track ages for detrial zircons. American Journal of Science, 292, 565-565.

Braun, J. (2002). Quantifying the effect of recent relief changes on age–elevation relationships. Earth and Planetary Science Letters, 200(3-4), 331-343.

Braun, J. (2003). Pecube: A new finite-element code to solve the 3D heat transport equation including the effects of a time-varying, finite amplitude surface topography. Computers & Geosciences, 29(6), 787-794.

Braun, J. (2016). Strong imprint of past orogenic events on the thermochronological record. Tectonophysics, 683, 325-332.

Braun, J., Van Der Beek, P., & Batt, G. (2006). Quantitative thermochronology: numerical methods for the interpretation of thermochronological data. Cambridge University Press.

Braun, J., Van Der Beek, P., Valla, P., Robert, X., Herman, F., Glotzbach, C., ... & Prigent, C. (2012). Quantifying rates of landscape evolution and tectonic processes by thermochronology and numerical modeling of crustal heat transport using PECUBE. Tectonophysics, 524, 1-28.

Braun, J., Gemignani, L., & Beek, P. V. D. (2018). Extracting information on the spatial variability in erosion rate stored in detrital cooling age distributions in river sands. Earth Surface Dynamics, 6(1), 257-270.

Brewer, I. D., Burbank, D. W., & Hodges, K. V. (2003). Modelling detrital cooling-age populations: insights from two Himalayan catchments. Basin Research, 15(3), 305-320.

Burbank, D. W., Derry, L. A., & France-Lanord, C. (1993). Reduced Himalayan sediment production 8 Myr ago despite an intensified monsoon. Nature, 364(6432), 48.

Burg, J. P., Brunel, M., Gapais, D., Chen, G. M., & Liu, G. H. (1984). Deformation of leucogranites of the crystalline Main Central Sheet in southern Tibet (China). Journal of Structural Geology, 6(5), 535-542.

Burg, J. P., Nievergelt, P., Oberli, F., Seward, D., Davy, P., Maurin, J. C., ... & Meier, M. (1998). The Namche Barwa syntaxis: evidence for exhumation related to compressional crustal folding. Journal of Asian Earth Sciences, 16(2-3), 239-252.

Burgess, W. P., Yin, A., Dubey, C. S., Shen, Z. K., & Kelty, T. K. (2012). Holocene shortening across the Main Frontal Thrust zone in the eastern Himalaya. Earth and Planetary Science Letters, 357, 152-167.

Byrne, T. B., & Liu, C. S. (Eds.). (2002). Geology and geophysics of an arc-continent collision, Taiwan (Vol. 358). Geological Society of America.

Byrne, T., Chan, Y. C., Rau, R. J., Lu, C. Y., Lee, Y. H., & Wang, Y. J. (2011). The arc–continent collision in Taiwan. In Arc-Continent Collision (pp. 213-245). Springer, Berlin, Heidelberg.

Calk, L. C., & Naeser, C. W. (1973). The thermal effect of a basalt intrusion on fission tracks in quartz monzonite. The Journal of Geology, 81(2), 189-198.

Carrapa, B. (2009). Tracing exhumation and orogenic wedge dynamics in the European Alps with detrital thermochronology. Geology, 37(12), 1127-1130.

Carrapa, B. (2010). Tracing exhumation and orogenic wedge dynamics in the European Alps with detrital thermochronology: REPLY. Geology, 38(11), e227-e227.

Carrapa, B., & DeCelles, P. G. (2008). Eocene exhumation and basin development in the Puna of northwestern Argentina. Tectonics, 27(1).

Carrapa, B., Wijbrans, J., & Bertotti, G. (2003). Episodic exhumation in the Western Alps. Geology, 31(7), 601-604.

Carrapa, B., Wijbrans, J., Bertotti, G., Bernet, M., & Spiegel, C. (2004). Detecting provenance variations and cooling patterns within the western Alpine orogen through $^{40}Ar/^{39}Ar$ geochronology on detrital sediments: The Tertiary Piedmont Basin, northwest Italy. Special Papers, Geological Society of America, 67-104.

Carroll, D. (1953). Weatherability of zircon. Journal of Sedimentary Research, 23(2), 106-116.

Carter, A. (2007). Heavy minerals and detrital fission-track thermochronology. Developments in Sedimentology, 58, 851-868.

Carter, A. (2019). Thermochronology on sand and sandstones for stratigraphic and provenance studies. In Fission-Track Thermochronology and its Application to Geology (pp. 259-268). Springer, Cham.

Carter, A., & Foster, G. L. (2009). Improving constraints on apatite provenance: Nd measurement on fission-track-dated grains. Geological Society, London, Special Publications, 324(1), 57-72.

Carter, A., & Moss, S. J. (1999). Combined detrital-zircon fission-track and U-Pb dating: A new approach to understanding hinterland evolution. Geology, 27(3), 235-238.

Carter, A., Najman, Y., Bahroudi, A., Bown, P., Garzanti, E., & Lawrence, R. D. (2010). Locating earliest records of orogenesis in western Himalaya: Evidence from Paleogene sediments in the Iranian Makran region and Pakistan Katawaz basin. Geology, 38(9), 807-810.

Cavazza, W., & Gandolfi, G. (1992). Diagenetic processes along a basin-wide marker bed as a function of burial depth. Journal of Sedimentary Research, 62(2), 261-272.

Cawood, P. A., Nemchin, A. A., Freeman, M., & Sircombe, K. (2003). Linking source and sedimentary basin: Detrital zircon record of sediment flux along a modern river system and implications for provenance studies. Earth and Planetary Science Letters, 210(1-2), 259-268.

Cerveny, P. F., Naeser, N. D., Zeitler, P. K., Naeser, C. W., & Johnson, N. M. (1988). History of uplift and relief of the Himalaya during the past 18 million years: Evidence from fission-track ages of detrital zircons from sandstones of the Siwalik Group. In New perspectives in basin analysis (pp. 43-61). Springer, New York, NY.

Challandes, N., Marquer, D., & Villa, I. M. (2008). PTt modelling, fluid circulation, and ^{39}Ar-^{40}Ar and Rb-Sr mica ages in the Aar Massif shear zones (Swiss Alps). Swiss Journal of Geosciences, 101(2), 269-288.

Chen, W. S., & Wang, Y. (1988). Development of deep-sea fan systems in Coastal Range basin, eastern Taiwan. Acta Geologica Taiwanica, 26, 36-56.

Chen, W. S., Yeh, J. J., & Syu, S. J. (2019). Late Cenozoic exhumation and erosion of the Taiwan orogenic belt: New insights from petrographic analysis of foreland basin sediments and thermochronological dating on the metamorphic orogenic wedge. Tectonophysics, 750, 56-69.

Chew, D. M., Sylvester, P. J., & Tubrett, M. N. (2011). U–Pb and Th–Pb dating of apatite by LA-ICPMS. Chemical Geology, 280(1-2), 200-216.

Chirouze, F., Bernet, M., Huyghe, P., Erens, V., Dupont-Nivet, G., & Senebier, F. (2012). Detrital thermochronology and sediment petrology of the middle Siwaliks along the Muksar Khola section in eastern Nepal. Journal of Asian Earth Sciences, 44, 94-106.

Cibin, U., Spadafora, E., Zuffa, G. G., & Castellarin, A. (2001). Continental collision history from arenites of episutural basins in the Northern Apennines, Italy. Geological Society of America Bulletin, 113(1), 4-19.

Cleary, W. J., & Conolly, J. R. (1972). Embayed quartz grains in soils and their significance. Journal of Sedimentary Research, 42(4).

Clift, P. D. (2017). Cenozoic sedimentary records of climate-tectonic coupling in the Western Himalaya. Progress in Earth and Planetary Science, 4(1), 39.

Clift, P., & Gaedicke, C. (2002). Accelerated mass flux to the Arabian Sea during the middle to late Miocene. Geology, 30(3), 207-210.

Clift, P. D., & Giosan, L. (2014). Sediment fluxes and buffering in the post-glacial Indus Basin. Basin Research, 26(3), 369-386.

Clift, P. D., & Webb, A. A. G. (2018). A history of the Asian monsoon and its interactions with solid Earth tectonics in Cenozoic South Asia. Geological Society, London, Special Publications, 483, SP483-1.

Clift, P. D., Blusztajn, J., & Nguyen, A. D. (2006). Large-scale drainage capture and surface uplift in eastern Tibet–SW China before 24 Ma inferred from sediments of the Hanoi Basin, Vietnam. Geophysical Research Letters, 33(19).

Clift, P. D., Hodges, K. V., Heslop, D., Hannigan, R., Van Long, H., & Calves, G. (2008). Correlation of Himalayan exhumation rates and Asian monsoon intensity. Nature geoscience, 1(12), 875.

Cochran, J.R., Stow, D.A.V., et al. (1990). Proc. ODP, Sci. Results, 116: College Station, TX (Ocean Drilling Program)

Colin, F., Alarcon, C., & Vieillard, P. (1993). Zircon: an immobile index in soils. Chemical Geology, 107(3-4), 273-276.

Copeland, P., & Harrison, T. M. (1990). Episodic rapid uplift in the Himalaya revealed by 40Ar/39Ar analysis of detrital K-feldspar and muscovite, Bengal fan. Geology, 18(4), 354-357.

Copeland, P., Harrison, T. M., & Heizler, M. T. (1990). $^{40}Ar/^{39}Ar$ single crystal dating of detrital muscovite and K-feldspar from Leg 116, southern Bengal Fan: Implications for the uplift and erosion of the Himalayas. In Proc. Ocean Drill. Program Sci. Results (Vol. 116, pp. 93-114).

Corrigan, J. D., & Crowley, K. D. (1990). Fission-track analysis of detrital apatites from sites 717 and 718, Leg 116, Central Indian Ocean. In Proc. Ocean Drill. Program Sci. Results (Vol. 116, pp. 75-92).

Corrigan, J. D., & Crowley, K. D. (1992). Unroofing of the Himalayas: A view from apatite fission-track analysis of Bengal fan sediments. Geophysical Research Letters, 19(23), 2345-2348.

Dadson, S. J., Hovius, N., Chen, H., Dade, W. B., Hsieh, M. L., Willett, S. D., ... & Lague, D. (2003). Links between erosion, runoff variability and seismicity in the Taiwan orogen. Nature, 426(6967), 648.

Dahl, P. S. (1997). A crystal-chemical basis for Pb retention and fission-track annealing systematics in U-bearing minerals, with implications for geochronology. Earth and Planetary Science Letters, 150(3-4), 277-290.

Dahlen, F. A., Suppe, J., & Davis, D. (1984). Mechanics of fold-and-thrust belts and accretionary wedges: Cohesive Coulomb theory. Journal of Geophysical Research: Solid Earth, 89(B12), 10087-10101.

Danišík, M. (2019). Integration of Fission-Track Thermochronology with Other Geochronologic Methods on Single Crystals. In Fission-Track Thermochronology and its Application to Geology (pp. 93-108). Springer, Cham.

Davis, D., Suppe, J., & Dahlen, F. A. (1983). Mechanics of fold-and-thrust belts and accretionary wedges. Journal of Geophysical Research: Solid Earth, 88(B2), 1153-1172.

DeCelles, P. G., Gehrels, G. E., Quade, J., Ojha, T. P., Kapp, P. A., & Upreti, B. N. (1998). Neogene foreland basin deposits, erosional unroofing, and the kinematic history of the Himalayan fold-thrust belt, western Nepal. Geological Society of America Bulletin, 110(1), 2-21.

DeCelles, P. G., Gehrels, G. E., Quade, J., LaReau, B., & Spurlin, M. (2000). Tectonic implications of U-Pb zircon ages of the Himalayan orogenic belt in Nepal. Science, 288(5465), 497-499.

DeCelles, P. G., Robinson, D. M., Quade, J., Ojha, T. P., Garzione, C. N., Copeland, P., & Upreti, B. N. (2001). Stratigraphy, structure, and tectonic evolution of the Himalayan fold-thrust belt in western Nepal. Tectonics, 20(4), 487-509.

DeCelles, P. G., Gehrels, G. E., Najman, Y., Martin, A. J., Carter, A., & Garzanti, E. (2004). Detrital geochronology and geochemistry of Cretaceous–Early Miocene strata of Nepal: implications for timing and diachroneity of initial Himalayan orogenesis. Earth and Planetary Science Letters, 227(3-4), 313-330.

DeCelles, P. G., Carrapa, B., Gehrels, G. E., Chakraborty, T., & Ghosh, P. (2016). Along-strike continuity of structure, stratigraphy, and kinematic history in the Himalayan thrust belt: The view from Northeastern India. Tectonics, 35(12), 2995-3027.

Dewey, J. F., Helman, M. L., Knott, S. D., Turco, E., & Hutton, D. H. W. (1989). Kinematics of the western Mediterranean. Geological Society, London, Special Publications, 45(1), 265-283.

Dickinson, W. R. (2008). Impact of differential zircon fertility of granitoid basement rocks in North America on age populations of detrital zircons and implications for granite petrogenesis. Earth and Planetary Science Letters, 275(1-2), 80-92.

Di Vincenzo, G., Viti, C., & Rocchi, S. (2003). The effect of chlorite interlayering on ^{40}Ar–^{39}Ar biotite dating: an ^{40}Ar–^{39}Ar laser-probe and TEM investigations of variably chloritised biotites. Contributions to Mineralogy and Petrology, 145(6), 643-658.

Dodson, M. H. (1973). Closure temperature in cooling geochronological and petrological systems. Contributions to Mineralogy and Petrology, 40(3), 259-274.

Dorsey, R. J. (1988). Provenance evolution and unroofing history of a modern arc-continent collision; evidence from petrography of Plio-Pleistocene sandstones, eastern Taiwan. Journal of Sedimentary Research, 58(2), 208-218.

Dorsey, R. J. (1992). Collapse of the Luzon Volcanic Arc during onset of arc-continent collision: Evidence from a Miocene-Pliocene unconformity, eastern Taiwan. Tectonics, 11(2), 177-191.

Dorsey, R. J., & Lundberg, N. (1988). Lithofacies analysis and basin reconstruction of the Plio-Pleistocene collisional basin, Coastal Range of eastern Taiwan. Acta Geol.Taiwan, (26), 57-132.

Doyle, L. J., Carder, K. L., & Steward, R. G. (1983). The hydraulic equivalence of mica. Journal of Sedimentary Research, 53(2), 643-648.

Dunkl, I., Di Giulio, A., & Kuhlemann, J. (2001). Combination of single-grain fission-track chronology and morphological analysis of detrital zircon crystals in provenance studies: sources of the Macigno Formation (Apennines, Italy). Journal of sedimentary research, 71(4), 516-525.

Dupré, B., Gaillardet, J., Rousseau, D., & Allègre, C. J. (1996). Major and trace elements of river-borne material: the Congo Basin. Geochimica et Cosmochimica Acta, 60(8), 1301-1321.

Ehlers, T. A., Chaudhri, T., Kumar, S., Fuller, C. W., Willett, S. D., Ketcham, R. A., ... & Dunai, T. J. (2005). Computational tools for low-temperature thermochronometer interpretation. Reviews in Mineralogy and Geochemistry, 58(1), 589-622.

England, P., & Molnar, P. (1990). Surface uplift, uplift of rocks, and exhumation of rocks. Geology, 18(12), 1173-1177.

Enkelmann, E., Ehlers, T. A., Zeitler, P. K., & Hallet, B. (2011). Denudation of the Namche Barwa antiform, eastern Himalaya. Earth and Planetary Science Letters, 307(3-4), 323-333.

Enkelmann, E., Sanchez Lohff, S. K., & Finzel, E. S. (2019). Detrital zircon double-dating of forearc basin strata reveals magmatic, exhumational, and thermal history of sediment source areas. Geological Society of America Bulletin.

Ewing, R. C., Meldrum, A., Wang, L., Weber, W. J., & Corrales, L. R. (2003). Radiation effects in zircon. Reviews in Mineralogy and geochemistry, 53(1), 387-425.

Farley, K. A. (2000). Helium diffusion from apatite: General behavior as illustrated by Durango fluorapatite. Journal of Geophysical Research: Solid Earth, 105(B2), 2903-2914.

Farley, K. A. (2002). (U-Th)/He dating: Techniques, calibrations, and applications. Reviews in Mineralogy and Geochemistry, 47(1), 819-844.

Fedele, J. J., & Paola, C. (2007). Similarity solutions for fluvial sediment fining by selective deposition. Journal of Geophysical Research: Earth Surface, 112(F2).

Fedo, C. M., Sircombe, K. N., & Rainbird, R. H. (2003). Detrital zircon analysis of the sedimentary record. Reviews in Mineralogy and Geochemistry, 53(1), 277-303.

Fellin, M., Sciunnach, D., Tunesi, A., Ando, S., Garzanti, E., & Vezzoli, G. (2005). Provenance of detrital apatites from the upper Gonfolite Lombarda Group (Miocene, NW Italy). GeoActa, 4, 43-56.

Fellin, M. G., Chen, C. Y., Willett, S. D., Christl, M., & Chen, Y. G. (2017). Erosion rates across space and timescales from a multi-proxy study of rivers of eastern Taiwan. Global and Planetary Change, 157, 174-193.

Fielding, P. E. (1970). The distribution of uranium, rare earths, and color centers in a crystal of natural zircon. American Mineralogist: Journal of Earth and Planetary Materials, 55(3-4_Part_1), 428-440.

Finnegan, N. J., Hallet, B., Montgomery, D. R., Zeitler, P. K., Stone, J. O., Anders, A. M., & Yuping, L. (2008). Coupling of rock uplift and river incision in the Namche Barwa–Gyala Peri massif, Tibet. Geological Society of America Bulletin, 120(1-2), 142-155.

Fisher, D. M., Willett, S., En-Chao, Y., & Clark, M. B. (2007). Cleavage fronts and fans as reflections of orogen stress and kinematics in Taiwan. Geology, 35(1), 65-68.

Fitzgerald, P. G., & Gleadow, A. J. (1988). Fission-track geochronology, tectonics and structure of the Transantarctic Mountains in northern Victoria Land, Antarctica. Chemical Geology: Isotope Geoscience section, 73(2), 169-198.

Fitzgerald, P. G., & Gleadow, A. J. (1990). New approaches in fission track geochronology as a tectonic tool: Examples from the Transantarctic Mountains. International Journal of Radiation Applications and Instrumentation. Part D. Nuclear Tracks and Radiation Measurements, 17(3), 351-357.

Fitzgerald, P. G., & Malusà, M. G. (2019). Concept of the Exhumed Partial Annealing (Retention) Zone and Age-Elevation Profiles in Thermochronology. In Fission-Track Thermochronology and its Application to Geology (pp. 165-189). Springer, Cham.

Fitzgerald, P. G., & Stump, E. (1997). Cretaceous and Cenozoic episodic denudation of the Transantarctic Mountains, Antarctica: New constraints from apatite fission track thermochronology in the Scott Glacier region. Journal of Geophysical Research: Solid Earth, 102(B4), 7747-7765.

Fitzgerald, P. G., Fryxell, J. E., & Wernicke, B. P. (1991). Miocene crustal extension and uplift in southeastern Nevada: Constraints from fission track analysis. Geology, 19(10), 1013-1016.

Fitzgerald, P. G., Stump, E., & Redfield, T. F. (1993). Late Cenozoic uplift of Denali and its relation to relative plate motion and fault morphology. Science, 259(5094), 497-499.

Fitzgerald, P. G., Sorkhabi, R. B., Redfield, T. F., & Stump, E. (1995). Uplift and denudation of the central Alaska Range: A case study in the use of apatite fission track thermochronology to determine absolute uplift parameters. Journal of Geophysical Research: Solid Earth, 100(B10), 20175-20191.

Fitzgerald, P. G., Baldwin, S. L., Webb, L. E., & O'Sullivan, P. B. (2006). Interpretation of (U–Th)/He single grain ages from slowly cooled crustal terranes: a case study from the Transantarctic Mountains of southern Victoria Land. Chemical Geology, 225(1-2), 91-120.

Fitzgerald, P. G., Duebendorfer, E. M., Faulds, J. E., & O'Sullivan, P. (2009). South Virgin–White Hills detachment fault system of SE Nevada and NW Arizona: Applying apatite fission track thermochronology to constrain the tectonic evolution of a major continental detachment fault. Tectonics, 28(2).

Fitzgerald, P. G., Malusà, M. G., & Muñoz, J. A. (2019). Detrital Thermochronology Using Conglomerates and Cobbles. In Fission-Track Thermochronology and its Application to Geology (pp. 295-314). Springer, Cham.

Flowers, R. M., Ketcham, R. A., Shuster, D. L., & Farley, K. A. (2009). Apatite (U–Th)/He thermochronometry using a radiation damage accumulation and annealing model. Geochimica et Cosmochimica acta, 73(8), 2347-2365.

Foster, D. A., Grice Jr, W. C., & Kalakay, T. J. (2010). Extension of the Anaconda metamorphic core complex: 40Ar/39Ar thermochronology and implications for Eocene tectonics of the northern Rocky Mountains and the Boulder batholith. Lithosphere, 2(4), 232-246.

Foster, G. L., & Carter, A. (2007). Insights into the patterns and locations of erosion in the Himalaya—a combined fission-track and in situ Sm–Nd isotopic study of detrital apatite. Earth and Planetary Science Letters, 257(3-4), 407-418.

Foster, D. A., & Gleadow, A. J. (1996). Structural framework and denudation history of the flanks of the Kenya and Anza Rifts, East Africa. Tectonics, 15(2), 258-271.

France-Lanord, C., Spiess, V., Klaus, A., & Schwenk, T. (2016). the Expedition 354 Scientists. Proceedings of the International Ocean Discovery Program. Bengal Fan, 354.

Fu, B., Page, F. Z., Cavosie, A. J., Fournelle, J., Kita, N. T., Lackey, J. S., ... & Valley, J. W. (2008). Ti-in-zircon thermometry: applications and limitations. Contributions to Mineralogy and Petrology, 156(2), 197-215.

Fuller, C. W., Willett, S. D., Fisher, D., & Lu, C. Y. (2006). A thermomechanical wedge model of Taiwan constrained by fission-track thermochronometry. Tectonophysics, 425(1-4), 1-24.

Granet, M., Chabaux, F., Stille, P., Dosseto, A., France-Lanord, C., & Blaes, E. (2010). U-series disequilibria in suspended river sediments and implication for sediment transfer time in alluvial plains: the case of the Himalayan rivers. Geochimica et Cosmochimica Acta, 74(10), 2851-2865.

Galbraith, R. F., & Laslett, G. M. (1993). Statistical models for mixed fission track ages. Nuclear tracks and radiation measurements, 21(4), 459-470.

Galbraith, R. F. (2005). Statistics for fission track analysis. Chapman and Hall/CRC.

Gallagher, K. (2012). Transdimensional inverse thermal history modeling for quantitative thermochronology. Journal of Geophysical Research: Solid Earth, 117(B2).

Gansser, A. (1964). Geology of the Himalayas. Interscience, New York.

Gansser, A. (1980). The significance of the Himalayan suture zone. Tectonophysics, 62(1-2), 37-52.

Gansser, A. (1982). The morphogenic phases of mountain building. Mountain Building Processes., 221-228.

Garver, J. I. (2003). Etching zircon age standards for fission-track analysis. Radiation Measurements, 37(1), 47-53.

Garver, J. I., & Brandon, M. T. (1994). Erosional denudation of the British Columbia Coast Ranges as determined from fission-track ages of detrital zircon from the Tofino basin, Olympic Peninsula, Washington. Geological Society of America Bulletin, 106(11), 1398-1412.

Garver, J. I., & Kamp, P. J. (2002). Integration of zircon color and zircon fission-track zonation patterns in orogenic belts: application to the Southern Alps, New Zealand. Tectonophysics, 349(1-4), 203-219.

Garver, J. I., Brandon, M. T., Roden-Tice, M., & Kamp, P. J. (1999). Exhumation history of orogenic highlands determined by detrital fission-track thermochronology. Geological Society, London, Special Publications, 154(1), 283-304.

Garzanti, E. (2019). The Himalayan Foreland Basin from collision onset to the present: a sedimentary–petrology perspective. Geological Society, London, Special Publications, 483, SP483-17.

Garzanti, E., & Malusà, M. G. (2008). The Oligocene Alps: Domal unroofing and drainage development during early orogenic growth. Earth and Planetary Science Letters, 268(3-4), 487-500.

Garzanti, E., Andò, S., & Vezzoli, G. (2008). Settling equivalence of detrital minerals and grain-size dependence of sediment composition. Earth and Planetary Science Letters, 273(1-2), 138-151.

Garzanti, E., Andò, S., & Vezzoli, G. (2009). Grain-size dependence of sediment composition and environmental bias in provenance studies. Earth and Planetary Science Letters, 277(3-4), 422-432.

Garzanti, E., Resentini, A., Vezzoli, G., Andò, S., Malusà, M., & Padoan, M. (2012). Forward compositional modelling of Alpine orogenic sediments. Sedimentary Geology, 280, 149-164.

Garzanti, E., Padoan, M., Andò, S., Resentini, A., Vezzoli, G., & Lustrino, M. (2013). Weathering and relative durability of detrital minerals in equatorial climate: sand petrology and geochemistry in the East African Rift. The Journal of Geology, 121(6), 547-580.

Garzanti, E., Resentini, A., Andò, S., Vezzoli, G., Pereira, A., & Vermeesch, P. (2015). Physical controls on sand composition and relative durability of detrital minerals during ultra-long distance littoral and aeolian transport (Namibia and southern Angola). Sedimentology, 62(4), 971-996.

Gautheron, C., Barbarand, J., Ketcham, R. A., Tassan-Got, L., van der Beek, P., Pagel, M., ... & Fialin, M. (2013). Chemical influence on α-recoil damage annealing in apatite: Implications for (U–Th)/He dating. Chemical Geology, 351, 257-267.

Gemignani, L., van der Beek, P. A., Braun, J., Najman, Y., Bernet, M., Garzanti, E., & Wijbrans, J. R. (2018). Downstream evolution of the thermochronologic age signal in the Brahmaputra catchment (eastern Himalaya): Implications for the detrital record of erosion. Earth and Planetary Science Letters, 499, 48-61.

Gleadow, A. J. W. (1990). Fission track thermochronology: reconstructing the thermal and tectonic evolution of the crust. In Proceedings of the Pacific Rim congress 90. Vol III.

Gleadow, A. J., & Brown, R. W. (2000). Fission-track thermochronology and the long-term denudational response to tectonics. Geomorphology and global tectonics, 57-75.

Gleadow, A. J. W., & Duddy, I. R. (1981). A natural long-term track annealing experiment for apatite. Nuclear Tracks, 5(1-2), 169-174.

Gleadow, A. J. W., & Fitzgerald, P. G. (1987). Uplift history and structure of the Transantarctic Mountains: new evidence from fission track dating of basement apatites in the Dry Valleys area, southern Victoria Land. Earth and planetary science letters, 82(1-2), 1-14.

Gleadow, A. J. W., & Lovering, J. F. (1974). The effect of weathering on fission track dating. Earth and Planetary Science Letters, 22(2), 163-168.

Gleadow, A. J. W., Hurford, A. J., & Quaife, R. D. (1976). Fission track dating of zircon: improved etching techniques. Earth and Planetary Science Letters, 33(2), 273-276.

Gleadow, A. J. W., Duddy, I. R., Green, P. F., & Lovering, J. F. (1986). Confined fission track lengths in apatite: a diagnostic tool for thermal history analysis. Contributions to Mineralogy and Petrology, 94(4), 405-415.

Glodny, J., Kühn, A., & Austrheim, H. (2008). Diffusion versus recrystallization processes in Rb–Sr geochronology: isotopic relics in eclogite facies rocks, Western Gneiss Region, Norway. Geochimica et Cosmochimica Acta, 72(2), 506-525.

Glotzbach, C., Bernet, M., & Van Der Beek, P. (2011). Detrital thermochronology records changing source areas and steady exhumation in the Western European Alps. Geology, 39(3), 239-242.

Glotzbach, C., Van Der Beek, P., Carcaillet, J., & Delunel, R. (2013). Deciphering the driving forces of erosion rates on millennial to million-year timescales in glacially impacted landscapes: An example from the Western Alps. Journal of Geophysical Research: Earth Surface, 118(3), 1491-1515.

Glotzbach, C., Busschers, F. S., & Winsemann, J. (2018). Detrital thermochronology of Rhine, Elbe and Meuse river sediment (Central Europe): implications for provenance, erosion and mineral fertility. International Journal of Earth Sciences, 107(2), 459-479.

Godard, V., Bourlès, D. L., Spinabella, F., Burbank, D. W., Bookhagen, B., Fisher, G. B., ... & Léanni, L. (2014). Dominance of tectonics over climate in Himalayan denudation. Geology, 42(3), 243-246.

Godin, L., Grujic, D., Law, R. D., & Searle, M. P. (2006). Channel flow, ductile extrusion and exhumation in continental collision zones: an introduction. Geological Society, London, Special Publications, 268(1), 1-23.

Gombosi, D. J., Garver, J. I., & Baldwin, S. L. (2014). On the development of electron microprobe zircon fission-track geochronology. Chemical Geology, 363, 312-321.

Goscombe, B., Gray, D., & Foster, D. A. (2018). Metamorphic response to collision in the Central Himalayan Orogen. Gondwana Research, 57, 191-265.

Graham, S. A., Dickinson, W. R., & Ingersoll, R. V. (1975). Himalayan-Bengal model for flysch dispersal in the Appalachian-Ouachita system. Geological Society of America Bulletin, 86(3), 273-286.

Green, P. F., Duddy, I. R., Gleadow, A. J. W., Tingate, P. R., & Laslett, G. M. (1986). Thermal annealing of fission tracks in apatite: 1. A qualitative description. Chemical Geology: Isotope Geoscience section, 59, 237-253.

Grujic, D., Coutand, I., Bookhagen, B., Bonnet, S., Blythe, A., & Duncan, C. (2006). Climatic forcing of erosion, landscape, and tectonics in the Bhutan Himalayas. Geology, 34(10), 801-804.

Guenthner, W. R., Reiners, P. W., Ketcham, R. A., Nasdala, L., & Giester, G. (2013). Helium diffusion in natural zircon: Radiation damage, anisotropy, and the interpretation of zircon (U-Th)/He thermochronology. American Journal of Science, 313(3), 145-198.

Guillot, S., Hodges, K., Fort, P. L., & Pêcher, A. (1994). New constraints on the age of the Manaslu leucogranite: Evidence for episodic tectonic denudation in the central Himalayas. Geology, 22(6), 559-562.

Handy, M. R., Schmid, S. M., Bousquet, R., Kissling, E., & Bernoulli, D. (2010). Reconciling plate-tectonic reconstructions of Alpine Tethys with the geological–geophysical record of spreading and subduction in the Alps. Earth-Science Reviews, 102(3-4), 121-158.

Harrison, T. M., & McDougall, I. (1980). Investigations of an intrusive contact, northwest Nelson, New Zealand—I. Thermal, chronological and isotopic constraints. Geochimica et cosmochimica acta, 44(12), 1985-2003.

Hay, D. C., & Dempster, T. J. (2009). Zircon alteration, formation and preservation in sandstones. Sedimentology, 56(7), 2175-2191.

He, M., Zheng, H., Bookhagen, B., & Clift, P. D. (2014). Controls on erosion intensity in the Yangtze River basin tracked by U–Pb detrital zircon dating. Earth-Science Reviews, 136, 121-140.

Herman, F., Copeland, P., Avouac, J. P., Bollinger, L., Mahéo, G., Le Fort, P., ... & Henry, P. (2010). Exhumation, crustal deformation, and thermal structure of the Nepal Himalaya derived from the inversion of thermochronological and thermobarometric data and modeling of the topography. Journal of Geophysical Research: Solid Earth, 115(B6).

Herman, F., Seward, D., Valla, P. G., Carter, A., Kohn, B., Willett, S. D., & Ehlers, T. A. (2013). Worldwide acceleration of mountain erosion under a cooling climate. Nature, 504(7480), 423.

Hippe, K., Kober, F., Zeilinger, G., Ivy-Ochs, S., Maden, C., Wacker, L., ... & Wieler, R. (2012). Quantifying denudation rates and sediment storage on the eastern Altiplano, Bolivia, using cosmogenic 10Be, 26Al, and in situ 14C. Geomorphology, 179, 58-70.

Hodges, K. V. (2000). Tectonics of the Himalaya and southern Tibet from two perspectives. Geological Society of America Bulletin, 112(3), 324-350.

Hodges, K. V., Parrish, R. R., & Searle, M. P. (1996). Tectonic evolution of the central Annapurna range, Nepalese Himalayas. Tectonics, 15(6), 1264-1291.

Hourigan, J. K., Reiners, P. W., & Brandon, M. T. (2005). U-Th zonation-dependent alpha-ejection in (U-Th)/He chronometry. Geochimica et Cosmochimica Acta, 69(13), 3349-3365.

Hsu, S. K., Liu, C. S., Shyu, C. T., Liu, S. Y., Sibuet, J. C., Lallemand, S., ... & Reed, D. (1998). New gravity and magnetic anomaly maps in the Taiwan-Luzon region and their preliminary interpretation. Terr. Atmos. Ocean. Sci, 9(3), 509-532.

Hsu, W. H., Byrne, T. B., Ouimet, W., Lee, Y. H., Chen, Y. G., Soest, M. V., & Hodges, K. (2016). Pleistocene onset of rapid, punctuated exhumation in the eastern Central Range of the Taiwan orogenic belt. Geology, 44(9), 719-722.

Hu, X., Garzanti, E., Wang, J., Huang, W., An, W., & Webb, A. (2016). The timing of India-Asia collision onset–Facts, theories, controversies. Earth-Science Reviews, 160, 264-299.

Huntington, K. W., Ehlers, T. A., Hodges, K. V., & Whipp Jr, D. M. (2007). Topography, exhumation pathway, age uncertainties, and the interpretation of thermochronometer data. Tectonics, 26(4).

Hurford, A. J. (2019). An historical perspective on fission-track thermochronology. In Fission-Track Thermochronology and its Application to Geology (pp. 3-23). Springer, Cham.

Huyghe, P., Mugnier, J. L., Gajurel, A. P., & Delcaillau, B. (2005). Tectonic and climatic control of the changes in the sedimentary record of the Karnali River section (Siwaliks of western Nepal). Island Arc, 14(4), 311-327.

Ingersoll, R. V. (2014). Provenance (geology). In AccessScience. McGraw-Hill Education. https://doi.org/10.1036/1097-8542.757524

Ingersoll, R. V., Dickinson, W. R., Graham, S. A., Chan, M. A., & Archer, A. W. (2003). Remnant-ocean submarine fans: largest sedimentary systems on Earth. Special Papers-Geological Society of America, 191-208.

Jacobs, J., Paoli, G., Rocchi, S., Ksienzyk, A. K., Sirevaag, H., & Elburg, M. A. (2018). Alps to Apennines zircon roller coaster along the Adria microplate margin. Scientific reports, 8(1), 2704.

Jamieson, R. A., & Beaumont, C. (2013). On the origin of orogens. Bulletin, 125(11-12), 1671-1702.

Ji, W. Q., Malusà, M. G., Tiepolo, M., Langone, A., Zhao, L., & Wu, F. Y. (2019). Synchronous Periadriatic magmatism in the Western and Central Alps in the absence of slab breakoff. Terra Nova, 31(2), 120-128.

Johnsson, M. J. (1993). The system controlling the composition of clastic sediments. Special Papers-Geological Society of America, 1-1.

Jolivet, L., & Faccenna, C. (2000). Mediterranean extension and the Africa-Eurasia collision. Tectonics, 19(6), 1095-1106.

Jourdan, S., Bernet, M., Tricart, P., Hardwick, E., Paquette, J. L., Guillot, S., ... & Schwartz, S. (2013). Short-lived, fast erosional exhumation of the internal western Alps during the late early Oligocene: Constraints from geothermochronology of pro-and retro-side foreland basin sediments. Lithosphere, 5(2), 211-225.

Jourdan, S., Bernet, M., Hardwick, E., Paquette, J. L., Tricart, P., Senebier, F., & Coeur, F. (2018). Geo-thermochronology of the Saint Antonin basin, south-eastern France. Bulletin de la Société Géologique de France, 189(3).

Kasuya, M., & Naeser, C. W. (1988). The effect of α-damage on fission-track annealing in zircon. International Journal of Radiation Applications and Instrumentation. Part D. Nuclear Tracks and Radiation Measurements, 14(4), 477-480.

Ketcham, R. A. (2005). Forward and inverse modeling of low-temperature thermochronometry data. Reviews in mineralogy and geochemistry, 58(1), 275-314.

Kirstein, L. A., Fellin, M. G., Willett, S. D., Carter, A., Chen, Y. G., Garver, J. I., & Lee, D. C. (2010). Pliocene onset of rapid exhumation in Taiwan during arc–continent collision: new insights from detrital thermochronometry. Basin Research, 22(3), 270-285.

Kirstein, L. A., Carter, A., & Chen, Y. G. (2014). Impacts of arc collision on small orogens: new insights from the Coastal Range detrital record, Taiwan. Journal of the Geological Society, 171(1), 5-8.

Kohn, B., Chung, L., & Gleadow, A. (2019). Fission-Track Analysis: Field Collection, Sample Preparation and Data Acquisition. In Fission-Track Thermochronology and its Application to Geology (pp. 25-48). Springer, Cham.

Komar, P. D. (2007). The entrainment, transport and sorting of heavy minerals by waves and currents. Developments in Sedimentology, 58, 3-48.

Komar, P. D., & Li, Z. (1988). Applications of grain-pivoting and sliding analyses to selective entrapment of gravel and to flow-competence evaluations. Sedimentology, 35(4), 681-695.

Komar, P. D., & Wang, C. (1984). Processes of selective grain transport and the formation of placers on beaches. The Journal of Geology, 92(6), 637-655.

Kuenen, P. H. (1959). Experimental abrasion; 3, fluviatile action on sand. American Journal of Science, 257(3), 172-190.

Kuenen, P. H. (1960). Experimental abrasion 4: eolian action. The Journal of Geology, 68(4), 427-449.

Kuhlemann, J., Dunkl, I., Brügel, A., Spiegel, C., & Frisch, W. (2006). From source terrains of the Eastern Alps to the Molasse Basin: Detrital record of non-steady-state exhumation. Tectonophysics, 413(3-4), 301-316.

Lång, L. O. (2000). Heavy mineral weathering under acidic soil conditions. Applied Geochemistry, 15(4), 415-423.

Lang, K. A., Huntington, K. W., Burmester, R., & Housen, B. (2016). Rapid exhumation of the eastern Himalayan syntaxis since the late Miocene. Geological Society of America Bulletin, 128(9-10), 1403-1422.

Lavarini, C., Attal, M., da Costa Filho, C. A., & Kirstein, L. A. (2018). Does pebble abrasion influence detrital age population statistics? A numerical investigation of natural data sets. Journal of Geophysical Research: Earth Surface, 123(10), 2577-2601.

Le Fort, P. (1975). Himalayas: the collided range. Present knowledge of the continental arc. American Journal of Science, 275(1), 1-44.

Le Roux, J. P. (2005). Grains in motion: A review. Sedimentary Geology, 178(3-4), 285-313.

Le Roux, G., Laverret, E., & Shotyk, W. (2006). Fate of calcite, apatite and feldspars in an ombrotrophic peat bog, Black Forest, Germany. Journal of the Geological Society, 163(4), 641-646.

Lee, Y. H., Chen, C. C., Liu, T. K., Ho, H. C., Lu, H. Y., & Lo, W. (2006). Mountain building mechanisms in the Southern Central Range of the Taiwan Orogenic Belt—From accretionary wedge deformation to arc–continental collision. Earth and Planetary Science Letters, 252(3-4), 413-422.

Lee, Y. H., Byrne, T., Wang, W. H., Lo, W., Rau, R. J., & Lu, H. Y. (2015). Simultaneous mountain building in the Taiwan orogenic belt. Geology, 43(5), 451-454.

Li, X., Zattin, M., & Olivetti, V. (2019). A detrital apatite fission-track study of the CIROS-2 sedimentary record: Tracing ice pathways in the Ross Sea area over the last 5 Ma. Terra Nova, 31(3), 271-280.

Liao, J., Malusà, M. G., Zhao, L., Baldwin, S. L., Fitzgerald, P. G., & Gerya, T. (2018a). Divergent plate motion drives rapid exhumation of (ultra) high pressure rocks. Earth and Planetary Science Letters, 491, 67-80.

Liao, J., Gerya, T., & Malusà, M. G. (2018b). 3D modeling of crustal shortening influenced by along-strike lithological changes: Implications for continental collision in the Western and Central Alps. Tectonophysics, 746, 425-438.

Lickorish, W. H., Ford, M., Burgisser, J., & Cobbold, P. R. (2002). Arcuate thrust systems in sandbox experiments: A comparison to the external arcs of the Western Alps. Geological Society of America Bulletin, 114(9), 1089-1107.

Lin, A. T., Watts, A. B., & Hesselbo, S. P. (2003). Cenozoic stratigraphy and subsidence history of the South China Sea margin in the Taiwan region. Basin Research, 15(4), 453-478.

Liu, T. K., Chen, Y. G., Chen, W. S., & Jiang, S. H. (2000). Rates of cooling and denudation of the Early Penglai Orogeny, Taiwan, as assessed by fission-track constraints. Tectonophysics, 320(1), 69-82.

Lonergan, L., & Johnson, C. (1998). Reconstructing orogenic exhumation histories using synorogenic detrital zircons and apatites: an example from the Betic Cordillera, SE Spain. Basin Research, 10(3), 353-364.

Lu, G., Winkler, W., Rahn, M., von Quadt, A., & Willett, S. D. (2018). Evaluating igneous sources of the Taveyannaz formation in the Central Alps by detrital zircon U–Pb age dating and geochemistry. Swiss Journal of Geosciences, 111(3), 399-416.

Lu, G., Di Capua, A., Winkler, W., Rahn, M., Guillong, M., von Quadt, A., & Willett, S. D. (2019). Restoring the source-to-sink relationships in the Paleogene foreland basins in the Central and Southern Alps (Switzerland, Italy, France): a detrital zircon study approach. International Journal of Earth Sciences, 1-18.

Lundberg, N., Reed, D. L., Liu, C. S., & Lieske Jr, J. (1997). Forearc-basin closure and arc accretion in the submarine suture zone south of Taiwan. Tectonophysics, 274(1-3), 5-23.

Malatesta, L. C., Avouac, J. P., Brown, N. D., Breitenbach, S. F., Pan, J., Chevalier, M. L., ... & Lavé, J. (2018). Lag and mixing during sediment transfer across the Tian Shan piedmont caused by climate-driven aggradation–incision cycles. Basin Research, 30(4), 613-635.

Malusà, M. G. (2019). A guide for interpreting complex detrital age patterns in stratigraphic sequences. In Fission-Track Thermochronology and its Application to Geology (pp. 279-293). Springer, Cham.

Malusà, M. G., & Balestrieri, M. L. (2012). Burial and exhumation across the Alps–Apennines junction zone constrained by fission-track analysis on modern river sands. Terra Nova, 24(3), 221-226.

Malusà, M. G., & Fitzgerald, P. G. (Eds.) (2019a). Fission-track Thermochronology and Its Application to Geology. Springer International Publishing.

Malusà, M. G., & Fitzgerald, P. G. (2019b). Application of thermochronology to geologic problems: bedrock and detrital approaches. In Fission-Track Thermochronology and its Application to Geology (pp. 191-209). Springer, Cham.

Malusà, M. G., & Fitzgerald, P. G. (2019c). From cooling to exhumation: Setting the reference frame for the interpretation of thermochronologic data. In Fission-Track Thermochronology and its Application to Geology (pp. 147-164). Springer, Cham.

Malusà, M. G., & Garzanti, E. (2012). Actualistic snapshot of the early Oligocene Alps: The Alps–Apennines knot disentangled. Terra Nova, 24(1), 1-6.

Malusà, M. G., & Garzanti, E. (2019). The sedimentology of detrital thermochronology. In Fission-Track Thermochronology and its Application to Geology (pp. 123-143). Springer, Cham.

Malusà, M. G., & Vezzoli, G. (2006). Interplay between erosion and tectonics in the Western Alps. Terra Nova, 18(2), 104-108.

Malusà, M. G., Polino, R., Zattin, M., Bigazzi, G., Martin, S., & Piana, F. (2005). Miocene to Present differential exhumation in the Western Alps: Insights from fission track thermochronology. Tectonics, 24(3).

Malusà, M. G., Zattin, M., Andò, S., Garzanti, E., & Vezzoli, G. (2009). Focused erosion in the Alps constrained by fission-track ages on detrital apatites. Geological Society, London, Special Publications, 324(1), 141-152.

Malusà, M. G., Villa, I. M., Vezzoli, G., & Garzanti, E. (2011a). Detrital geochronology of unroofing magmatic complexes and the slow erosion of Oligocene volcanoes in the Alps. Earth and Planetary Science Letters, 301(1-2), 324-336.

Malusà, M. G., Faccenna, C., Garzanti, E., & Polino, R. (2011b). Divergence in subduction zones and exhumation of high pressure rocks (Eocene Western Alps). Earth and Planetary Science Letters, 310(1-2), 21-32.

Malusà, M. G., Carter, A., Limoncelli, M., Villa, I. M., & Garzanti, E. (2013). Bias in detrital zircon geochronology and thermochronometry. Chemical Geology, 359, 90-107.

Malusà, M. G., Faccenna, C., Baldwin, S. L., Fitzgerald, P. G., Rossetti, F., Balestrieri, M. L., ... & Piromallo, C. (2015). Contrasting styles of (U) HP rock exhumation along the Cenozoic Adria-Europe plate boundary (Western Alps, Calabria, Corsica). Geochemistry, Geophysics, Geosystems, 16(6), 1786-1824.

Malusà, M. G., Danišík, M., & Kuhlemann, J. (2016a). Tracking the Adriatic-slab travel beneath the Tethyan margin of Corsica–Sardinia by low-temperature thermochronometry. Gondwana Research, 31, 135-149.

Malusà, M. G., Resentini, A., & Garzanti, E. (2016b). Hydraulic sorting and mineral fertility bias in detrital geochronology. Gondwana Research, 31, 1-19.

Malusà, M. G., Anfinson, O. A., Dafov, L. N., & Stockli, D. F. (2016c). Tracking Adria indentation beneath the Alps by detrital zircon U-Pb geochronology: Implications for the Oligocene–Miocene dynamics of the Adriatic microplate. Geology, 44(2), 155-158.

Malusà, M. G., Wang, J., Garzanti, E., Liu, Z. C., Villa, I. M., & Wittmann, H. (2017). Trace-element and Nd-isotope systematics in detrital apatite of the Po river catchment: Implications for provenance discrimination and the lag-time approach to detrital thermochronology. Lithos, 290, 48-59.

Mancktelow, N. S., & Grasemann, B. (1997). Time-dependent effects of heat advection and topography on cooling histories during erosion. Tectonophysics, 270(3-4), 167-195.

Meade, B. J. (2007). Present-day kinematics at the India-Asia collision zone. Geology, 35(1), 81-84.

Meesters, A. G. C. A., & Dunai, T. J. (2002). Solving the production–diffusion equation for finite diffusion domains of various shapes: Part II. Application to cases with α-ejection and nonhomogeneous distribution of the source. Chemical Geology, 186(1-2), 57-73.

Meigs, A. J., Burbank, D. W., & Beck, R. A. (1995). Middle-late Miocene (> 10 Ma) formation of the Main Boundary thrust in the western Himalaya. Geology, 23(5), 423-426.

Mesalles, L., Mouthereau, F., Bernet, M., Chang, C. P., Tien-Shun Lin, A., Fillon, C., & Sengelen, X. (2014). From submarine continental accretion to arc-continent orogenic evolution: The thermal record in southern Taiwan. Geology, 42(10), 907-910.

Métivier, F., Gaudemer, Y., Tapponnier, P., & Klein, M. (1999). Mass accumulation rates in Asia during the Cenozoic. Geophysical Journal International, 137(2), 280-318.

Mezger, K., & Krogstad, E. J. (1997). Interpretation of discordant U-Pb zircon ages: An evaluation. Journal of metamorphic Geology, 15(1), 127-140.

Miller, S. R., Fitzgerald, P. G., & Baldwin, S. L. (2010). Cenozoic range-front faulting and development of the Transantarctic Mountains near Cape Surprise, Antarctica: Thermochronologic and geomorphologic constraints. Tectonics, 29(1).

Milliken, K. L. (2007). Provenance and diagenesis of heavy minerals, Cenozoic units of the northwestern Gulf of Mexico sedimentary basin. Developments in Sedimentology, 58, 247-261.

Mitchell, S. G., & Reiners, P. W. (2003). Influence of wildfires on apatite and zircon (U-Th)/He ages. Geology, 31(12), 1025-1028.

Moecher, D. P., & Samson, S. D. (2006). Differential zircon fertility of source terranes and natural bias in the detrital zircon record: Implications for sedimentary provenance analysis. Earth and Planetary Science Letters, 247(3-4), 252-266.

Molnar, P., England, P., & Martinod, J. (1993). Mantle dynamics, uplift of the Tibetan Plateau, and the Indian monsoon. Reviews of Geophysics, 31(4), 357-396.

Montario, M. J., & Garver, J. I. (2009). The thermal evolution of the Grenville Terrane revealed through U-Pb and fission-track analysis of detrital zircon from Cambro-Ordovician quartz arenites of the Potsdam and Galway Formations. The Journal of Geology, 117(6), 595-614.

Montemagni, C., Montomoli, C., Iaccarino, S., Carosi, R., Jain, A. K., Massonne, H. J., & Villa, I. M. (2019). Dating protracted fault activities: microstructures, microchemistry and geochronology of the Vaikrita Thrust, Main Central Thrust zone, Garhwal Himalaya, NW India. Geological Society, London, Special Publications, 481(1), 127-146.

Moore, M. A., & England, P. C. (2001). On the inference of denudation rates from cooling ages of minerals. Earth and Planetary Science Letters, 185(3-4), 265-284.

Morton, A. C. (1979). Surface features of heavy mineral grains from Palaeocene sands of the central North Sea. Scottish Journal of Geology, 15(4), 293-300.

Morton, A. C. (2012). Value of heavy minerals in sediments and sedimentary rocks for provenance, transport history and stratigraphic correlation. Quantitative mineralogy and microanalysis of sediments and sedimentary rocks. Mineralogical Association of Canada Short Course Series, 42, 133-165.

Morton, A. C., & Hallsworth, C. R. (1999). Processes controlling the composition of heavy mineral assemblages in sandstones. Sedimentary Geology, 124(1-4), 3-29.

Morton, A. C., & Hallsworth, C. (2007). Stability of detrital heavy minerals during burial diagenesis. Developments in Sedimentology, 58, 215-245.

Mouthereau, F., & Lacombe, O. (2006). Inversion of the Paleogene Chinese continental margin and thick-skinned deformation in the Western Foreland of Taiwan. Journal of Structural Geology, 28(11), 1977-1993.

Murakami, M. (2010). Average shear work estimation of Nojima fault from fission-track analytical data. Earth Monthly, 32, 24-29.

Murakami, M., & Tagami, T. (2004). Dating pseudotachylyte of the Nojima fault using the zircon fission-track method. Geophysical Research Letters, 31(12).

Naeser, C. W. (1976). Fission track dating. US Geological Survey Open-File Report 76-190.

Najman, Y., Bickle, M., Garzanti, E., Pringle, M., Barfod, D., Brozovic, N., ... & Ando, S. (2009). Reconstructing the exhumation history of the Lesser Himalaya, NW India, from a multitechnique provenance study of the foreland basin Siwalik Group. Tectonics, 28(5).

Najman, Y., Appel, E., Boudagher-Fadel, M., Bown, P., Carter, A., Garzanti, E., ... & Parrish, R. (2010a). Timing of India-Asia collision: Geological, biostratigraphic, and palaeomagnetic constraints. Journal of Geophysical Research: Solid Earth, 115(B12).

Najman, Y., Bickle, M., Garzanti, E., Pringle, M., Barfod, D., Brozovic, N., ... & Ando, S. (2010b). Correction to "Reconstructing the exhumation history of the Lesser Himalaya, NW India, from a multitechnique provenance study of the foreland basin Siwalik Group". Tectonics, 29(6).

Najman, Y., Mark, C., Barfod, D. N., Carter, A., Parrish, R., Chew, D., & Gemignani, L. (2019). Spatial and temporal trends in exhumation of the Eastern Himalaya and syntaxis as determined from a multitechnique detrital thermochronological study of the Bengal Fan. Geological Society of America Bulletin.

Nickel, E. (1973). Experimental dissolution of light and heavy minerals in comparison with weathering and intrastratal solution. Contributions to Sedimentology, 1, 1-68.

Niemi, N. A., Buscher, J. T., Spotila, J. A., House, M. A., & Kelley, S. A. (2013). Insights from low-temperature thermochronometry into transpressional deformation and crustal exhumation along the San Andreas fault in the western Transverse Ranges, California. Tectonics, 32(6), 1602-1622.

O'Sullivan, G. J., Chew, D. M., Morton, A. C., Mark, C., & Henrichs, I. A. (2018). An integrated apatite geochronology and geochemistry tool for sedimentary provenance analysis. Geochemistry, Geophysics, Geosystems, 19(4), 1309-1326.

Ohishi, S., & Hasebe, N. (2012). Observations of fission-tracks in zircons by atomic force microscope. Radiation Measurements, 47(7), 548-556.

Painter, C. S., Carrapa, B., DeCelles, P. G., Gehrels, G. E., & Thomson, S. N. (2014). Exhumation of the North American Cordillera revealed by multi-dating of Upper Jurassic–Upper Cretaceous foreland basin deposits. Bulletin, 126(11-12), 1439-1464.

Parrish, R. R., & Hodges, V. (1996). Isotopic constraints on the age and provenance of the Lesser and Greater Himalayan sequences, Nepalese Himalaya. Geological Society of America Bulletin, 108(7), 904-911.

Peacock, S. M. (1996). Thermal and petrologic structure of subduction zones. Subduction: top to bottom, 96, 119-133.

Piromallo, C., & Faccenna, C. (2004). How deep can we find the traces of Alpine subduction?. Geophysical Research Letters, 31(6).

Pupin, J. P. (1980). Zircon and granite petrology. Contributions to Mineralogy and Petrology, 73(3), 207-220.

Rahl, J. M., Ehlers, T. A., & van der Pluijm, B. A. (2007). Quantifying transient erosion of orogens with detrital thermochronology from syntectonic basin deposits. Earth and Planetary Science Letters, 256(1-2), 147-161.

Rahl, J. M., Harbor, D. J., Galli, C. I., & O'Sullivan, P. (2018). Foreland basin record of uplift and exhumation of the Eastern Cordillera, northwest Argentina. Tectonics, 37(11), 4173-4193.

Rahn, M. K., Brandon, M. T., Batt, G. E., & Garver, J. I. (2004). A zero-damage model for fission-track annealing in zircon. American Mineralogist, 89(4), 473-484.

Raymo, M. 1. (1994). The Himalayas, organic carbon burial, and climate in the Miocene. Paleoceanography, 9(3), 399-404.

Reiners, P. W. (2005). Zircon (U-Th)/He thermochronometry. Reviews in Mineralogy and Geochemistry, 58(1), 151-179.

Reiners, P. W., & Brandon, M. T. (2006). Using thermochronology to understand orogenic erosion. Annu. Rev. Earth Planet. Sci., 34, 419-466.

Reiners, P. W., & Ehlers, T. A. (Eds.). (2005). Low-Temperature Thermochronology: Techniques, Interpretations, and Applications (Vol. 58). Reviews in Mineralogy and Geochemistry.

Reiners, P. W., & Farley, K. A. (2001). Influence of crystal size on apatite (U–Th)/He thermochronology: an example from the Bighorn Mountains, Wyoming. Earth and Planetary Science Letters, 188(3-4), 413-420.

Reiners, P. W., Thomson, S. N., McPhillips, D., Donelick, R. A., & Roering, J. J. (2007). Wildfire thermochronology and the fate and transport of apatite in hillslope and fluvial environments. Journal of Geophysical Research: Earth Surface, 112(F4).

Resentini, A., & Malusà, M. G. (2012). Sediment budgets by detrital apatite fission-track dating (Rivers Dora Baltea and Arc, Western Alps). Geological Society of America Special Papers, 487, 125-140.

Resentini, A., Malusà, M. G., & Garzanti, E. (2013). MinSORTING: An Excel® worksheet for modelling mineral grain-size distribution in sediments, with application to detrital geochronology and provenance studies. Computers & geosciences, 59, 90-97.

Resentini, A., Goren, L., Castelltort, S., & Garzanti, E. (2017). Partitioning sediment flux by provenance and tracing erosion patterns in Taiwan. Journal of Geophysical Research: Earth Surface, 122(7), 1430-1454.

Reverman, R. L., Fellin, M. G., Herman, F., Willett, S. D., & Fitoussi, C. (2012). Climatically versus tectonically forced erosion in the Alps: Thermochronometric constraints from the Adamello Complex, Southern Alps, Italy. Earth and Planetary Science Letters, 339, 127-138.

Ricci Lucchi, F. (1986). The Oligocene to Recent foreland basins of the northern Apennines. In Foreland basins (Vol. 8, pp. 105-139). Blackwell Scientific Oxford.

Ricci Lucchi, F. (2003). Turbidites and foreland basins: an Apenninic perspective. Marine and Petroleum Geology, 20(6-8), 727-732.

Rittenhouse, G. (1943). Transportation and deposition of heavy mineral. Bulletin of the geological Society of America, 54(12), 1725-1780.

Rolland, Y., Mahéo, G., Guillot, S., & Pêcher, A. (2001). Tectono-metamorphic evolution of the Karakorum Metamorphic complex (Dassu–Askole area, NE Pakistan): exhumation of mid-crustal HT–MP gneisses in a convergent context. Journal of Metamorphic Geology, 19(6), 717-737.

Rosenberg, C. L., Berger, A., Bellahsen, N., & Bousquet, R. (2015). Relating orogen width to shortening, erosion, and exhumation during Alpine collision. Tectonics, 34(6), 1306-1328.

Rubatto, D., & Hermann, J. (2001). Exhumation as fast as subduction?. Geology, 29(1), 3-6.

Rubey, W. W. (1933). The size distribution of heavy minerals within a water-laid sandstone. Journal of Sedimentary Research, 3(1), 3-29.

Ruiz, G., & Seward, D. (2006). The Punjab foreland basin of Pakistan: a reinterpretation of zircon fission-track data in the light of Miocene hinterland dynamics. Terra Nova, 18(4), 248-256.

Ruiz, G. M. H., Seward, D., & Winkler, W. (2004). Detrital thermochronology-a new perspective on hinterland tectonics, an example from the Andean Amazon Basin, Ecuador. Basin Research, 16(3), 413-430.

Russell, R. D., & Taylor, R. E. (1937). Roundness and shape of Mississippi River sands. The Journal of Geology, 45(3), 225-267.

Saylor, J. E., Stockli, D. F., Horton, B. K., Nie, J., & Mora, A. (2012). Discriminating rapid exhumation from syndepositional volcanism using detrital zircon double dating: Implications for the tectonic history of the Eastern Cordillera, Colombia. Bulletin of the Geological Society of America, 124(5-6), 762-779.

Saylor, J. E., Knowles, J. N., Horton, B. K., Nie, J., & Mora, A. (2013). Mixing of source populations recorded in detrital zircon U-Pb age spectra of modern river sands. The Journal of Geology, 121(1), 17-33.

Schmid, S. M., Fügenschuh, B., Kissling, E., & Schuster, R. (2004). Tectonic map and overall architecture of the Alpine orogen. Eclogae Geologicae Helvetiae, 97(1), 93-117.

Schmidt, J. L. et al (2014). Little Devil's postpile revisited: behavior of multiple thermochronometers in a contact aureole. In: Abstracts of the 14th international conference on thermochronology, Chamonix, France, 8–14 Sept 2014

Schneider, D. A., & Issler, D. R. (2019). Application of low-temperature thermochronology to hydrocarbon exploration. In Fission-Track Thermochronology and its Application to Geology (pp. 315-333). Springer, Cham.

Schuiling, R. D., Scholten, M. J., de Meijer, R. J., & Riezebos, H. J. (1985). Grain size distribution of different minerals in a sediment as a function of their specific density. Geologie en Mijnbouw, 64(2), 199-203.

Searle, M. P., Law, R. D., Godin, L., Larson, K. P., Streule, M. J., Cottle, J. M., & Jessup, M. J. (2008). Defining the Himalayan main central thrust in Nepal. Journal of the Geological Society, 165(2), 523-534.

Seno, T., Stein, S., & Gripp, A. E. (1993). A model for the motion of the Philippine Sea plate consistent with NUVEL-1 and geological data. Journal of Geophysical Research: Solid Earth, 98(B10), 17941-17948.

Shen, T., Wang, G., Leloup, P. H., van der Beek, P., Bernet, M., Cao, K., ... & Zhang, K. (2016). Controls on Cenozoic exhumation of the Tethyan Himalaya from fission-track thermochronology and detrital zircon U-Pb geochronology in the Gyirong basin area, southern Tibet. Tectonics, 35(7), 1713-1734.

Silver, L. T., Williams, I. S., & Woodhead, J. A. (1981). Uranium in granites from southwestern United States: actanide parent–daughter system, sites and mobilization US Department of Energy. Open File Report, GJBX-45, 315.

Simoes, M., Avouac, J. P., Beyssac, O., Goffé, B., Farley, K. A., & Chen, Y. G. (2007). Mountain building in Taiwan: A thermokinematic model. Journal of Geophysical Research: Solid Earth, 112(B11).

Slingerland, R., & Smith, N. D. (1986). Occurrence and formation of water-laid placers. Annual Review of Earth and Planetary Sciences, 14(1), 113-147.

Spear, F. S. (1993). Metamorphic phase equilibria and pressure-temperature-time paths. Mineralogical Society of America Monograph, 352-356.

Spiegel, C., Siebel, W., Kuhlemann, J., & Frisch, W. (2004). Toward a comprehensive provenance analysis: A multi-method approach and its implications for the evolution of the Central Alps. Special Papers, Geological Society of America, 37-50.

Spotila, J. A. (2005). Applications of low-temperature thermochronometry to quantification of recent exhumation in mountain belts. Reviews in Mineralogy and Geochemistry, 58(1), 449-466.

Stalder, N. F., Fellin, M. G., Caracciolo, L., Guillong, M., Winkler, W., Milli, S., ... & Critelli, S. (2018). Dispersal pathways in the early Messinian Adriatic foreland and provenance of the Laga Formation (Central Apennines, Italy). Sedimentary geology, 375, 289-308.

Stickroth, S. F., Carrapa, B., DeCelles, P. G., Gehrels, G. E., & Thomson, S. N. (2019). Tracking the growth of the Himalayan fold-and-thrust belt from lower Miocene foreland basin strata: Dumri Formation, western Nepal. Tectonics. doi: 10.1029/2018TC005390

Stock, G. M., Ehlers, T. A., & Farley, K. A. (2006). Where does sediment come from? Quantifying catchment erosion with detrital apatite (U-Th)/He thermochronometry. Geology, 34(9), 725-728.

Stockli, D. F. (2005). Application of low-temperature thermochronometry to extensional tectonic settings. Reviews in Mineralogy and Geochemistry, 58(1), 411-448.

Stolar, D. B., Willett, S. D., & Montgomery, D. R. (2007). Characterization of topographic steady state in Taiwan. Earth and Planetary Science Letters, 261(3-4), 421-431.

Stübner, K., Grujic, D., Dunkl, I., Thiede, R., & Eugster, P. (2018). Pliocene episodic exhumation and the significance of the Munsiari thrust in the northwestern Himalaya. Earth and Planetary Science Letters, 481, 273-283.

Stüwe, K., & Barr, T. D. (1998). On uplift and exhumation during convergence. Tectonics, 17(1), 80-88.

Stüwe, K., White, L., & Brown, R. (1994). The influence of eroding topography on steady-state isotherms. Application to fission track analysis. Earth and Planetary Science Letters, 124(1-4), 63-74.

Sun, W., Zhao, L., Malusà, M. G., Guillot, S., & Fu, L. Y. (2019). 3-D Pn tomography reveals continental subduction at the boundaries of the Adriatic microplate in the absence of a precursor oceanic slab. Earth and Planetary Science Letters, 510, 131-141.

Suppe, J. (1981). Mechanics of mountain building and metamorphism in Taiwan. Mem. Geol. Soc. China, 4(6), 67-89.

Suppe, J. (1984). Kinematics of arc-continent collision, flipping of subduction, and back-arc spreading near Taiwan. Memoir. Geol. Soc. China, 6, 21-33Sláma, J., & Košler, J. (2012). Effects of sampling and mineral separation on accuracy of detrital zircon studies. Geochemistry, Geophysics, Geosystems, 13(5).

Szopa, K., Skreczko, S., Chew, D., Krzykawski, T., & Szymczyk, A. (2019). Multi-tool (LA-ICPMS, EMPA and XRD) investigation on heavy minerals from selected Holocene peat-bog deposits from the upper Vistula River Valley, Poland. Minerals, in press.

Szulc, A. G., Najman, Y., Sinclair, H. D., Pringle, M., Bickle, M., Chapman, H., ... & DeCelles, P. (2006). Tectonic evolution of the Himalaya constrained by detrital 40Ar^ 39Ar, Sm-Nd and petrographic data from the Siwalik foreland basin succession, SW Nepal. Basin Research, 18(4), 375-391.

Tagami, T. (2019). Application of Fission-Track Thermochronology to Understand Fault Zones. In Fission-Track Thermochronology and its Application to Geology (pp. 221-233). Springer, Cham.

Tagami, T., Ito, H., & Nishimura, S. (1990). Thermal annealing characteristics of spontaneous fission tracks in zircon. Chemical Geology: Isotope Geoscience Section, 80(2), 159-169.

Tagami, T., Carter, A., & Hurford, A. J. (1996). Natural long-term annealing of the zircon fission-track system in Vienna Basin deep borehole samples: constraints upon the partial annealing zone and closure temperature. Chemical Geology, 130(1-2), 147-157.

Tatzel, M., Dunkl, I., & von Eynatten, H. (2017). Provenance of Palaeo-Rhine sediments from zircon thermochronology, geochemistry, U/Pb dating and heavy mineral assemblages. Basin Research, 29, 396-417.

Thiede, R. C., & Ehlers, T. A. (2013). Large spatial and temporal variations in Himalayan denudation. Earth and Planetary Science Letters, 371, 278-293.

Thiede, R. C., Bookhagen, B., Arrowsmith, J. R., Sobel, E. R., & Strecker, M. R. (2004). Climatic control on rapid exhumation along the Southern Himalayan Front. Earth and Planetary Science Letters, 222(3-4), 791-806.

Thomson, S. N., Gehrels, G. E., Ruiz, J., & Buchwaldt, R. (2012). Routine low-damage apatite U-Pb dating using laser ablation–multicollector–ICPMS. Geochemistry, Geophysics, Geosystems, 13(2).

Tranel, L. M., Spotila, J. A., Kowalewski, M. J., & Waller, C. M. (2011). Spatial variation of erosion in a small, glaciated basin in the Teton Range, Wyoming, based on detrital apatite (U-Th)/He thermochronology. Basin Research, 23(5), 571-590.

Tremblay, M. M., Fox, M., Schmidt, J. L., Tripathy-Lang, A., Wielicki, M. M., Harrison, T. M., ... & Shuster, D. L. (2015). Erosion in southern Tibet shut down at∼ 10 Ma due to enhanced rock uplift within the Himalaya. Proceedings of the National Academy of Sciences, 112(39), 12030-12035.

Van Der Beek, P., Robert, X., Mugnier, J. L., Bernet, M., Huyghe, P., & Labrin, E. (2006). Late Miocene-Recent exhumation of the central Himalaya and recycling in the foreland basin assessed by apatite fission-track thermochronology of Siwalik sediments, Nepal. Basin Research, 18(4), 413-434.

Van Loon, A. T., & Mange, M. A. (2007). 'In situ'dissolution of heavy minerals through extreme weathering, and the application of the surviving assemblages and their dissolution characteristics to correlation of Dutch and German silver sands. Developments in Sedimentology, 58, 189-213.

Vance, D., Bickle, M., Ivy-Ochs, S., & Kubik, P. W. (2003). Erosion and exhumation in the Himalaya from cosmogenic isotope inventories of river sediments. Earth and Planetary Science Letters, 206(3-4), 273-288.

Vannay, J. C., Grasemann, B., Rahn, M., Frank, W., Carter, A., Baudraz, V., & Cosca, M. (2004). Miocene to Holocene exhumation of metamorphic crustal wedges in the NW Himalaya: Evidence for tectonic extrusion coupled to fluvial erosion. Tectonics, 23(1).

Velbel, M. A. (1999). Bond strength and the relative weathering rates of simple orthosilicates. American Journal of Science, 299(7-9), 679-696.

Vermeesch, P. (2004). How many grains are needed for a provenance study?. Earth and Planetary Science Letters, 224(3-4), 441-451.

Vermeesch, P. (2007). Quantitative geomorphology of the White Mountains (California) using detrital apatite fission track thermochronology. Journal of Geophysical Research: Earth Surface, 112(F3).

Vermeesch, P. (2012). On the visualisation of detrital age distributions. Chemical Geology, 312, 190-194.

Vermeesch, P. (2019). Statistics for Fission-Track Thermochronology. In Fission-Track Thermochronology and its Application to Geology (pp. 109-122). Springer, Cham.

Vernon, A. J., van Der Beek, P. A., Sinclair, H. D., & Rahn, M. K. (2008). Increase in late Neogene denudation of the European Alps confirmed by analysis of a fission-track thermochronology database. Earth and Planetary Science Letters, 270(3-4), 316-329.

Villa, I. M. (1998). Isotopic closure. Terra Nova, 10(1), 42–47.

Villa, I. M. (2010). Disequilibrium textures versus equilibrium modelling: geochronology at the crossroads. Geological Society, London, Special Publications, 332(1), 1-15.

Viola, G., Mancktelow, N. S., & Seward, D. (2001). Late Oligocene-Neogene evolution of Europe-Adria collision: New structural and geochronological evidence from the Giudicarie fault system (Italian Eastern Alps). Tectonics, 20(6), 999-1020.

von Eynatten, H., & Dunkl, I. (2012). Assessing the sediment factory: the role of single grain analysis. Earth-Science Reviews, 115(1-2), 97-120.

Wagner, G. A. (1972). The geological interpretation of fission track ages. Trans Am Nucl Soc, 15,117.

Wagner, G. A., & Reimer, G. M. (1972). Fission track tectonics: the tectonic interpretation of fission track apatite ages. Earth and Planetary Science Letters, 14(2), 263-268.

Wagner, G.A., Reimer, G.M., & Jäger, E. (1977). Cooling ages derived by apatite fission-track, mica Rb-Sr and K-Ar dating: the uplift and cooling history of the Central Alps. Mem Inst Geol Mineral Univ Padova, 30, 1–27.

Wagner, G. A., Miller, D. S., & Jäger, E. (1979). Fission track ages on apatite of Bergell rocks from central Alps and Bergell boulders in Oligocene sediments. Earth and Planetary Science Letters, 45(2), 355-360.

Watson, E. B., Wark, D. A., & Thomas, J. B. (2006). Crystallization thermometers for zircon and rutile. Contributions to Mineralogy and Petrology, 151(4), 413.

Weinberg, R. F. (2016). Himalayan leucogranites and migmatites: nature, timing and duration of anatexis. Journal of Metamorphic Geology, 34(8), 821-843.

White, N. M., Pringle, M., Garzanti, E., Bickle, M., Najman, Y., Chapman, H., & Friend, P. (2002). Constraints on the exhumation and erosion of the High Himalayan Slab, NW India, from foreland basin deposits. Earth and Planetary Science Letters, 195(1-2), 29-44.

Whitmarsh, R. B., Manatschal, G., & Minshull, T. A. (2001). Evolution of magma-poor continental margins from rifting to seafloor spreading. Nature, 413(6852), 150.

Willett, S. D., & Brandon, M. T. (2013). Some analytical methods for converting thermochronometric age to erosion rate. Geochemistry, Geophysics, Geosystems, 14(1), 209-222.

Willett, S. D., Fisher, D., Fuller, C., En-Chao, Y., & Chia-Yu, L. (2003). Erosion rates and orogenic-wedge kinematics in Taiwan inferred from fission-track thermochronometry. Geology, 31(11), 945-948.

Williams, M. L., Jercinovic, M. J., & Hetherington, C. J. (2007). Microprobe monazite geochronology: understanding geologic processes by integrating composition and chronology. Annu. Rev. Earth Planet. Sci., 35, 137-175.

Wittmann, H., Von Blanckenburg, F., Maurice, L., Guyot, J. L., & Kubik, P. W. (2011). Recycling of Amazon floodplain sediment quantified by cosmogenic ^{26}Al and ^{10}Be. Geology, 39(5), 467-470.

Wittmann, H., Malusà, M. G., Resentini, A., Garzanti, E., & Niedermann, S. (2016). The cosmogenic record of mountain erosion transmitted across a foreland basin: Source-to-sink analysis of in situ ^{10}Be, ^{26}Al and ^{21}Ne in sediment of the Po river catchment. Earth and Planetary Science Letters, 452, 258-271.

Wolf, R. A., Farley, K. A., & Kass, D. M. (1998). Modeling of the temperature sensitivity of the apatite (U–Th)/He thermochronometer. Chemical Geology, 148(1-2), 105-114.

Worden, R. H., & Burley, S. D. (2003). Sandstone diagenesis: the evolution of sand to stone. Sandstone Diagenesis: Recent and Ancient, 4, 3-44.

Yin, A., & Harrison, T. M. (2000). Geologic evolution of the Himalayan-Tibetan orogen. Annual review of earth and planetary sciences, 28(1), 211-280.

Yu, S. B., Chen, H. Y., & Kuo, L. C. (1997). Velocity field of GPS stations in the Taiwan area. Tectonophysics, 274(1-3), 41-59.

Zanchetta, S., Malusà, M. G., & Zanchi, A. (2015). Precollisional development and Cenozoic evolution of the Southalpine retrobelt (European Alps). Lithosphere, 7(6), 662-681.

Zattin, M., Talarico, F. M., & Sandroni, S. (2010). Integrated provenance and detrital thermochronology studies on the ANDRILL AND-2A drill core: Late Oligocene–Early Miocene exhumation of the Transantarctic Mountains (southern Victoria Land, Antarctica). Terra Nova, 22(5), 361-368.

Zeitler, P. K., Johnson, N. M., Briggs, N. D., & Naeser, C. W. (1986). Uplift history of the NW Himalaya as recorded by fission-track ages on detrital Siwalik zircons. In Proceedings of the Symposium on Mesozoic and Cenozoic Geology. Jiqing H (ed) Geological Publishing House, Beijing (pp. 481-494).

Zeitler, P. K., Meltzer, A. S., Koons, P. O., Craw, D., Hallet, B., Chamberlain, C. P., ... & Shroder, J. (2001). Erosion, Himalayan geodynamics, and the geomorphology of metamorphism. GSA Today, 11(1), 4-9.

Zeitler, P. K., Meltzer, A. S., Brown, L., Kidd, W. S., Lim, C., & Enkelmann, E. (2014). Tectonics and topographic evolution of Namche Barwa and the easternmost Lhasa block, Tibet. Toward an Improved Understanding of Uplift Mechanisms and the Elevation History of the Tibetan Plateau: Geological Society of America Special Paper, 507, 23-58.

Zhang, J. Y., Yin, A., Liu, W. C., Wu, F. Y., Lin, D., & Grove, M. (2012). Coupled U-Pb dating and Hf isotopic analysis of detrital zircon of modern river sand from the Yalu River (Yarlung Tsangpo) drainage system in southern Tibet: Constraints on the transport processes and evolution of Himalayan rivers. Geological Society of America Bulletin, 124(9-10), 1449-1473.

Zhao, L., Paul, A., Guillot, S., Solarino, S., Malusà, M. G., Zheng, T., ... & Zhu, R. (2015). First seismic evidence for continental subduction beneath the Western Alps. Geology, 43(9), 815-818.

Zhao, L., Paul, A., Malusà, M. G., Xu, X., Zheng, T., Solarino, S., ... & Aubert, C. (2016). Continuity of the Alpine slab unraveled by high-resolution P wave tomography. Journal of Geophysical Research: Solid Earth, 121(12), 8720-8737.

Zhao, W., Nelson, K. D., Che, J., Quo, J., Lu, D., Wu, C., & Liu, X. (1993). Deep seismic reflection evidence for continental underthrusting beneath southern Tibet. Nature, 366(6455), 557.

Zhuang, G., Najman, Y., Guillot, S., Roddaz, M., Antoine, P. O., Métais, G., ... & Solangi, S. H. (2015). Constraints on the collision and the pre-collision tectonic configuration between India and Asia from detrital geochronology, thermochronology, and geochemistry studies in the lower Indus basin, Pakistan. Earth and Planetary Science Letters, 432, 363-373.

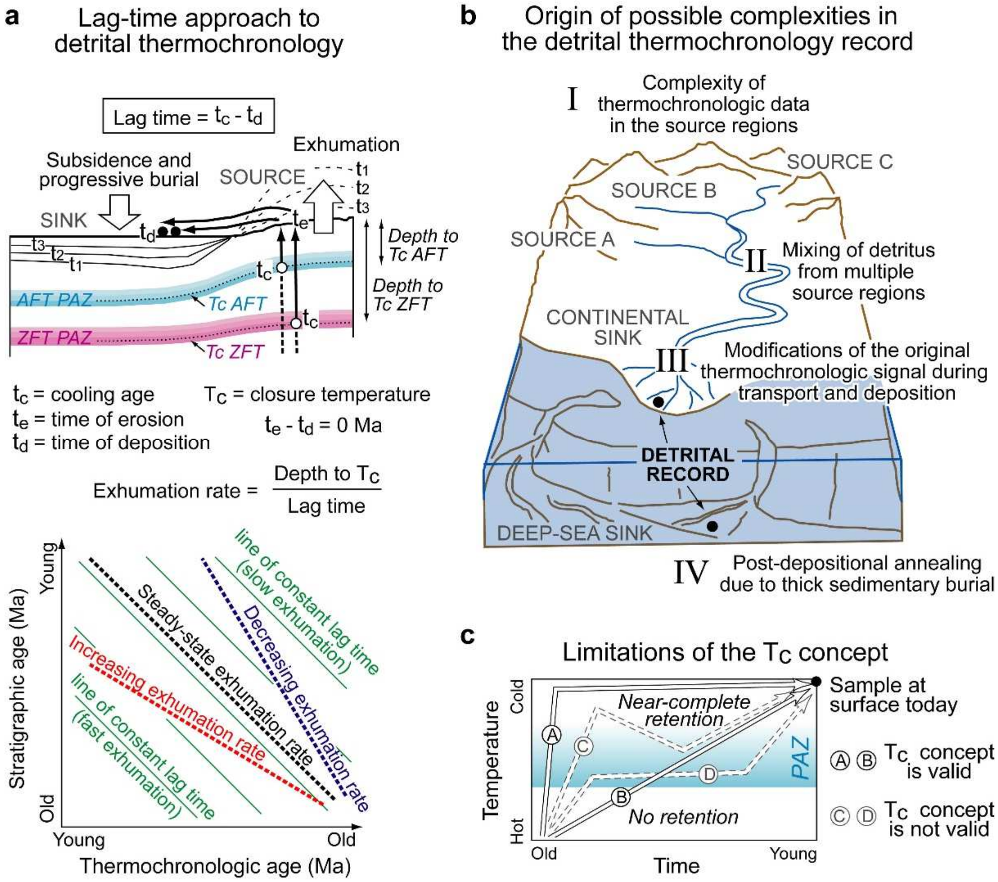

(1.5 column fitting image)

Fig. 1. **(a)** Classic lag-time approach to detrital thermochronology (modified after Cerveny et al., 1988; Garver et al., 1999). Upper panel: rocks are exhumed across the partial annealing zones (PAZ) of the fission-track systems in zircon (ZFT) and apatite (AFT), cross the corresponding closure temperatures T_c at the cooling age t_c, and reach the Earth's surface at time t_e. Apatite and zircon grains are then eroded from bedrock and deposited in a sedimentary basin at time t_d, where t_d is independently constrained, for example by biostratigraphy. According to this simple conceptual scheme, the lag time between t_c and t_d would provide, under the assumptions summarized in Fig. 2, an estimate of the average exhumation rate from the depth corresponding to the T_c isotherm to Earth's surface. Lower panel: typical lag-time diagram, reporting stratigraphic age vs. thermochronologic age (lines of equal lag time are indicated in green). Decreasing lag-time values up section (in red) would suggest increasing exhumation rates, constant lag-time values (in black) would suggest steady-state exhumation rates, increasing lag-time values (in blue) would suggest decreasing exhumation rates. These relationships are sometimes used to infer whether an eroding mountain belt is under a constructional, steady-state or decay stage of evolution (e.g., Spotila, 2005) and to provide indications on orogenic wedge dynamics (Carrapa, 2009). **(b)** The simplified conceptual scheme in (a) clashes against the thermochronologic complexities characterizing sedimentary successions because of factors I to IV. **(c)** The closure temperature and cooling age concepts, representing the basis of the lag-time approach shown in (a), can be applied to rocks that have cooled monotonically from higher to lower temperatures (A, B) (Dodson, 1973), but cannot be applied to rocks that have followed more complex cooling paths during exhumation towards the Earth surface (C, D).

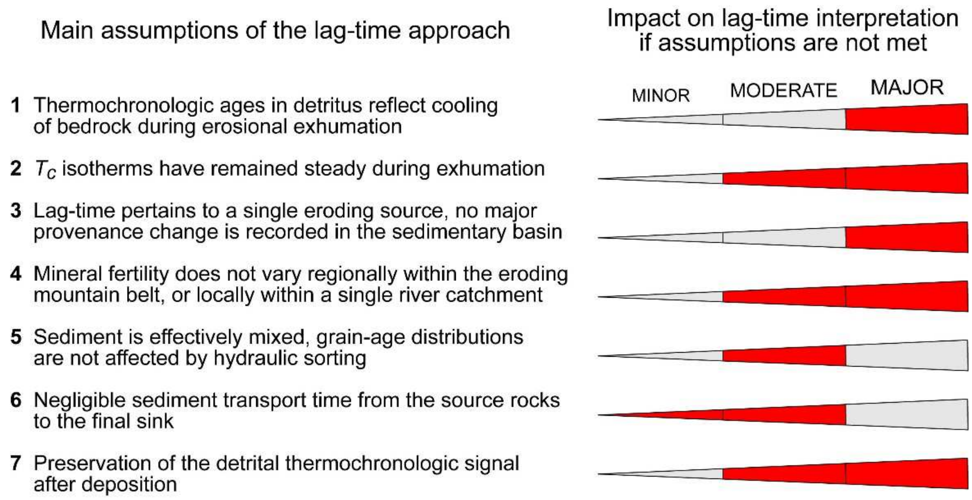

(1.5 column fitting image)

Fig. 2. Main assumptions of the lag-time approach and their potential impact on lag-time interpretation (Major: inferred scenarios could be incorrect if assumptions are not met; Moderate: inferred scenarios are broadly correct, but inferred exhumation rates are either underestimated or overestimated; Minor: the impact on interpretation is generally negligible). Assumptions 1-to-7 should be evaluated on a case by case basis. Most of them (1-3 and 6-7) can be tested by inspecting the thermochronologic age trends through a stratigraphic succession (see Sections 3 to 6); assumption 4 can be tested by direct mineral fertility measurements, which require that the source area has not been completely eroded away (see Section 4.5); assumption 5 can be tested by inspecting the relationships between grain age and grain size (see Section 5.1).

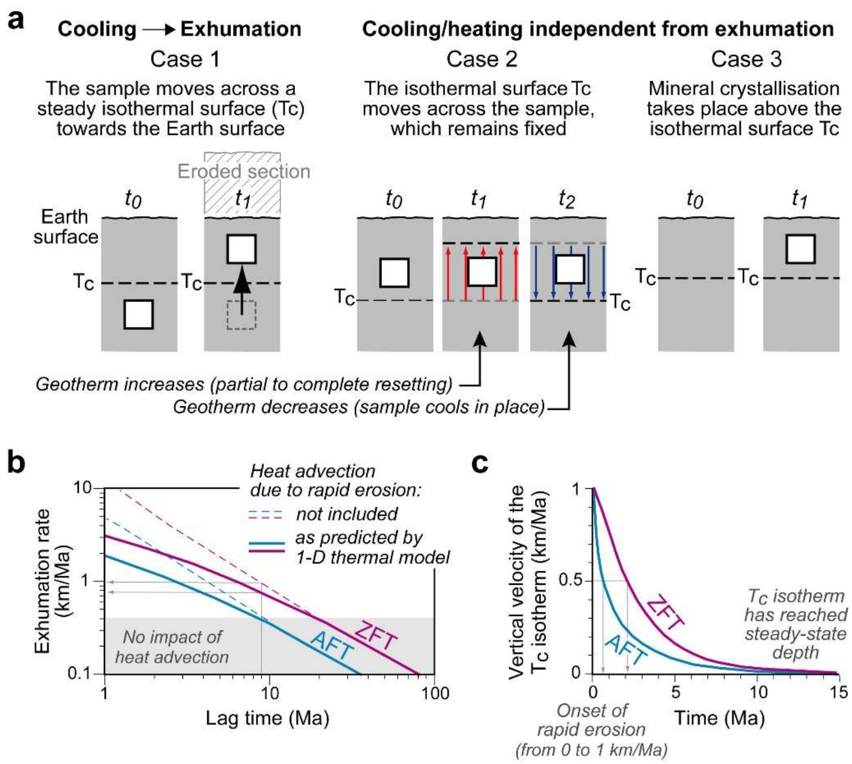

(1.5 column fitting image)

Fig. 3. **(a)** Cooling recorded by low-temperature thermochronometers may reflect different scenarios either related to exhumation, and thus relevant for lag-time analysis, or independent from exhumation: Case 1 - the movement (exhumation) of rocks towards Earth's surface because of overburden removal. Case 2 - in this scenario transient rising of isothermal surfaces (i.e., an increase in the geothermal gradient) results in partial or complete resetting of low-temperature thermochronometers, which record subsequent thermal relaxation (i.e., a decrease in the geothermal gradient). Case 3 - crystallization of minerals occurs at shallow crustal depth, above the T_c isotherm (modified from Malusà and Fitzgerald, 2019c). **(b)** Exhumation rate as a function of the lag time for fission-tracks in apatite (AFT) and zircon (ZFT). For fast exhumation (i.e., short lag time), the lag-time approach may strongly overestimate the exhumation rate because of the impact of heat advection due to rapid surface erosion. This problem can be minimized using thermal models that consider heat advection due to surface erosion (modified after Braun et al., 2006). **(c)** Response of the T_c isotherms to the sudden onset of rapid erosion from 0 to 1 km/Ma. The T_c isotherms initially move with the same velocity as the rock relative to Earth's surface, then the vertical velocities decrease (50% decrease in less than 1 Ma for AFT and ~2 Ma for ZFT) until isotherms reach a steady-state depth. Higher-temperature isotherms take longer to reach steady state compared to lower-temperature isotherms (modified after Reiners and Brandon, 2006).

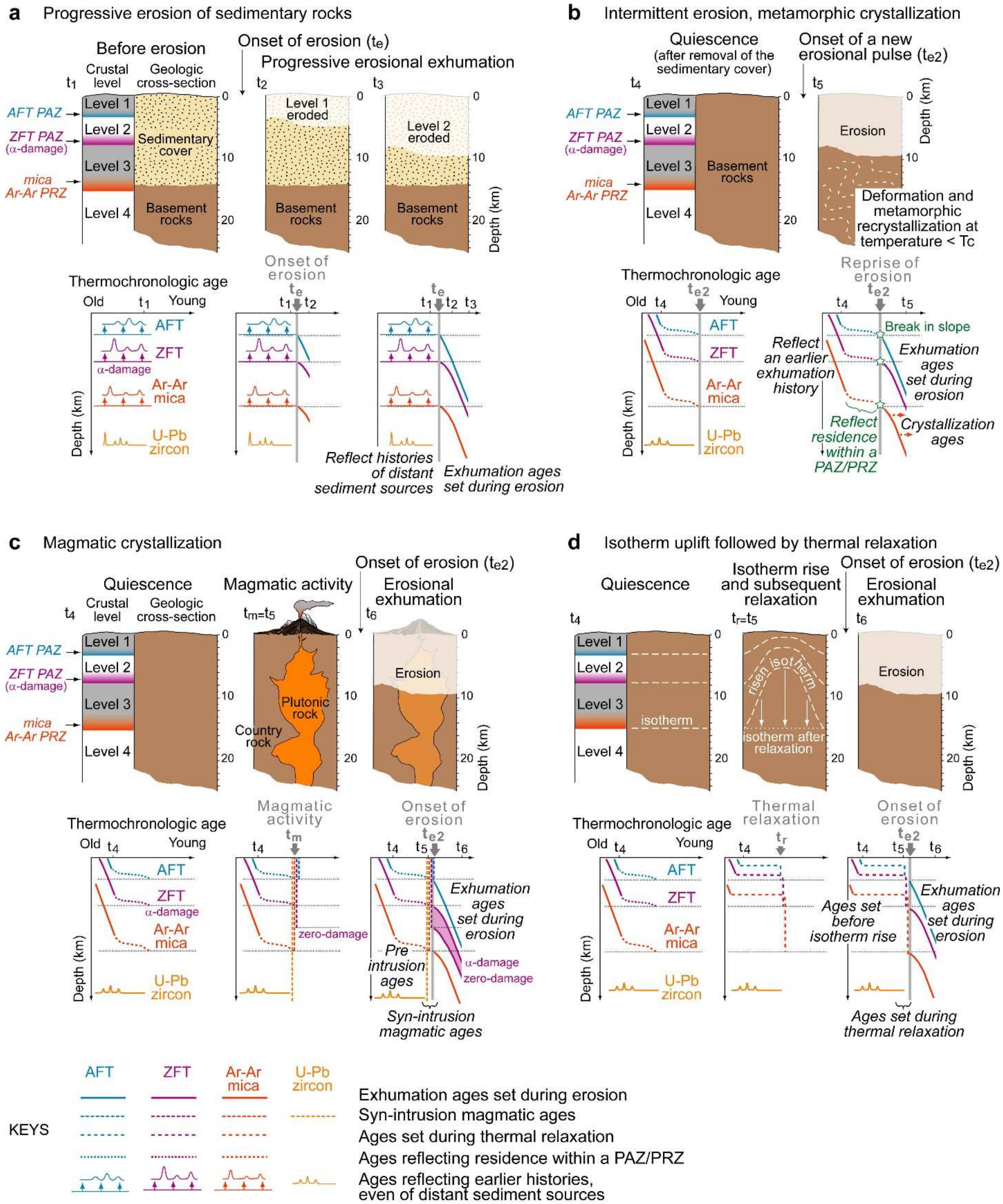

(2 column fitting image)

Fig. 4. Conceptual geologic cross-sections (upper rows) and corresponding age-depth diagrams (lower rows) illustrating the progressive setting of thermochronologic ages in bedrock and the specific age patterns expected for different geologic processes (see text for details). **(a)** Progressive erosion of sedimentary rocks and exhumation of underlying basement rocks. **(b)** Intermittent erosion of basement rocks, and possible recrystallization of metamorphic minerals at depth. **(c)** Intrusion of magma and growth of volcanoes at the surface followed by erosional unroofing. **(d**) Rising of isothermal

surfaces and subsequent thermal relaxation, e.g., due to continental rifting or rapid exhumation of deep rocks. Age-depth diagrams include the impact of heat advection after the onset of erosion, calculated for an erosion rate of 1 km/Ma and an initial geothermal gradient of 30°C/km according to a transient advection–diffusion equation for homogeneous media (Ehlers et al., 2005). Crustal levels 1 to 4 are delineated by the partial annealing zone (PAZ) of the apatite fission-track (AFT) system (lower boundary of level 1), the PAZ of α-damaged zircon fission-track (ZFT) system (lower boundary of level 2), and the partial retention zone (PRZ) of the mica Ar-Ar system (lower boundary of level 3). Note that only ages marked by a thick continuous line reflect exhumation during erosion and can be used to infer past exhumation rates.

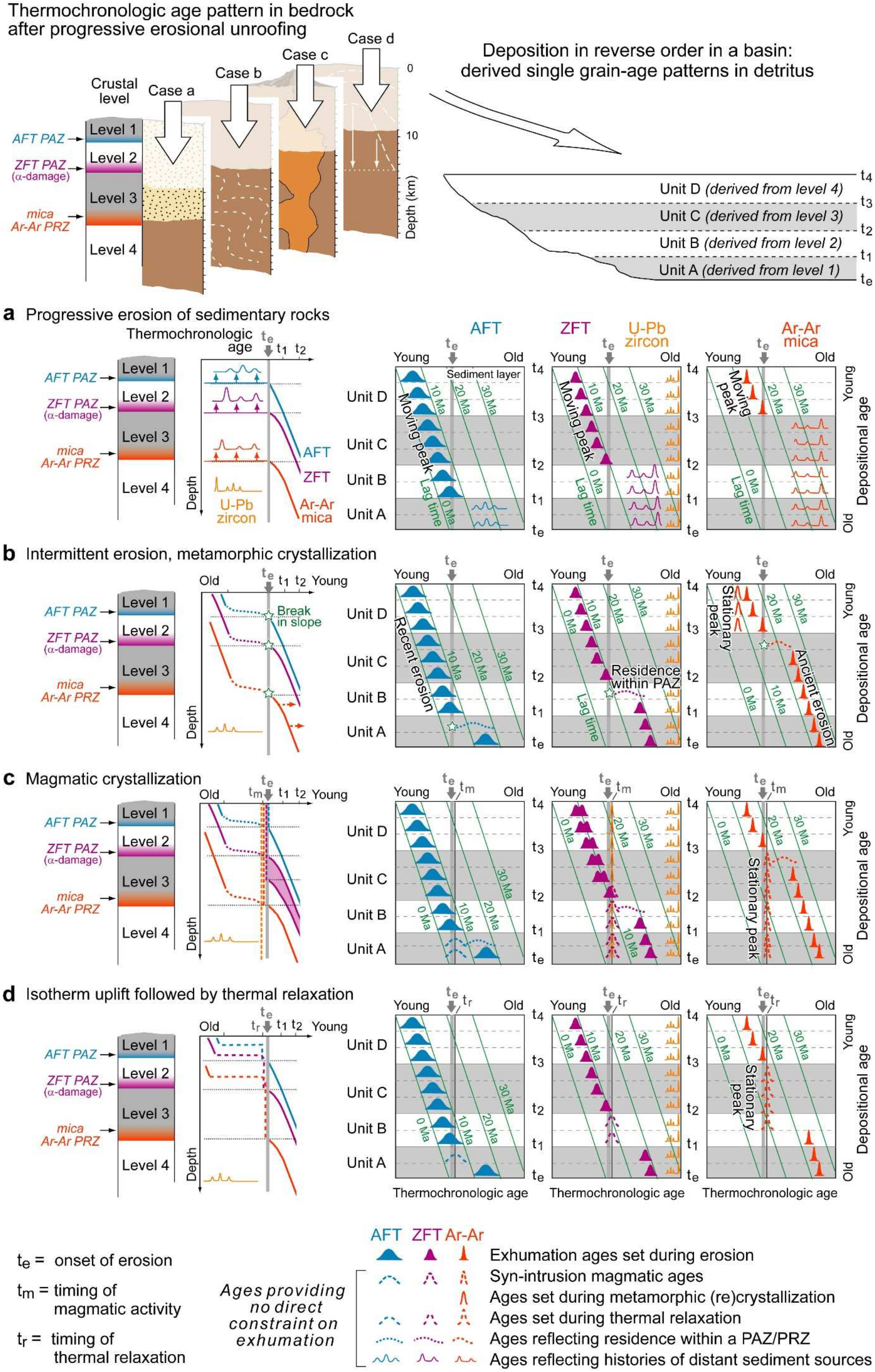
Thermochronologic age pattern in bedrock after progressive erosional unroofing
Crustal level
Case a
Case b
Case c
Case d
AFT PAZ
ZFT PAZ (α-damage)
mica Ar-Ar PRZ
Level 1
Level 2
Level 3
Level 4
Depth (km)
0
10
Deposition in reverse order in a basin: derived single grain-age patterns in detritus
Unit D (derived from level 4)
Unit C (derived from level 3)
Unit B (derived from level 2)
Unit A (derived from level 1)
t4
t3
t2
t1
te
a Progressive erosion of sedimentary rocks
Thermochronologic age
U-Pb zircon
AFT
ZFT
Ar-Ar mica
Depth
Young
Old
Sediment layer
Moving peak
Lag time
0 Ma
10 Ma
20 Ma
30 Ma
Unit D
Unit C
Unit B
Unit A
Depositional age
b Intermittent erosion, metamorphic crystallization
Break in slope
Recent erosion
Residence within PAZ
Stationary peak
Ancient erosion
c Magmatic crystallization
tm
Stationary peak
d Isotherm uplift followed by thermal relaxation
tr
Thermochronologic age
te = onset of erosion
tm = timing of magmatic activity
tr = timing of thermal relaxation
Ages providing no direct constraint on exhumation
AFT ZFT Ar-Ar
Exhumation ages set during erosion
Syn-intrusion magmatic ages
Ages set during metamorphic (re)crystallization
Ages set during thermal relaxation
Ages reflecting residence within a PAZ/PRZ
Ages reflecting histories of distant sediment sources

(2 column fitting image)

Fig. 5. Thermochronologic age patterns in a sedimentary basin expected after progressive erosion of crustal levels 1 to 4 in bedrock. The reference bedrock age-depth relationships (cases a-to-d on the left) reflect the different geologic processes illustrated in Fig. 4. Each of the four hypothetical stratigraphic units A to D (on the right) is exclusively derived from the progressive erosion, and deposition in reverse order in the basin, of one of the four crustal levels identified in the source (t_e = onset of erosion and stratigraphic age of the oldest sedimentary rocks in the basin). Different geologic processes produce diagnostic combinations of stationary and moving age peaks in detrital grain-age distributions. Moving age peaks (marked by full bells) are defined by thermochronologic ages set during bedrock erosion. These moving peaks get progressively younger up section and can be used to infer past exhumation rates. Stationary age peaks remain fixed up section and are defined by thermochronologic ages set during episodes of magmatic/metamorphic crystallization or episodes of thermal relaxation (Fig. 3, cases 2 and 3), and cannot be used to infer past exhumation rates.

Note that: *1)* The first appearance of a moving age peak occurs in detritus well after the onset of erosion, and with a time delay that is greater for higher-temperature thermochronologic systems (see case a). *2)* For a given thermochronologic system, only one moving age peak is expected from a single eroding source (cases a to d). *3)* Within a given stratigraphic interval, moving age peaks defined by different thermochronologic systems are potentially related to exhumation events of different age (see units B and C of case b). *4)* Detrital thermochronology ages reflecting former residence of mineral grains within a PAZ/PRZ are found at different levels of a stratigraphic succession, depending on the thermochronologic systems under consideration (see cases b and c). *5)* Stationary age peaks due to metamorphic crystallization are not expected in the lowermost units of a sedimentary basin, unless related to much older metamorphic events (see case b). *6)* Stationary peaks defined by magmatic crystallization ages are potentially detected starting from the lowermost units of a sedimentary basin, and for different thermochronologic systems within the same stratigraphic level (see case c) or even in the same mineral (see Fig. 6a). *7)* Stationary age peaks due to magmatic or metamorphic crystallization can be associated with a moving age peak that is always older than the stationary age peak from the same source (see cases b and c, and Fig. 6b). *8)* Stationary age peaks due to thermal relaxation are never associated with moving age peaks from the same source within the same stratigraphic level, and they are found in progressively younger stratigraphic units for progressively higher-temperature thermochronologic systems (see case d).

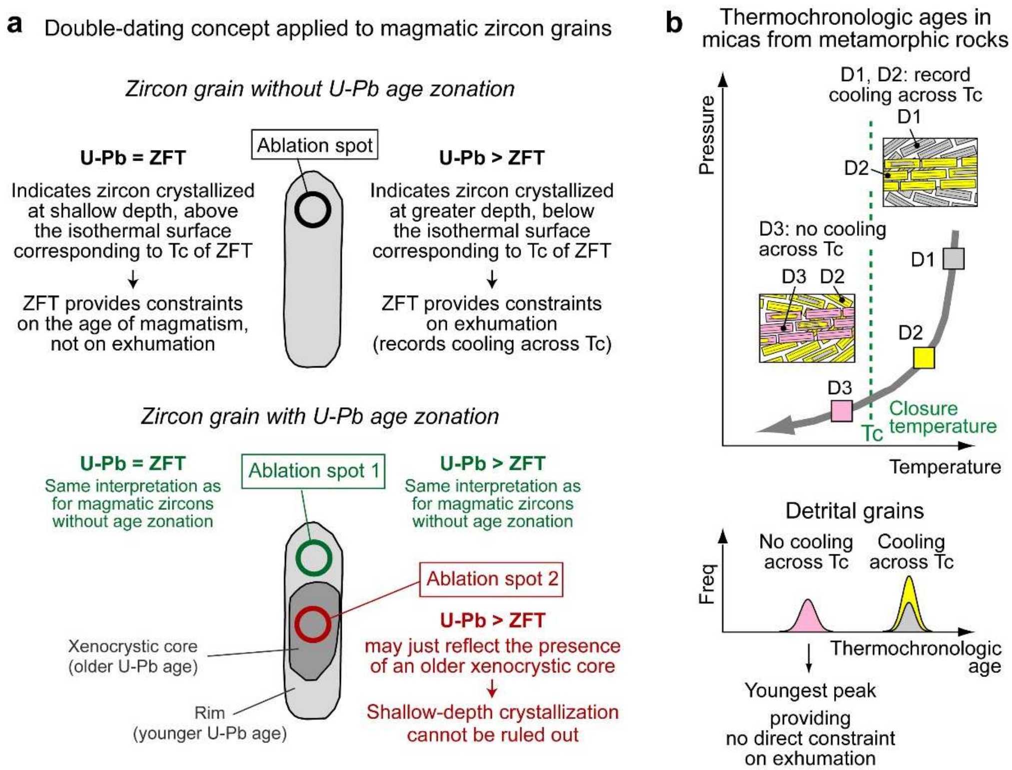

(1.5 column fitting image)

Fig. 6. (a) Identification of syn-intrusion magmatic ages in detrital zircon grains by double dating (U-Pb and ZFT). Magmatic zircons crystallized at shallow depth (i.e., from volcanic or shallow-level plutonic rocks) display identical U-Pb and ZFT ages within error (Carter and Moss 1999), because of rapid magma crystallization in the upper crust where country rocks are at temperatures cooler than the PAZ of the ZFT system. Zircon grains crystallized at greater depth and recording cooling across T_c during exhumation display a ZFT age younger than the corresponding U-Pb age. These ZFT ages can be used to contrain the long-term exhumation history of the source rocks using the lag-time approach (Bernet, 2019). However, if the ablation spot is located in the centre of the grain (lower row; e.g., Jourdan et al., 2018), U-Pb > ZFT may just reflect the presence of an older xenocrystic core, and shallow-depth crystallization of the zircon rim (also controlling the ZFT age) cannot be safely ruled out. Detrital zircon grains that have undergone removal of their external rims by abrasion during transport from source to sink are particularly prone to misinterpretation. **(b)** Conceptual pressure-temperature exhumation path of a metamorphic rock, with micas grown along different foliation planes during deformation stages D1 to D3. D1 and D2 indicate micas grown at higher temperature than the isotopic closure of the $^{40}Ar/^{39}Ar$ system. These micas will cross the T_c isothermal surface of the $^{40}Ar/^{39}Ar$ system during exhumation. D3 indicates micas that have grown at lower temperature than the diffusion-only isotopic closure of the $^{40}Ar/^{39}Ar$ system (e.g., Villa, 2010). These micas will not cross the T_c isothermal surface during exhumation. When eroded, micas D1 and D2 will define a moving age peak in detritus (cf. Fig. 5) that can be used to constrain the long-term exhumation history of the source rocks using the lag-time approach. Micas D3 will however define a stationary age peak (Fig. 5b) which is younger than the moving age peak and provides no direct constraints on exhumation (from Malusà, 2019; reproduced with permission from Springer).

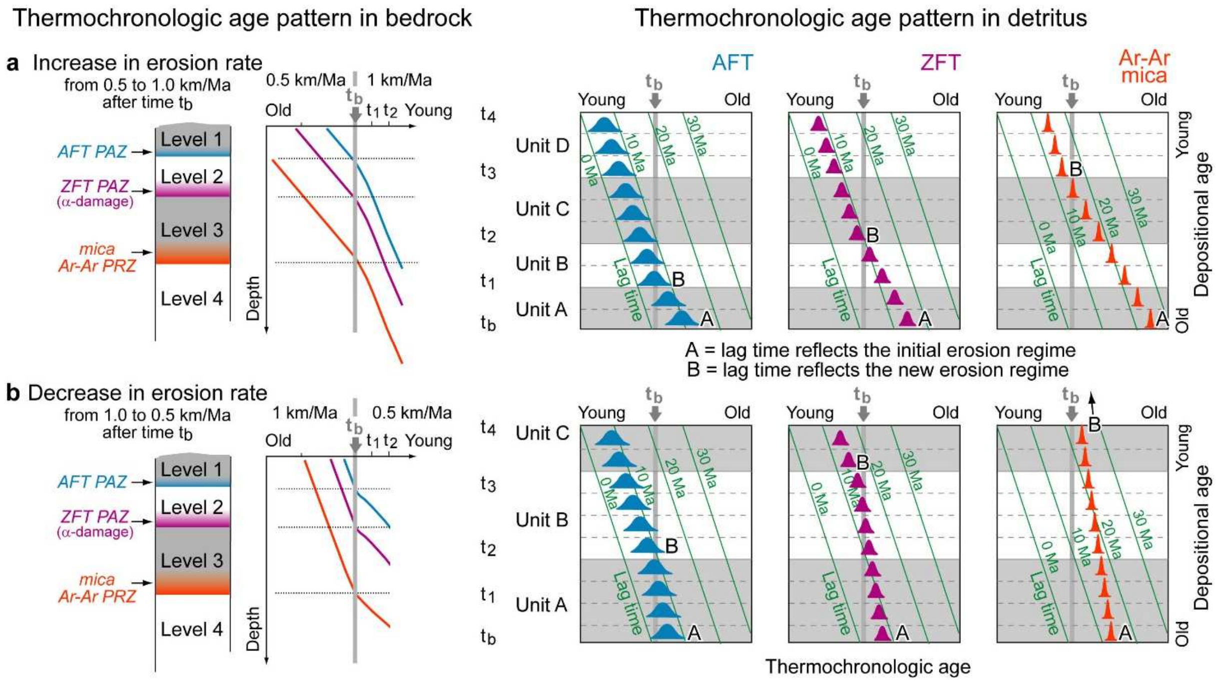

(2 column fitting image)

Fig. 7. (a) Sensitivity of the detrital thermochronology record to a sharp increase in exhumation rate in the source region at time t_b (from 0.5 to 1.0 km/Ma). Time t_b also marks the onset of sedimentation in the hypothetical sedimentary basin (on the right). In the basal part of the basin, labelled with "A", lag-time reflects the erosion rate before time t_b. In the overlying strata, lag-time values progressively decrease up section until they reflect, starting from "B", the new bedrock erosion rate. The time elapsed between A and B is shorter for lower-temperature systems and much longer for higher-temperature systems (>10 Ma for the Ar-Ar system on mica that mirrors the new erosion rate only after time t_3). Notably, a sharp change in erosion rate is hardly distinguishable from a more progressive change in erosion rate on a detrital thermochronologic basis, especially in the case of higher-temperature thermochronologic systems. **(b)** Sensitivity to a sharp decrease in exhumation rate at time t_b (from 1.0 to 0.5 km/Ma). Because of slower bedrock exhumation compared to (a), lag-time values reflecting the new erosion rate values will be observed in much younger strata of the sedimentary succession, and the higher-temperature thermochronologic systems may even fail to fully reveal the new erosion regime.

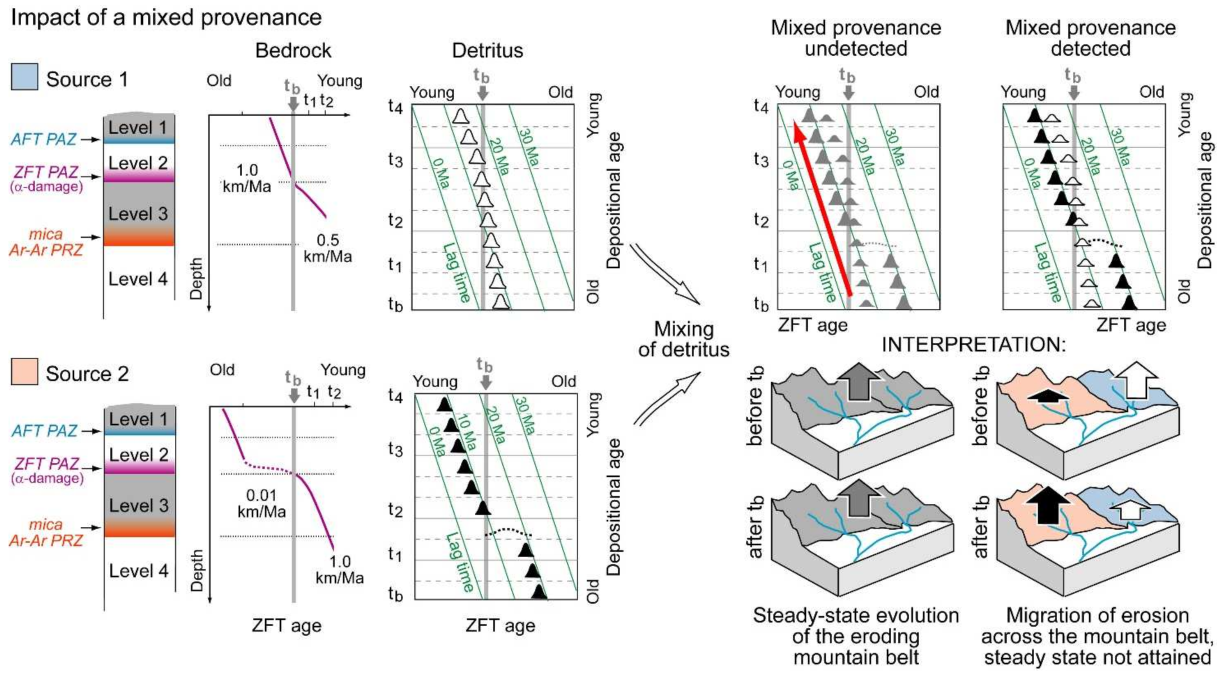

(2 column fitting image)

Fig. 8. Potential impact of a mixed provenance on lag-time analysis. On the left: ZFT age-depth relationships and corresponding single grain-age distributions expected in detritus for source 1 (same as Fig. 7b) and source 2 (same as Fig. 5c). Source 1 underwent a decrease in erosion rate from 1 km /Ma to 0.5 km/Ma at time t_b. Source 2 underwent an increase in erosion rate from 0.01 km /Ma to 1 km/Ma at time t_b. On the right: resulting lag-time diagram after sediment mixing in the final sink (sedimentation in the basin starts at time t_b). The two sediment sources have similar areas and zircon fertilities, but the faster erosion rate in source 2 implies a greater amount of zircon grains derived from that source in the final sink. If mixed provenance remains undetected, the constant lag-time values defined by the youngest age peaks (marked by the red arrow) may lead to an incorrect interpretation in terms of steady-state evolution of the eroding mountain belt (on the left), which is not attained (on the right; the big arrows on the bottom-right are proportional to the exhumation rate before and after t_b). This underlines the importance of independent provenance discriminations of dated mineral grains.

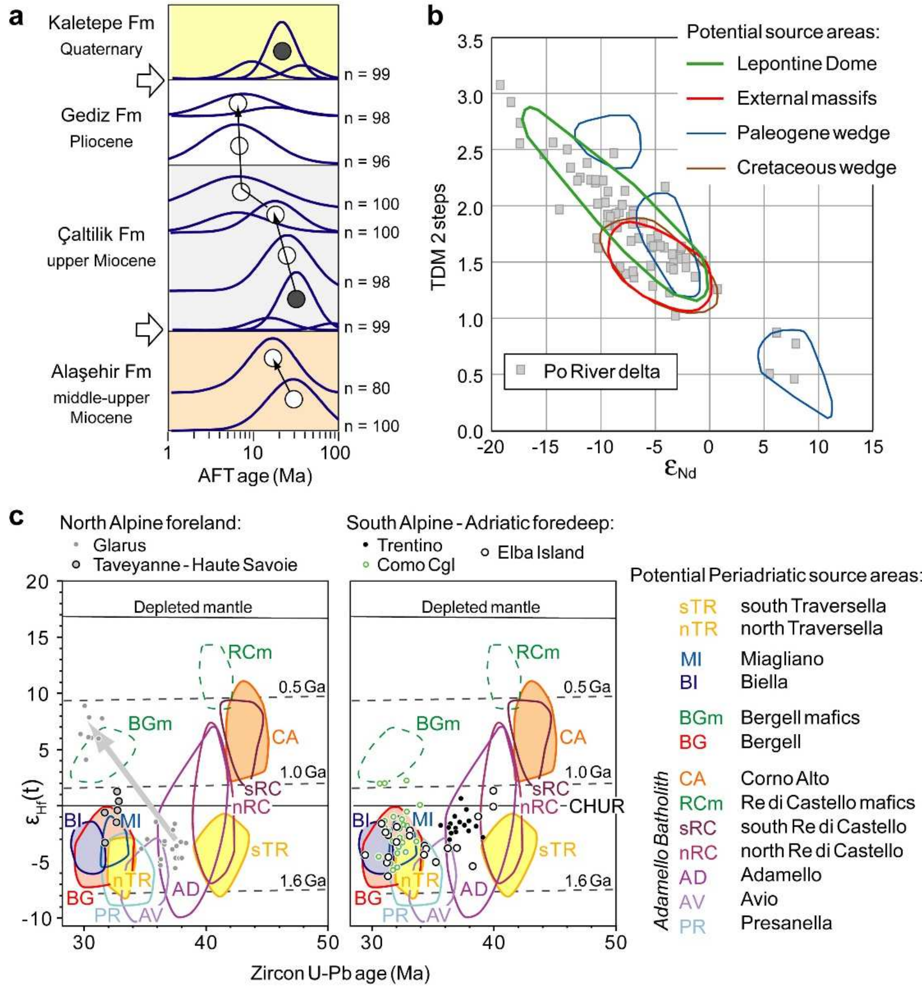

(1.5 column fitting image)

Fig. 9. Detection of provenance changes and approaches to provenance discrimination of apatite and zircon grains. **(a)** AFT age populations in sedimentary rocks of the Gediz Graben, western Turkey (Asti et al., 2018). The appearance of older grain-age populations moving up section along the stratigraphic sequence is supportive of major provenance changes (black dots mark jump to an older age-peak indicating change of provenance, which is also marked by the white arrows). **(b)** Example of provenance discrimination based on Nd isotopes, as applied to detrital apatite grains (grey squares) derived from erosion of the European Alps (Malusà et al., 2017): most of the grains are exclusively consistent with a Lepontine source; TDM = Nd-isotopic model ages. **(c)** Examples of provenance discrimination based on zircon U-Pb ages and Hf isotopic compositions, as applied to magmatic zircon grains in sedimentary rocks of the Alpine foreland basin and the Adriatic foredeep (based on data from Jacobs et al., 2018; Lu et al., 2018). The reference fields for the potential Periadriatic source areas are from Ji et al. (2019) (the Bergell and Re di Castello mafic rocks, indicated by green dashed lines, are volumetrically minor). South of the Alps, sedimentary rock samples from Trentino include zircon grains exclusively derived from the Adamello magmatic unit (AD), whereas samples from the Gonfolite succession (Como Conglomerate) include zircon grains from the Bergell pluton (BG) but likely no grain from the Biella (BI) and Traversella (nTR, sTR) plutons; the same provenances are documented in samples from Elba Island. North of the Alps, zircon grains are initially consistent with an Adamello source (AD), but zircon grains in younger sedimentary rocks follow a trend of progressive $\varepsilon_{Hf}(t)$ increase that is different from the boomerang-shaped trend defined by the Periadriatic plutons, which may suggest a different source area and a provenance change up section.

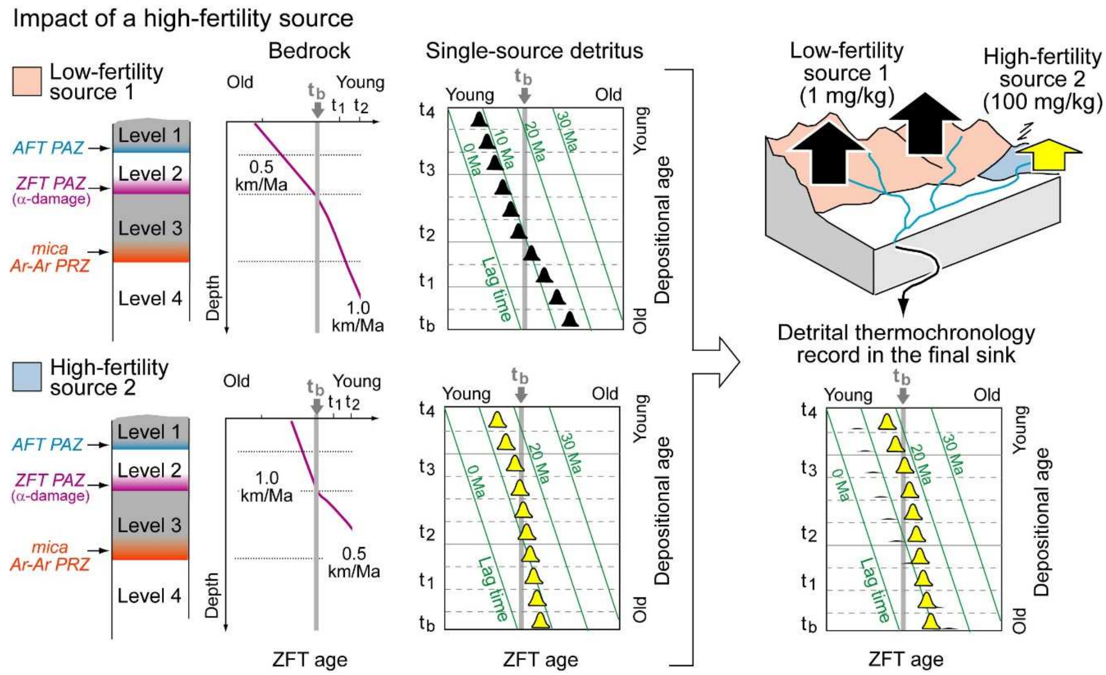

(2 column fitting image)

Fig. 10. Impact of high-fertility source areas on lag-time analysis. On the left: ZFT age-depth relationships and detrital grain-age distributions expected for source 1 (same as Fig. 7a) and source 2 (same as Fig. 7b). In source 1, characterized by zircon fertility around 1 mg/kg, the erosion rate increases from 1 km /Ma to 0.5 km/Ma at time t_b. In the much smaller source 2, characterized by higher zircon fertility around 100 mg/kg, the erosion rate decreases from 1.0 km /Ma to 0.5 km/Ma at time t_b. On the right: resulting lag-time diagram after mixing of detritus in the final sink (sedimentation in the basin starts at time t_b). In spite of the larger area and the higher erosion rate characterizing source 1, zircon grains from source 2 are overwhelming in the final sink due to the higher zircon fertility of source 2. According to this hypothetical scenario, the detrital thermochronology record in the final sink is prone to be incorrectly interpreted in terms of decreasing exhumation rates in the whole orogen, despite that most of the orogen underwent an increase in exhumation rate at time t_b. This underlines the importance of a reliable mineral fertility determination before any interpretations of the detrital thermochronology record.

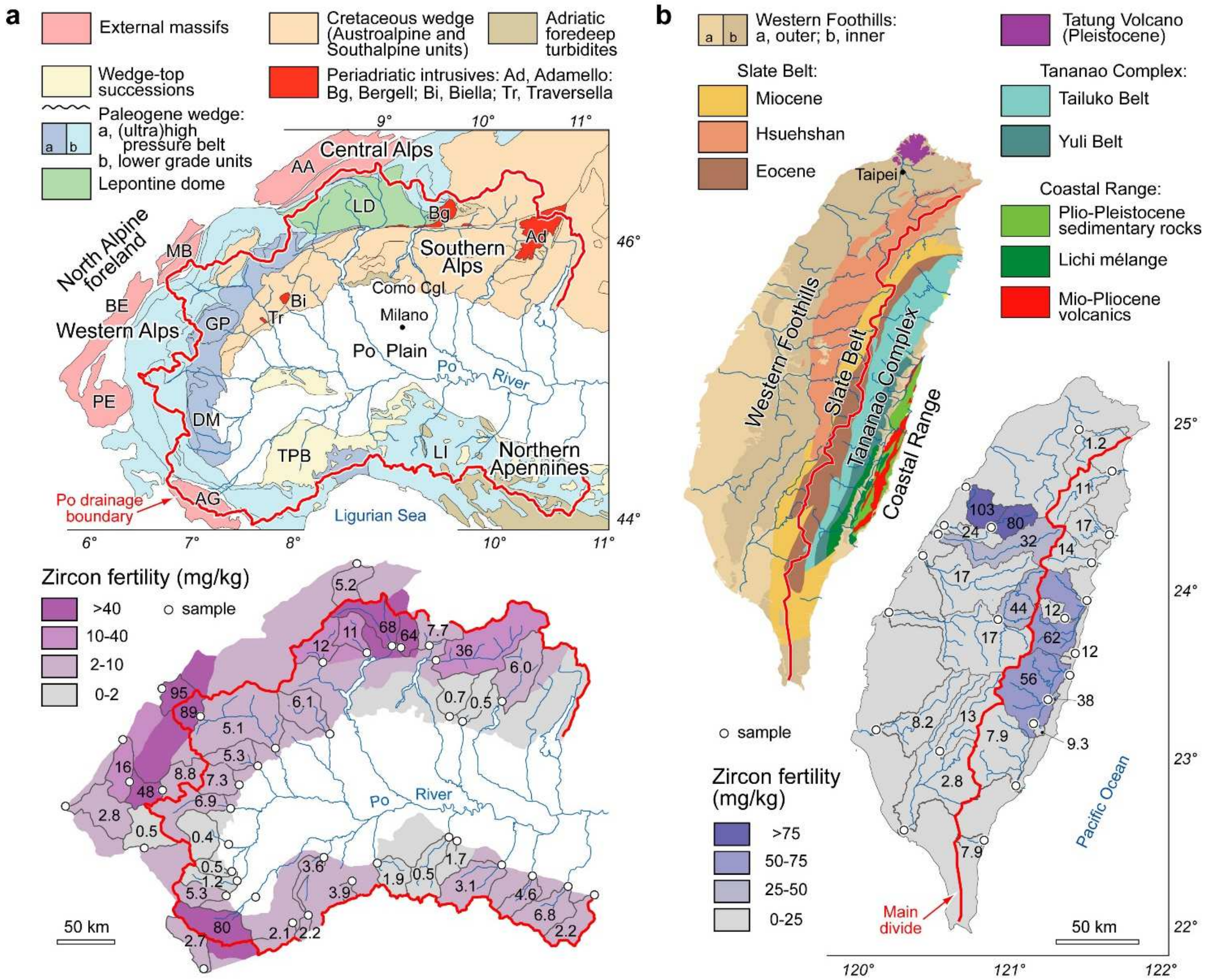

(2 column fitting image)

Fig. 11. (a) Tectonic sketch map (top) and zircon fertility map (bottom) of the European Alps based on mineral concentrations measured in modern river sand samples (white dots) (Malusà et al., 2016b). As in the example of Fig. 10, zircon fertility values span over two orders of magnitude, from ~0.4 mg/kg in the Dora-Maira (DM) to ~95 mg/kg in the Mont Blanc massif (MB). Other acronyms: AA, Aar; AG, Argentera; BE, Belledonne; GP, Gran Paradiso; LD, Lepontine dome; LI, Ligurian units of the Northern Apennines; PE, Pelvoux; TPB, Tertiary Piedmont Basin. **(b)** Tectonic sketch map (left) and zircon fertility map (right) of Taiwan based on the same approach applied in (a). Also in this case, zircon fertility values span over two orders of magnitude, from ~1.2 to >100 mg/kg (Resentini et al., in review).

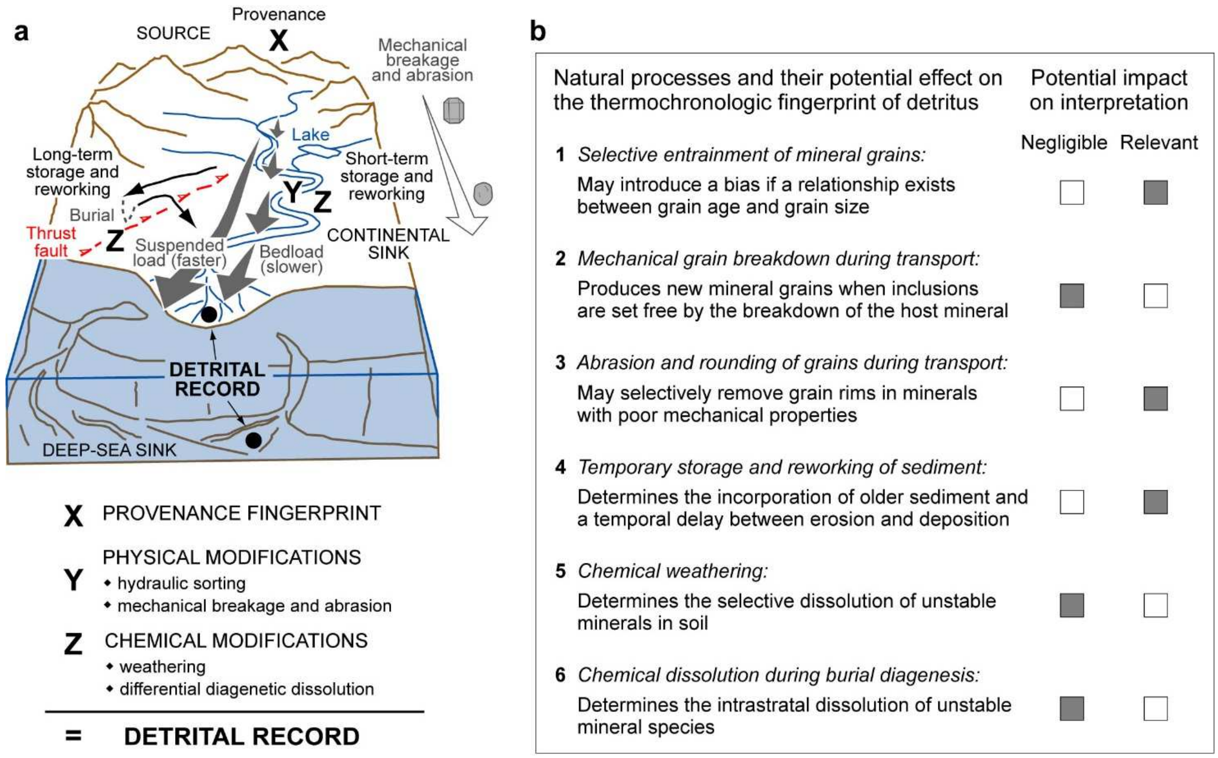

(2 column fitting image)

Fig. 12. (a) The detrital thermochronology fingerprint of the source area (X) can be modified by physical (Y) and chemical (Z) processes during sediment transport towards the final sink and subsequent burial diagenesis. Because solving for three variables requires an equal number of independent equations, using the detrital thermochronology record to obtain provenance information (X) requires that both physical and chemical modifications (Y and Z) during transport and deposition are constrained independently (from Malusà and Garzanti, 2019; reproduced with permission from Springer). **(b)** Summary of the natural processes that may modify the original thermochronologic fingerprint of detritus, and their potential impact on data interpretation using the lag-time approach (see text for details).

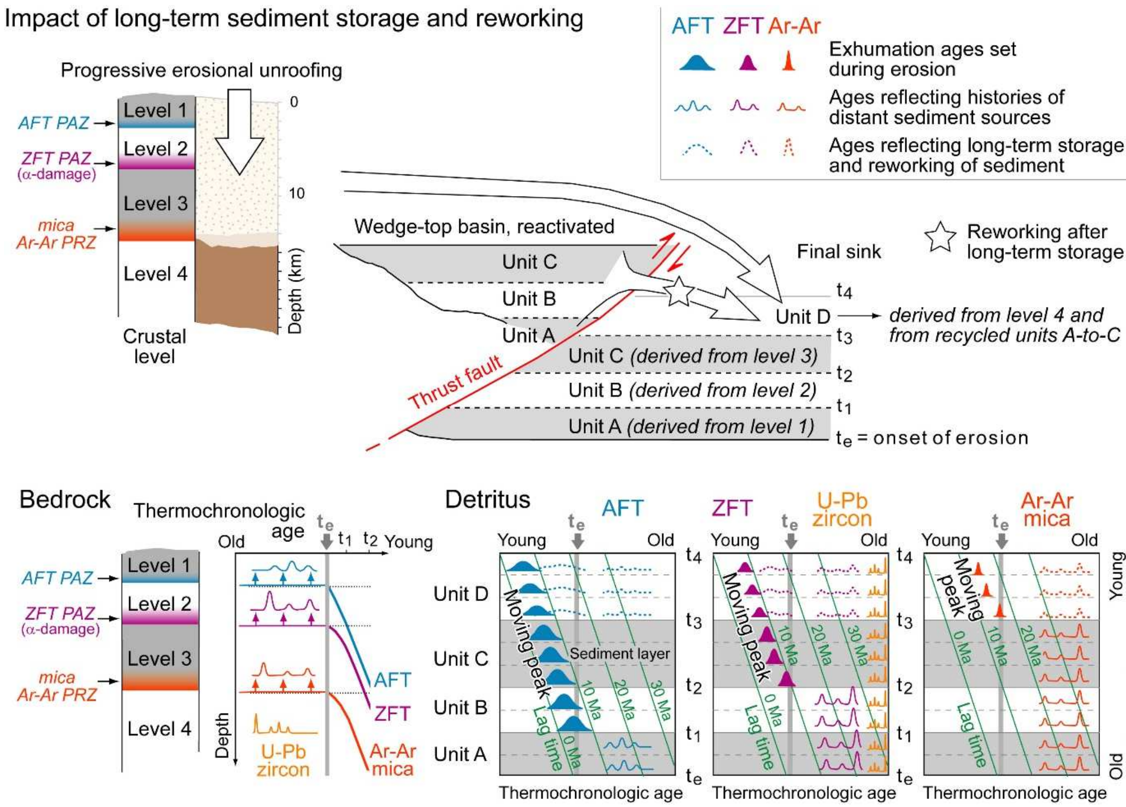

(2 column fitting image)

Fig. 13. Impact of long-term sediment storage and reworking on thermochronologic age trends (the thermochronologic age structure in bedrock is the same as in Fig. 4a). Detritus derived from erosion of levels 1 to 3, and temporarily stored in a wedge-top basin (for example), after time t_3 is reworked and admixed in the final sink along with detritus derived from erosion of level 4. As a result, unit D will include not only a young moving age peak that provides direct constraints on exhumation, but also all of the major age peaks inherited from sedimentary units A-to-C (dashed lines). Small grain-age populations recognized in units A-to-C may remain undetected in unit D, if below the detection limit after sediment mixing.

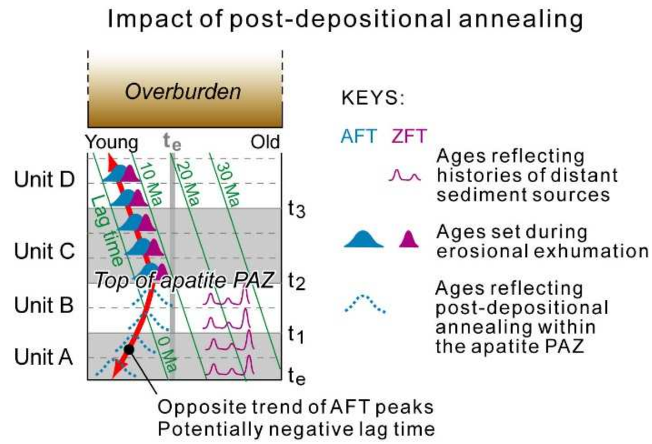

(single column fitting image)

Fig. 14. Impact of post-depositional annealing towards the base of a thick sedimentary succession (initial age structure as in Fig. 5a). In the lowermost units, the AFT age peaks become increasingly younger down section, showing the opposite trend (marked by the red arrow) to that observed in the uppermost stratigraphic levels. Such a reversal is not observed in higher T_c systems within the same stratigraphic level. Post-depositional annealing may lead to negative lag-time values.

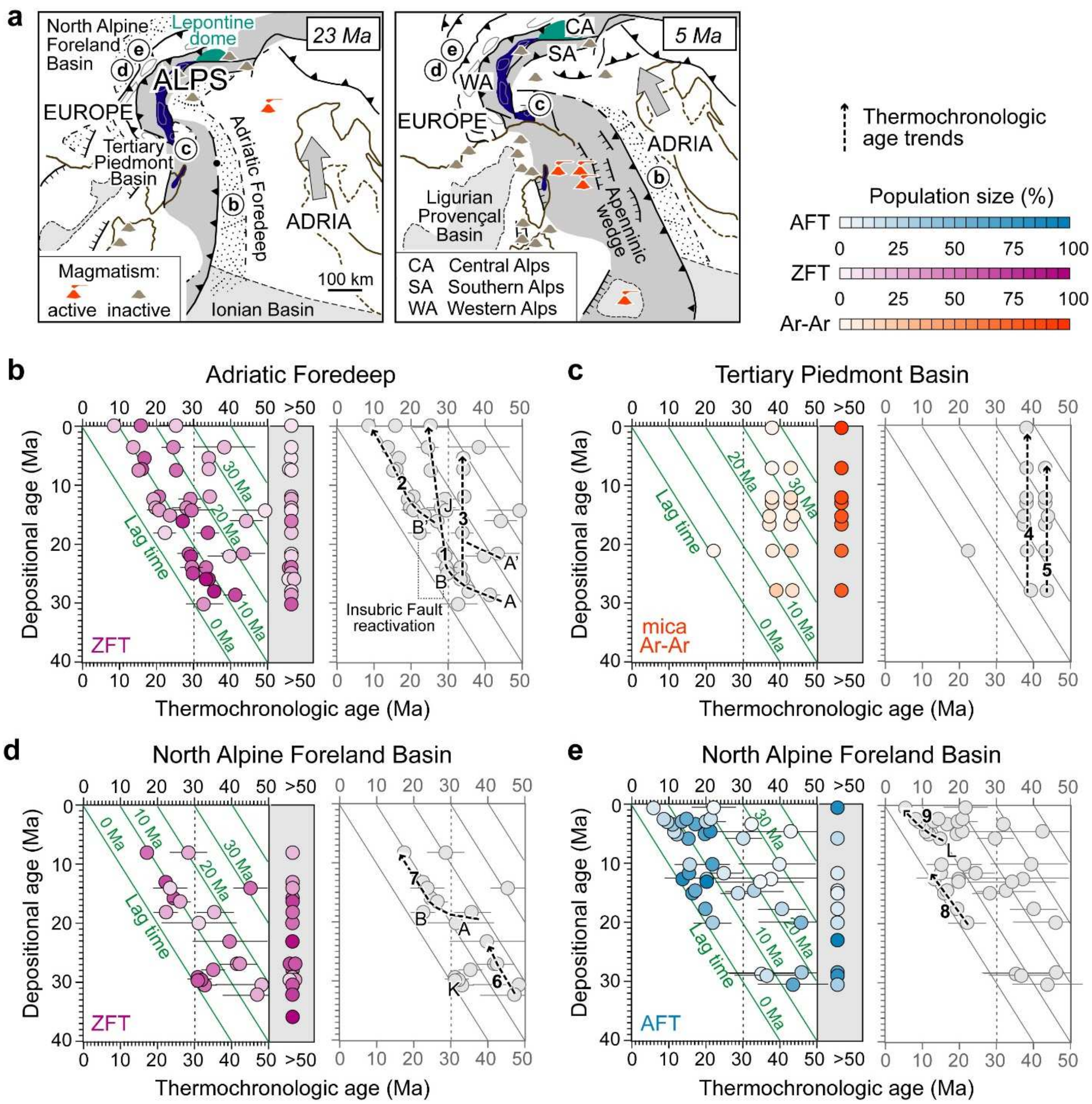

(2 column fitting image)

Fig. 15. Synthesis of detrital thermochronology data from the European Alps and surrounding sedimentary basins. **(a)** Tectonic sketch map showing the location of analyzed sedimentary basins (b-to-e) relative to the growing Alps at 23 and 5 Ma (after Malusà et al., 2015). The Eocene Eclogite belt is indicated in blue, the Lepontine dome is indicated in green. The grey arrow indicates the relative Adria-Europe plate motion (after Dewey et al., 1989). **(b)** Detrital ZFT data from the Adriatic foredeep (Bernet et al., 2001; 2009; Dunkl et al., 2001; Stalder et al., 2018); **(c)** Detrital mica Ar-Ar data from the Tertiary Piedmont Basin (Carrapa et al., 2003; 2004); **(d)** Detrital ZFT data from the North Alpine foreland basin (Bernet et al., 2009; Jourdan et al., 2013); **(e)** Detrital AFT data from the North Alpine foreland basin (Glotzbach et al., 2011; Jourdan et al., 2013). Different color intensities in the lag-time diagrams indicate the relative percentages of each grain-age population (see color bars on the top-right). Grains older than 50 Ma are indicated as a single grain-age population for the sake of simplicity. The vertical dashed line at 30 Ma marks the end of the Alpine magmatic climax. The greyscale diagrams on the right side of frames b-to-e show the interpretive age trends discussed in the main text.

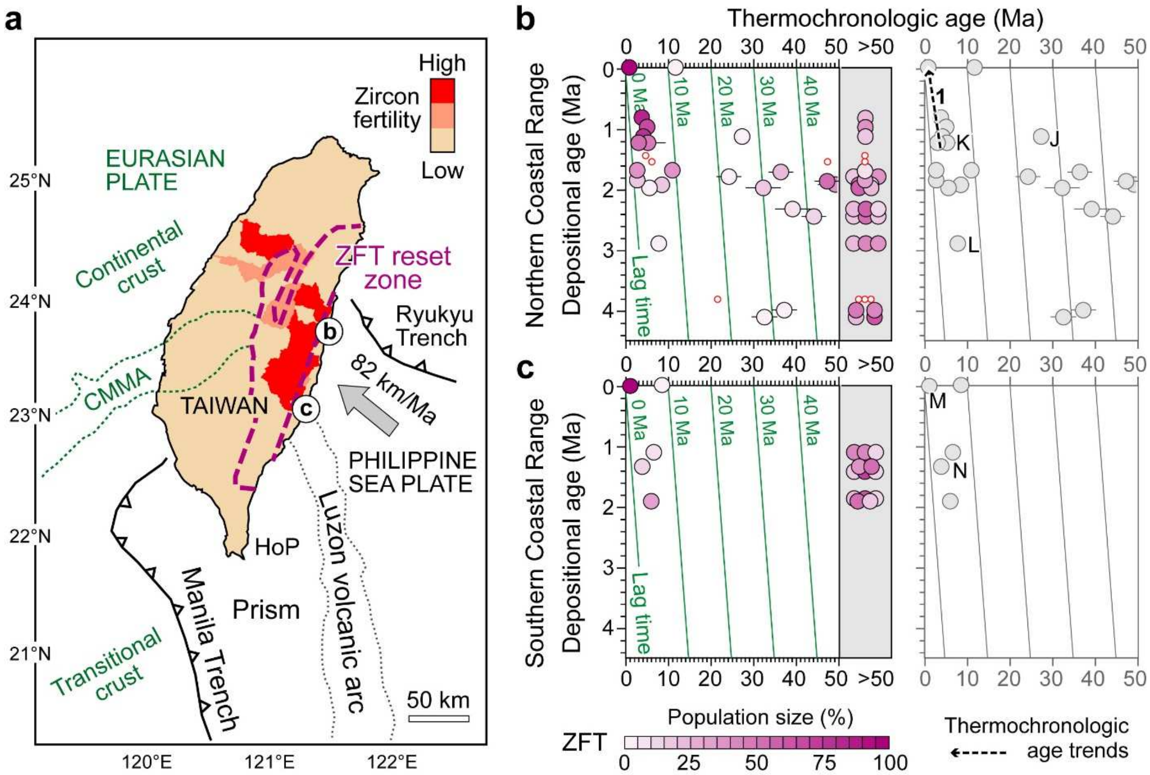

(2 column fitting image)

Fig. 16. Detrital thermochronology datasets from Taiwan. **(a)** Plate-tectonic setting (after Byrne et al., 2011) portraying the boundary of the zone of reset ZFT ages (purple dashed line, from Lee et al., 2015) and regions with higher zircon fertility (see Fig. 11b). Grey arrow = relative motion between Eurasia and Philippine Sea plates (Yu et al., 1997); CMMA = continental margin magnetic anomaly (Hsu et al., 1998); HoP = Hengchun Peninsula; “b” and “c” = location of datasets from the northern and southern Coastal Range, illustrated to the right. **(b, c)** Detrital ZFT data from the Taiwan-derived Plio-Pleistocene successions of the northern (Kirstein et al., 2010) and southern (Kirstein et al., 2014) Coastal Range, and corresponding modern sediments (Fellin et al., 2017). Different color intensities in the lag-time diagrams indicate the different size of each grain-age population (see color bar below). Small red dots indicate grain-age populations in sediments from the orogen pro-side (Mesalles et al., 2014). The greyscale diagrams on the right side of frames b and c show the interpretive age trends discussed in the main text.

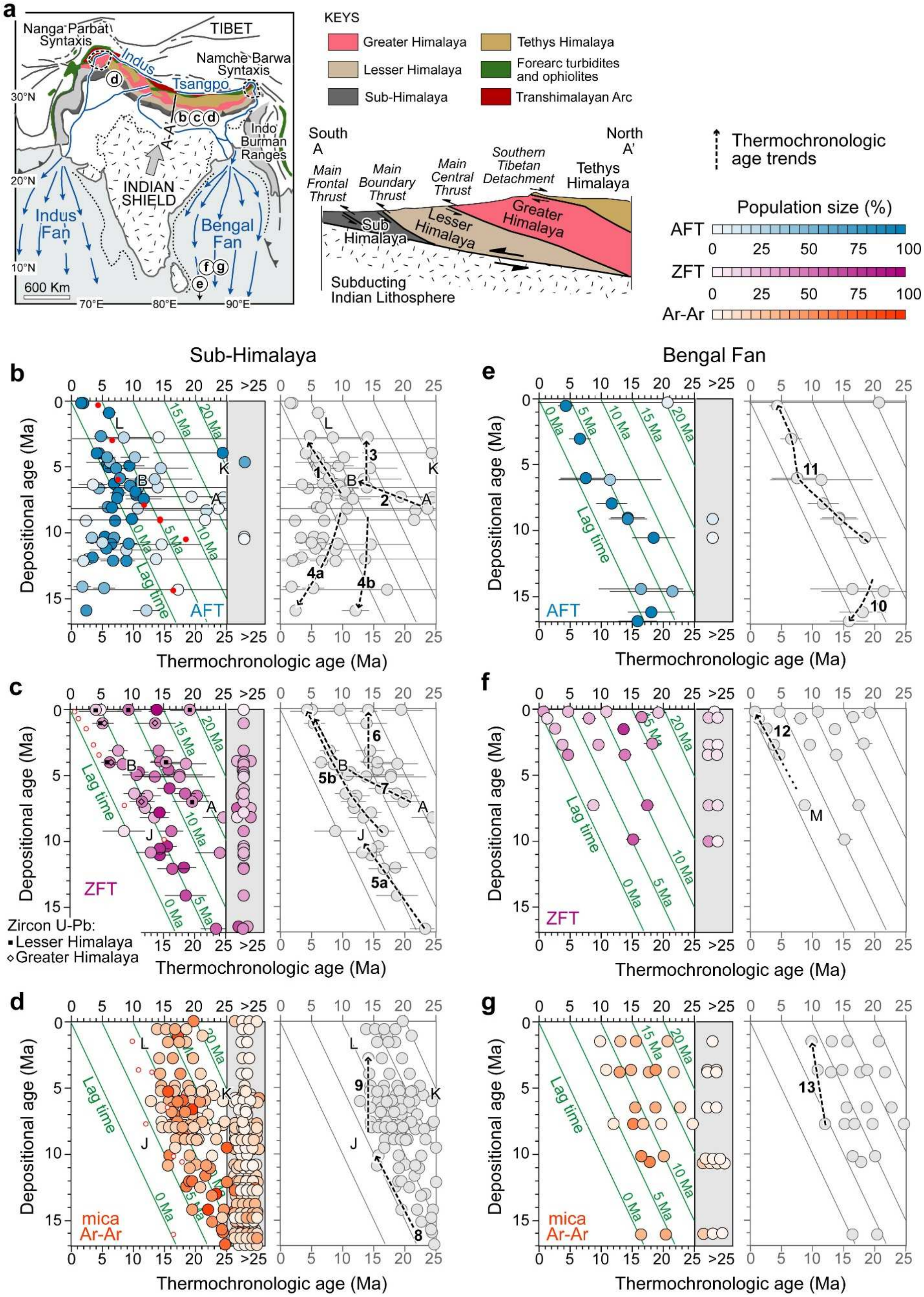

(2 column fitting image)

Fig. 17. Detrital thermochronology data from stratigraphic successions of the Himalaya and adjacent sedimentary basins (0-17 Ma stratigraphic interval). **(a)** Tectonic sketch map of the Himalayan region (Gansser, 1964; 1980) showing India-Eurasia relative plate motion (grey arrow, after Meade, 2007) and the location of sedimentary successions and associated detrital thermochronology data sets illustrated in frames b-to-g (Sub-Himalaya = b-to-d; Bengal Fan = e-to-g). On the bottom-right a simplified geologic cross-section across the central-eastern Himalaya (after Beaumont et al., 2001 and Goscombe et al., 2018). **(b)** Detrital AFT data from the Siwaliks of southwestern Nepal (van der Beek et al., 2006) and eastern Nepal (Chirouze et al., 2012); **(c)** Detrital ZFT data from the Siwaliks of southern Nepal (Bernet et al., 2006; Chirouze et al., 2012; Stickroth et al., 2019); for double-dated samples, ZFT age populations with a Lesser Himalaya U-Pb age fingerprint (i.e., including U-Pb ages at 1.8 and 2.5 Ga) or a Greater Himalaya U-Pb age fingerprint (i.e., with dominant ages at 1.1 Ga and subordinate ages at 1.5, 1.7 and 2.5 Ga) are also indicated by a full square or an empty lozenge, respectively; **(d)** Detrital mica Ar-Ar data from the Dharamsala and Siwalik formations of northwestern India (White et al., 2002; Najman et al., 2009) and the Siwalik and Dumri Formations of southern Nepal (Szulc et al., 2006; Stickroth et al., 2019); **(e)** Detrital AFT data from the distal Bengal Fan, Ocean Drilling Program Leg 116, sites 717 and 718 (Corrigan and Crowley, 1990, as recalculated by van der Beek et al., 2006). **(f)** Detrital ZFT data from the mid-Bengal Fan, IODP Expedition 354 (Najman et al., 2019); **(g)** Detrital mica Ar-Ar data from the mid-Bengal Fan, IODP Expedition 354 (Najman et al., 2019). Different color intensities indicate the different size of each grain-age population (see color bars on the top-right). Grains older than 25 Ma are indicated as distinct grain-age populations, if any, to highlight different provenances (grain-age populations for mica Ar-Ar are calculated by the normal mixture deconvolution algorithm of Galbraith (2005), implemented in "auto" mode in DensityPlotter by Vermeesch, 2012). Red dots in diagrams b-to-d (on the left) indicate the youngest grain-age populations in the corresponding diagrams for the Bengal Fan (e-to-g, on the right). The greyscale diagrams on the right side of frames b-to-g show the interpretive age trends discussed in the main text.